THE NUCLEAR ELASTIC SCATTERING OF FAST PROTONS

(PROTON-PROTON SCATTERING EXPERIMENTS USING A POLARIZED BEAM)

P. CHRISTMAS

(THESIS)

SEPTEMBER 1961

CONTENTS

Ch. IV. Experimental Measurements.

1) Adjustment of Apparatus.
   - (a) general remarks
   - (b) setting up the beam
   - (c) adjustment of counter voltages and delays
   - (d) zero angles for telescopes

2) Measurement of beam energy.

3) Measurement of beam polarization.
   - (a) asymmetry in p-carbon scattering
   - (b) analysis of data
   - (c) scattering at 20°
   - (d) polarization of beam from asymmetry
   - (e) scattering at 15°
   - (f) conclusions

4) Proton-proton scattering
   - (a) accumulation of data
   - (b) background counts
   - (c) random counts
   - (d) dead-time losses
   - (e) estimation of mean energy and energy spread
   - (f) angular resolution

Ch. V. Results

1) Analysis of data.

2
   - (a) calculation of polarization
   - (b) additional information from the data
   - (c) calculation of statistical errors

2) Tabulated results.

3) Accuracy
   - (a) sources of error
   - (b) statistical analysis

Ch. VI. Discussion of Results

1) Energy dependence of the polarization at 45° c.m.
   - (a) power law $P = aE^{b}$
   - (b) use of power law for interpolation
   - (c) significance of power law $p = aE^{b}$

2) Phase shift analyses of proton-proton scattering
   - (a) phase shift analyses at 40 MeV and below
   - (b) p-p scattering above 40 MeV

3) Conclusions.

Ch. VII. The Depolarization in Proton-Proton Scattering Near 150 MeV.

1) Introduction
   (a) general remarks
   (b) principle of the measurement
   (c) time-reversal invariance in p-p scattering
2) Previous measurements of D at 142 MeV
   (a) general remarks
   (b) results
3) The second Harwell depolarization measurement .
   (a) principle
   (b) apparatus
   (c) accumulation of data
   (d) systematic errors
   (e) results
   (f) discussion

Appendix I. Phase Shifts in Nucleon-Nucleon Elastic Scattering

1) Scattering of spin-zero particles
2) Scattering of spin-one-half particles
   (a) pure nuclear scattering
   (b) Coulomb effects in p-p scattering

Appendix II. Formalism of Nucleon-Nucleon Scattering

1) The M-Matrix
2) Observables
   (a) double scattering experiments
   (b) triple scattering experiments
   (c) spin correlation experiments
   (d) relativistic corrections.
3) Observables in terms of phase shifts

Appendix III. Multiple Coulomb Scattering

1) Theory
2) Applications

References

ABSTRACT

Proton-proton elastic scattering has been studied in counter experiments using the 150 MeV. 48 percent polarized proton beam from The Harwell 110-inch synchocyclotron.

The polarization in p-p scattering has been measured at various energies between about 27 MeV. and 100 MeV. The beam energy was reduced to the required values in a suitable absorber, and the energy of each measurement was defined by an anti-coincidence arrangement in conjunction with telescope absorbers. A liquid hydrogen target was employed and solenoids were used to rotate the polarisation of the beam through $\pm$ 180° in order to eliminate geometrical false asymmetries.

The Wolfenstein depolarization parameter in p-p scattering at 143 MeV. has been measured using similar techniques.

STATEMENT OF AUTHOR'S CONTRIBUTION TO THE EXPERIMENTS

I was responsible for the design and construction of much of the apparatus for the polarization experiment and was largely responsible for carrying out the measurements. I also analysed all the data. In the depolarization experiment I assisted in the assembly and testing of the liquid hydrogen target and participated in some of the preliminary measurements and in the collection of data.

ACKNOWLEDGEMENTS

I am particularly indebted to Mr. B. Rose who suggested the polarisation experiment and who has provided advice and encouragement at all times, and to Mr. A.E. Taylor for much useful advice and criticism and for his active participation in the earlier stages of the measurements. Until his departure for CERN, Geneva, in January, 1961, Mr. Taylor was my supervisor; that burden has since been borne by Mr. Rose.

I am also grateful to Dr. J.K. Perring and Dr. H.N.J. Phillips for useful discussions, to Mr. E. Wood, Mr. L. Bird and Mr. I.L. Watkins for their assistance with the measurements and to all the members of the synchocyclotron crew for their co-operation.

Chapter I.

INTRODUCTION

1. Nuclear Forces and Nucleon - Nucleon Scattering.

It is well established that all atomic nuclei are composed of protons and neutrons in roughly equal numbers. The nature of the forces which these particles exert upon one another is however less well known and provides the central problem in nuclear physics.

In many respects the proton and the neutron are very similar; for this reason, and as a matter of general convenience, they are often referred to collectively as nucleons. This notation finds formal expression in the isotopic spin formalism.

The peculiar features of the nucleon - nucleon interaction, namely its great strength and extremely short range, were first demonstrated by Wigner (R.1.). Since then a great deal of work, both experimental and theoretical, has been carried out with the object of learning more about nuclear forces. Attention has been concentrated mainly upon systems containing only two particles, chiefly because of the theoretical difficulties associated with multi-particle systems; it is also supposed that nuclear forces are additive, so that more complex structures can be explained in terms of the two-nucleon interaction.

The only known stable system of two nucleons is the deuteron,

comprising a proton and neutron in a bound state of binding energy about 2.23 MeV. The properties of the deuteron have provided important information about nuclear forces. Most of our knowledge has however derived from scattering experiments in which protons have provided the target and the bombarding particles have been either protons or neutrons. The absence of a suitable target of neutrons has precluded any direct study of neutron-neutron scattering.

Much of this introduction is devoted to a general survey of nucleon-nucleon scattering experiments and their interpretation. The concluding section is less general and gives the background to the proton-proton scattering experiments which form the subject of this thesis. Before embarking upon these topics it will be convenient, in the following section, to make some acquaintance with the language used by the physicist to describe the scattering of one particle by another.

2. The Interpretation of Scattering Experiments.

The simplest model of nucleon-nucleon scattering ignores both the spins of the particles and the possibility of inelastic processes. The scattering then reduces to the elastic scattering of one particle by another of equal mass at rest in the laboratory. This is a well-known problem in quantum mechanics; transferred to the centre-of-mass system it involves the solution of the Schroedinger equation for the scattering of a particle of reduced

mass by the potential which describes the interaction. The only difference between this problem and that of finding the bound states, if any, of the particle in the potential is that the total energy is now positive rather than negative. The wave function describing the scattering contains a sum over spherical harmonics, each of which is identified with a particular orbital momentum. Associated with each spherical harmonic is a radial term which reduces, at large distances, to an ingoing and an outgoing spherical wave. A similar solution describes the particles in the absence of the potential. In the latter case the symmetry arises merely from the choice of a particular point as origin; it is reduced one degree by choosing the coefficients of the various terms in the wave function so that they combine into a plane wave, corresponding to a beam of particles. More specifically, the plane wave solution is a sum of terms, each corresponding to a specific angular momentum l and having the asymptotic form

$$e^{i(kr - \frac{1}{2}l\pi)} - e^{-i(kr-\frac{1}{2}l\pi)} \qquad 1.1.$$

Where k is the de Broglie wave number of the particle in the centre-of-mass system.

When the potential is present the corresponding part of the solution takes the form

$$e^{i(kr - \frac{1}{2}l\pi + 2\delta_l)} - e^{-i(kr - \frac{1}{2}l\pi)} \qquad 1.2.$$

The solutions with and without the potential differ only by a change

in the phase of each outgoing "partial wave". For each angular momentum ℓ there is a real "phase shift" δ_ℓ which describes the scattering. Phase shifts are discussed more fully in Appendix I.

The significance of the partial wave approach to scattering lies in the fact that for a given energy only states with angular momenta below a certain value can participate; higher angular momenta correspond classically to particles with impact parameters larger than the range of the potential. It is, therefore, possible to describe the scattering at any particular energy in terms of a limited number of phase shifts. For example, it is shown in Appendix I that the differential cross-section can be written

$$I(\theta) = \frac{1}{k^2} \left| \sum_{\ell=0}^{\infty} (2\ell + 1) P_\ell (\cos\theta) \sin\delta_\ell \right|^2 \qquad 1.3.$$

In general only the first few terms of the sum over ℓ are significant, and equation 1.3 can be written as a sum over a few powers of $\cos\theta$ whose coefficients contain the phase shifts. If the cross-section data are accurate enough then the phase shifts may be extracted from them.

In general a potential cannot be derived from the phase shifts, but phase shifts can be calculated from an assumed potential and compared with those extracted from the data. In this way the validity of the potential can be ascertained.

The simple model discussed above does not contain all that is known about the nucleon-nucleon system. Several additional

features are required and these will now be mentioned. So far attention has been confined to elastic scattering of spin-zero particles. Inelastic scattering is included by allowing the phase shifts to be complex, so that the amplitude as well as the phase of each partial wave can change. The spins of the particles must also be taken into account. As a result of the spin-dependence of the interaction the number of phase shifts is increased. Further, orbital angular momentum need no longer always be conserved and it is necessary to extend the definition of phase shifts given above; this point is considered in Appendix I.

A final point is that the partial wave approach to scattering is useful only if the range of the potential is finite. If the range is infinite then all partial waves are scattered and the extraction of phase shifts is impossible; this is the case for the Coulomb interaction in proton-proton scattering . However, the form of the Coulomb potential is known and its effects can be calculated. Allowing for these effects, information about the nuclear part of the proton-proton interaction can be obtained from the data (see Appendix I).

3. A Survey of Nucleon-Nucleon Scattering .

(a) Summary. By about the year 1940 the general features of the nucleon-nucleon interaction appeared to have emerged, largely from low energy scattering experiments and the observed properties of the deuteron. Since about 1945 numerous high energy scattering

experiments have been performed. It was hoped that these could be described by potentials similar to those required by the low energy data, and that they would provide information about the shape of the potentials, about which nothing was known.

The first part of the present section deals briefly with the low energy data and the features which emerged from them; for a more detailed account the book by Blatt and Weisskopf should be consulted (R.2.). Some discussion then follows of high energy scattering and the extent to which the results could be understood in terms of potential models. Mention is also made of attempts to obtain a more fundamental understanding of the interaction. These topics are described more fully in various review articles. (e.g. R.3, 4, 5.)

(b) Nucleon-Nucleon Scattering below 10 MeV. Most of the experimental data prior to 1940 referred to Neutron-proton scattering below 10 MeV. In this region the scattering is predominantly S-wave and elastic; photo production of deuterons is significant only below 0.1 eV., while the modifications needed below 1eV to account for chemical binding of the target proton were quite well understood, The observed scattering, together with the binding energy of the deuteron, were explained in terms of an attractive central potential the details of which, as pointed out by Wigner, depended upon the total spin, i.e., upon whether the scattering takes place in the singlet or triplet spin state. The deuteron was at this stage regarded as a pure S-state. For each spin state the energy-

dependence of the S-wave phase shift was shown to be the following:

$$k \quad = \; -a_0^{-1} + \tfrac{1}{2} r_0 k^2 - P r_0^3 k^4 + \ldots . \qquad 1.4$$

k is the de Broglie wave number in the centre-of-mass system:

$$k^2 = 0.012E \times 10^{26} \text{ cm}^{-2} \qquad 1.5.$$

where E is the laboratory kinetic energy in MeV (The de Broglie wavelength is $\lambda = 1/k$)

a_0 is the "zero energy scattering length"; it is related to the strength of the potential. r_0 is the "effective range", equation 1.4 being known as the effective range expansion. The "shape parameter" P is related to the radial dependence of the potential. Additional terms not shown on the right-hand side of equation 1.4 contain higher powers of k; since r_0 is about 2×10^{-13} cm., it follows that these are negligible at energies below about 20 MeV. Below 10 MeV the term containing P is also negligible and equation 1.4 reduces to the "shape-independent approximation". Neutron-proton scattering data below 10 MeV have helped to provide accurate values of the scattering length and effective range for both singlet and triplet scattering, but they can be fitted by any reasonable shape of attractive potential. Measurements of proton-proton scattering have been confined to energies greater than 0.1 MeV, since Coulomb scattering predominates at lower energies. The presence of the Coulomb potential provides the first dissimilarity with n-p scattering ; this point has already been mentioned and is discussed further in Appendix I. The second difference derives from the identity of the two particles. The cross-section is symmetric about 90^0 c.m.; formally this is a consequence

of the antisymmetisation of the scattering matrix. Also, the Pauli principle requires that the wave functions shall be antisymmetric under exchange of the two protons, so that only spatially symmetric (even-parity) singlet states and antisymmetric (odd-parity) triplet states are permitted. The number of phase shifts required for p-p scattering is thus less than the number required for n-p scattering at the same energy.

Proton-proton scattering below 10 MeV is susceptible to a shape-independent approximation similar to that for n-p scattering, but now only the singlet state is involved. Further, the data are not inconsistent with charge-independence, i.e., with equality of the n-p and p-p forces. The data already mentioned could be fitted with a central potential. However, the asymmetry of the deutron ground state wave function, implied by its observed electric quadrupole moment, demanded an additional, non-central term in the interaction. The latter is the "Tensor potential", described by the operator.

$$S_{12} = 3\,\underline{\sigma_1}\cdot\underline{s}\,\underline{\sigma_2}\cdot\underline{s} - \underline{\sigma_1}\cdot\underline{\sigma_2} \qquad 1.6.$$

where $\underline{\sigma_1}$, $\underline{\sigma_2}$ are the Pauli operators of the nucleons and $\underline{s}$ is a unit vector parallel to the line joining them. The tensor interaction vanishes in the singlet state. In the triplet state it allows coupling of states of different orbital angular momentum, providing parity is conserved. As a result the deuteron ground-state can contain a small amount of D-state, and the latter suffices to explain the observed magnetic moment.

The two-nucleon data below 10 MeV are consistent with attractive

central-plus-tensor potentials. However, this type of potential does not give the observed saturation of nuclear forces. The latter was first explained in terms of interactions which can be attractive or repulsive according to the symmetry properties of the wave function under the exchange of same or all of the co-ordinates of the particles. Such interactions are said to involve "exchange forces". More recently saturation has come to be regarded rather as a consequence of a repulsive "hard core" in the potential.

Both the shell model of the nucleus and certain features of high energy scattering demand a second non-central term in the two-nucleon potential, the velocity-dependent spin-orbit ($\underline{L}.\underline{S}$) potential.

Information about the nucleon-nucleon interaction can also be derived from general conservation theorems. These predict that the interaction is

(1) invariant under spatial rotations (conservation of angular momentum)
(2) invariant under spatial reflections (conservation of parity),
(3) invariant under time-reversal.

In the absence of evidence to the contrary it has been usual to assume also that the interaction is (4) charge-independent and (5) at most linear in the relative momentum.

A general form can be written for the potential subject to these five conditions. The various terms of which it is composed are just those which occur in the combined central, tensor and spin-orbit potential predicted experimentally. A potential of this kind can be written for each of the four combinations of spin and parity; the

non-central terms vanish for singlet scattering.

The general features of the two-nucleon interaction thus seemed to be well-established, at least at low energies. It remained to be seen whether or not the same features could account for scattering at high energies.

(c) Nucleon-Nucleon Scattering above 10 MeV. During the past 15 years or so the construction of high energy particle accelerators has resulted in a wealth of new data from nucleon-nucleon scattering experiments, most of which have been performed at energies much greater than 10 MeV. It was hoped that high energy scattering would reveal something of the shape of the two-nucleon potential, about which very little information is provided by low energy data. This point may be appreciated by an appeal to the Uncertainty Principle, according to which the minimum uncertainty in the position of a particle is about equal to its de Broglie wavelength; it follows that a scattering experiment can at best provide information only about the average of the potential over this distance. It has been seen that the range of the nuclear potential is of the order 10^{-13} cm. (= 1 fermi). At 10 MeV the de Broglie wavelength of a nucleon in the centre-of-mass system is about 3×10^{-13} cm. and so nothing can be learnt about the shape of the potential. At 300 MeV, on the other hand, the situation is very different since the wavelength is only 0.5×10^{-13} cm. Also, several partial waves are involved; the S-wave scattering relates to the central region of the potential and higher partial waves to the outer regions.

The multiplicity of partial waves in high energy scattering means that many more phase shifts are involved. For each singlet state there is one phase shift. In triplet states the tensor part of the interaction implies that orbital angular momentum need no longer be conserved and it follows that each triplet state with ℓ greater than 1 requires 4 phase parameters (see Appendix I), namely 3 phase shifts and a mixing parameter. For example, it now appears that S-, P-, D- and F- waves are required at energies below 100 MeV; these give 9 phase shifts for p-p scattering and 16 for n-p scattering, whereas the number of independent parameters which can be extracted from the differential cross-section is only $\ell_{max} + 1 = 4$ for the former and $2\ell_{max} + 1 = 7$ for the latter. At higher energies the situation is even worse. Measurements are clearly needed of quantities other than the cross-section. The additional observables are the double- and triple- scattering and spin-correlation parameters defined by Wolfenstein and discussed in Appendix II. The relevant experiments require "polarized" beams, in which the spins of the nucleons are aligned predominantly along one direction, and these became available in 1954 (the method of producing polarized beams by scattering is described in Appendix II). The occurrence of polarization effects in scattering is readily appreciated in terms of a spin-orbit potential; particles scattered to the left and to the right correspond classically to opposite directions of their angular momentum vectors. For a tensor potential the effect is less obvious (R.6.). In the nucleon-nucleon system polarization effects can occur

only in triplet scattering. For a spin-orbit potential the orbital angular momentum must be greater than zero.

Above 400 MeV. pion production becomes significant (threshold 290 MeV.) and complex phase shifts are necessary. The number of real parameters involved is thereby doubled and it becomes unlikely that any detailed information can be extracted from the data. For this reason attention has concentrated very largely upon energies below 400 MeV.

Many attempts have been made to fit the high energy data with potentials which embrace some or all of the features described earlier. Quite simple functions, with at most one or two parameters, have usually been employed for the radial dependence. No attempt will be made to describe the various potential models that have been proposed; all have had limited applications. The most significant feature to emerge has been the need for a "hard core" or infinite repulsion at small distances. The most successful of the purely phenomenological potentials has been that of Gammel and Thaler (R.7), based on the 310 MeV. phase shift analysis of Stapp et. al. (R.8). It gives quite good agreement with most of the data up to 310 MeV.

During recent years emphasis has moved away from phenomenological potentials. It has rather become concentrated upon the extraction of unique sets of phase shifts at those energies at which there is sufficient data to make this feasible. It is hoped that when all the phase shifts are known as functions of energy it will be possible to construct a satisfactory potential. References to the numerous published analyses of n-p and p-p scattering are given in the review

articles already mentioned. In the earlier phase shift analyses it was often necessary to restrict the number of partial waves involved to what is now considered an unrealistic extent, in order to reduce the computation to a reasonable level. This limitation has been largely removed by advances in computer technology. One of the most successful analyses prior to 1958 was that of Stapp et al. at 310 MeV. already mentioned. More recently, analyses have been reported in which data at various energies were treated simultaneously, the phase shifts being extracted as functions of the energy.

Scattering experiments can provide information about how nucleons interact, but they cannot answer the question "why do they interact?" The answer to this question must come from field theory in terms of some more fundamental process; a great deal of effort continues to be expended upon this subject. The nucleon-nucleon interaction is now thought to proceed through the exchange of mesons. The outer parts of the potential are associated with pion exchange; n-pion exchange forces give a contribution of range λ/n where λ is the pion Compton wavelength ($\lambda = 1.4 \times 10^{-13}$ cm.). Approximate calculations have been made of the one- and two- pion exchange processes and these are quite successful in explaining low energy scattering. Attempts to extend these calculations to higher energies have so far involved making assumptions about the inner region of the potential. Signell and Marshak (R9) added a spin-orbit term to the Gartenhaus meson-theoretic potential and thereby obtained quite good fits to the data up to 150 MeV. Qualitatively their potential is very similar to that of Gammel and

Thaler.

Recently, meson theory has been applied to high energy scattering data in a different way. It has been shown that phase shifts calculated in Born approximation from one- pion exchange can be used for the higher partial waves, the remainder of which are treated by the usual analysis. Cziffra et al.(H10) have extended the Stapp analysis by this method, using calculated phase shifts for $l > 5$. In addition to the phase shifts for $l \leqslant 5$, a reasonable value was also obtained for the pion-nucleon coupling constant, which entered the analysis as a free parameter.

4. The State of Proton-Proton Scattering in 1958

(a) Summary. It is convenient to conclude the introduction with some remarks about the state of the two-nucleon problem as it appeared at about the end of 1958. The emphasis is upon those features which bear most directly upon the experiments which form the subject of this thesis. Discussion is devoted largely to proton-proton scattering not only because of the smaller number of phase shifts involved at a given energy as compared with neutron-proton scattering, but also because the available data were, and remain, more numerous and of greater precision. Interest had, as mentioned above, become concentrated upon extracting unique sets of phase shifts from the data at various energies. The prospects of achieving this aim appeared good for p-p scattering at the higher energies. At 310 MeV the modified analysis of Cziffra et al. had already reduced the number of possible solutions to two and it appeared

that a measurement of the correlation parameter C_{kp} at 45° c.m. would distinguish these. A programme of p-p triple-scattering measurements was already under way at 150 MeV and similar experiments were planned at 210 MeV.

(b) The D Parameter in Proton-Proton Scattering at 150 MeV.

The Wolfenstein D parameter, or depolarisation, in p-p scattering at about 150 MeV had been measured both at Harwell and at Harvard. This measurement was of particular interest because the values predicted by the Gammel-Thaler and Signell-Marshak potentials were quite different. However, the two sets of measurements were themselves in definite disagreement. The Harvard data favoured the Gammel-Thaler predictions, the Harwell data those of Signell and Marshak. It was decided to repeat the measurement at Harwell in the hope that the ambiguity would thereby be removed; the writer was a member of the team which performed this measurement and a description is given in Chapter 7.

(c) Low Energy Proton-Proton Polarization. Below 100 MeV the prospects for obtaining unique phase shift solutions appeared less good. Only cross-section data and a few polarization measurements were available.

There were a number of cross-section measurements, although some of these dated back several years and were of a lower accuracy than the more recent data. Apart from measurements at 98 MeV reported from Harwell, the only polarisation data below 100 MeV were those from Harvard. There, Palmeiri et al. (Ml1) had obtained the angular distribution of the polarisation in p-p scattering at several energies down to 68 MeV, and in addition, values of the polarisation at 45° c.m.

at 56 MeV and 46 MeV. There were no other p-p scattering data. Triple-scattering experiments at low energies were exceedingly difficult, for reasons related to the small size of the polarization in proton-nuclear scattering. These were the small beam polarization obtainable by the usual methods, and the small analysing power of any third scatterer. It appeared that triple-scattering experiments would require a linear accelerator with a polarized ion source, while a correlation-type measurement would need a polarized target; neither of these were available.

Interest in the energy region below 100 MeV had become concentrated near 40 MeV, largely owing to accurate cross-section data at that energy reported in 1957 from Minnisota (H12). This data was analysed later in the same year by Noyes (H13); this analysis referred to preliminary data, the final version appeared in 1958 (H14).

The object of Noyes' analysis was to learn more about the singlet even-parity part of the p-p interaction. At 40 MeV the effective range expansion (Section 1.3) is sensitive to the shape of the potential; limited information about the latter should follow from a sufficiently precise knowledge of the S-wave phase shift at that energy. P-waves were known to be present at 40 MeV from the form of the Coulomb nuclear interference minimum; however, the data could not be fitted by S- and P- waves alone. When D- waves were included the data were fitted, but with S- and D- wave phase shifts which differed widely from the expected values while in addition polarizations of about 20 per cent were predicted. Noyes concluded that accurate polarization data were

the least requirement for a unique solution. Also, if the polarization at 45° c.m. was appreciably smaller than 20 per cent, then the presence of F- waves at 40 MeV would be confirmed. The Harvard group obtained a value of (1.2 ± 1.3) per cent for the polarization at 45° c.m. at 40 MeV. Noyes and MacGregor, in the published account of the 40 MeV analysis, suggested that this provided conclusive evidence for F- waves at that energy. They also suggested that a single polarization measurement was unlikely to be of very much help, but that the ambiguity in the solutions at 40 MeV might be resolved by measurements of the angular distribution and polarization as functions of energy.

It was with the remarks of the last paragraph in mind that the polarization measurements with which this thesis is largely concerned were embarked upon. The measurements were aimed at extending the data of Palmeiri et al. to lower energies, to 30 MeV for example where there were angular distribution data, and also at obtaining accurate values near 40 MeV. The energy dependence of the polarization at low energies was itself of interest, since the Harvard data did not preclude for this a more complicated form than that predicted by Gammel and Thaler, according to whom the polarization falls monotonically to zero as the energy decreases (see Fig. 14). An absolute error of ± 0.5 per cent in each measurement was hoped for.

The polarization experiment is described in the next five chapters. Chapters 2, 3 and 4 are devoted to various aspects of the measurements. The results are presented in chapter 5 and in chapter 6 they are discussed with reference to the Noyes' analysis and also to other phase shift analyses which have since been reported.

Chapter II

POLARIZATION FROM DOUBLE SCATTERING

1. The Left-Right Asymmetry in Double Scattering.

Polarization effects in nucleon-nucleon scattering are described in Appendix II. It is shown there that information about the polarisation can be obtained from measurements of double scattering. The extraction of this information will now be discussed in more detail. Following this, some of the difficulties of the double scattering experiment will be mentioned, and the ways in which these were overcome in the present work.

From equation A2.12 of Appendix II the differential cross-section for the scattering of a polarised beam is given by

$$I(\theta) = I_o(\theta)\,(1 + \underline{P_1} \cdot \underline{P_2}) \quad . \qquad 2.1.$$

$I_o(\theta)$ is the unpolarised cross-section, $\underline{P_1}$ the beam polarisation and $\underline{P_2}$ the polarisation that would result from the scattering if $\underline{P_1}$ were zero. $\underline{P_1}$ and $\underline{P_2}$ are parallel to the unit vectors $\underline{n_1}$ and $\underline{n_2}$ which define the first and second scattering planes respectively. It will be assumed that $\underline{n_1}$ is upward, i.e., that the first scattering is in the horizontal plane and to the left.

The azimuthal angle ϕ between $\underline{n_1}$ and $\underline{n_2}$ will be defined as follows:-

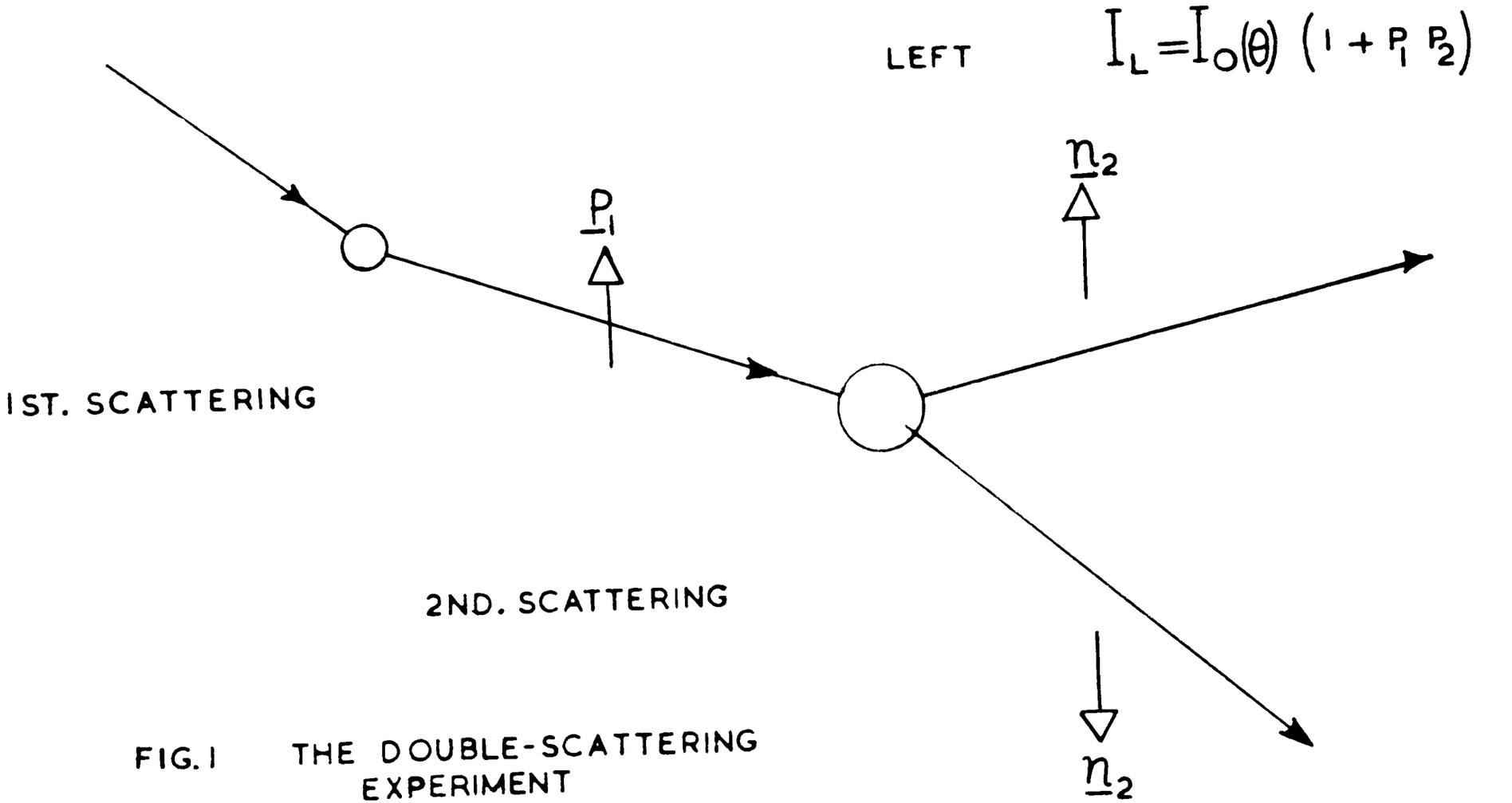

FIG. 1 THE DOUBLE-SCATTERING EXPERIMENT

$$\cos\phi = \underline{n_1} \cdot \underline{n_2} \quad , \quad \sin\phi = (\underline{n_1} \wedge \underline{n_2}) \cdot \underline{k_2} \qquad 2.2$$

Equation 2.1 may now be written

$$I(\Theta) = Io(\Theta)\,(1 + P_1 P_2 \cos\phi). \qquad 2.3$$

Referring to the second scattering, $\phi = 0^\circ$ and $\phi = 180^\circ$ correspond respectively to scattering to the left and to the right. If the corresponding cross-sections are I(L) and I(R) then

$$\begin{aligned} I(L) &= Io(\Theta)\,(1 + P_1 P_2) \quad , \\ I(R) &= Io(\Theta)\,(1 - P_1 P_2) \end{aligned} \qquad 2.4$$

The measured quantity is the "left-right asymmetry", $\sum$, defined as follows:-

$$\sum = \frac{I(L) - I(R)}{I(L) + I(R)} = P_1 P_2 \qquad 2.5.$$

See also Fig. I.

At this juncture two points about notation must be mentioned. In the first place, reference to an "asymmetry" will hereafter mean the left-right asymmetry defined in equation 2.5, rather than the quantity Δ defined in Appendix II. In the second place, a double scattering experiment will refer to the measurement of an asymmetry; recently, polarized ion sources have been fitted to some accelerators so that the asymmetry measurement may now involve only one scattering.

Measurements of the asymmetry can be used to determine either P_1 or P_2, the other being known. In principle the experiment is a simple one, the procedure being as follows: The polarized beam is directed onto the target and scattered particles are detected by a counter telescope which can be rotated in the horizontal plane about an axis through the centre of the target. Scattered particles are

counted for a given time with the telescope at the required angle to the beam, first on the left and then on the right. The asymmetry is then calculated from the two counts according to equation 2.5.

2. Features of the Double Scattering Experiment.

(a) False Asymmetries. The measurement described at the end of the preceding section will in general be subject to error unless the two angles of scattering are accurately the same. The error, referred to as a "false asymmetry", derives from the variation with angle of the differential cross-section. For example, if the angle of scattering to the left exceeds that for scattering to the right by an amount $2\Delta\theta$, then equations 2.4 must be replaced by

$$I(L) = (I_o(\theta) + I_o^1(\theta)\Delta\theta)(1 + P_1 P_2), \qquad 2.6$$
$$I(R) = (I_o(\theta) - I_o^1(\theta)\Delta\theta)(1 - P_1 P_2)$$

θ is the mean scattering angle and $I_o^1(\theta)$ is the derivative of $I_o(\theta)$ with respect to θ. Instead of equation 2.5, the following is obtained:

$$= \frac{I_o^1(\theta)\Delta\theta + I_o(\theta) P_1 P_2}{I_o(\theta) + I_o^1(\theta)\Delta\theta P_1 P_2} \qquad 2.7$$

$$= P_1 P_2 + \frac{I_o^1(\theta)}{I_o(\theta)} (1 - P_1^2 P_2^2)\Delta\theta \ ;$$

an asymmetry is observed even if the incident beam is unpolarised. For a polarised beam the variation of polarization with angle provides an additional false asymmetry. Effects of this kind may completely obscure

any genuine asymmetry; to avoid them, all alignment and measurement of angles must be done with great care.

False asymmetries may be reduced by mounting the counters upon a table which can be rotated through 180° about the axis of the incident beam. However, the beam must be aligned very carefully along the axis of rotation.

(b) The Use of Solenoids. Reference to Fig. 1 shows that the asymmetry measurement could be made without moving the telescope relative to the beam, if it were possible to rotate the polarization of the latter through 180° in the vertical plane. Such an experiment would be free from the false asymmetries discussed above. The necessary rotation of the polarization can be achieved by passing the beam along the axis of a solenoid. The magnetic moment of each nucleon experiences a couple which causes it to precess about the direction of the field. For nucleons of given energy the amount of rotation is determined by the length of the solenoid and the number of ampere-turns.

The use of a solenoid in a double scattering experiment was first described by Hillman et al.(R15). It is now becoming a standard technique for experiments with beams of polarized nucleons. For neutrons there are no difficulties, apart from those associated with the energy spread in the beam; other factors being equal the amount of precession is proportional to the time spent in the magnetic field. For protons there are, however, undesirable side-effects due to the electric charge carried by the particles. The

solenoid field invariably contains small radial components which will deflect the beam, while the main part of the field will focus a non-parallel beam. These effects have been described by Edwards and Rose (R16). They can be minimized by adjusting the position of the solenoid so that its axis coincides with that of the beam.

(c) Self-Monitoring Systems. In order to obtain reliable results from an asymmetry measurement, it is essential that the counts recorded for the two positions of the telescope, or for the two settings of the solenoid, shall correspond to equal integrated fluxes of particles into the target. A precise monitor of the beam intensity is required; if it is not available then the accuracy of the determination will suffer. However, if in conjunction with a solenoid two similar telescopes are used, set one on each side of the beam and at as nearly as possible the same angle, then the system is rendered self-monitoring (see Chapter V). In contrast to the case where two telescopes are used without a solenoid, the efficiencies of the telescopes do not appear in the expression for the asymmetry. The ratio of the efficiencies can however be obtained from the data and its constancy used to check that the apparatus is functioning properly.

3. The Proton-Proton Polarization Measurement.

In the measurements to which the greater part of this thesis is devoted, the polarization in proton-proton scattering was

obtained from the asymmetry in the scattering of a polarized proton beam by a liquid hydrogen target. The polarized proton beam from the Harwell 110-inch synchrocyclotron was used. The beam energy was reduced to the required value by the appropriate amounts of a suitable absorber. It was estimated that the loss of beam intensity by multiple Coulomb scattering in the absorber would not be excessive, while Wolfenstein (R17) has shown that there is no significant depolarization of the beam during the slowing-down process. The energy and energy spread of each determination were defined by an anti coincidence range method. The measured asymmetries were expected to be of the order 1 per cent or less; it was therefore extremely important to eliminate false asymmetries. Accordingly a solenoid was used, and a self-monitoring counter array. The current through the solenoid could be reversed, enabling both senses of the 180° rotation of the polarization to be achieved, and use of this facility further reduced the likelihood of systematic errors.

Chapter III

APPARATUS

1. Beam Handling and Hydrogen Target.

(a) General Description. The external polarized proton beam of the Harwell synchrocyclotron, of energy about 150 MeV, is obtained by scattering at approximately 8° in the horizontal plane from an internal carlon target, followed by extraction through a magnetic channel. The polarization is approximately 48 per cent, with spin-up predominating, and the mean intensity is of the order of 3×10^{6} protons per second.

The general arrangement of the apparatus is shown in Fig. 2. The emergent beam was collimated into an evacuated tube which passed in turn through the solenoid, two small steering magnets, a pair of quadrupole focussing magnets and finally through the concrete shielding wall into the experimental area. Emerging into air, the beam traversed an air-filled ionization chamber beam monitor and was then collimated on to a one-inch-thick liquid hydrogen target. The energy degrader was inserted between the monitor and the second collimator.

(b) Beam Optics. The "Solenoid" used in this experiment did in fact comprise two similar solenoids connected in series. This was

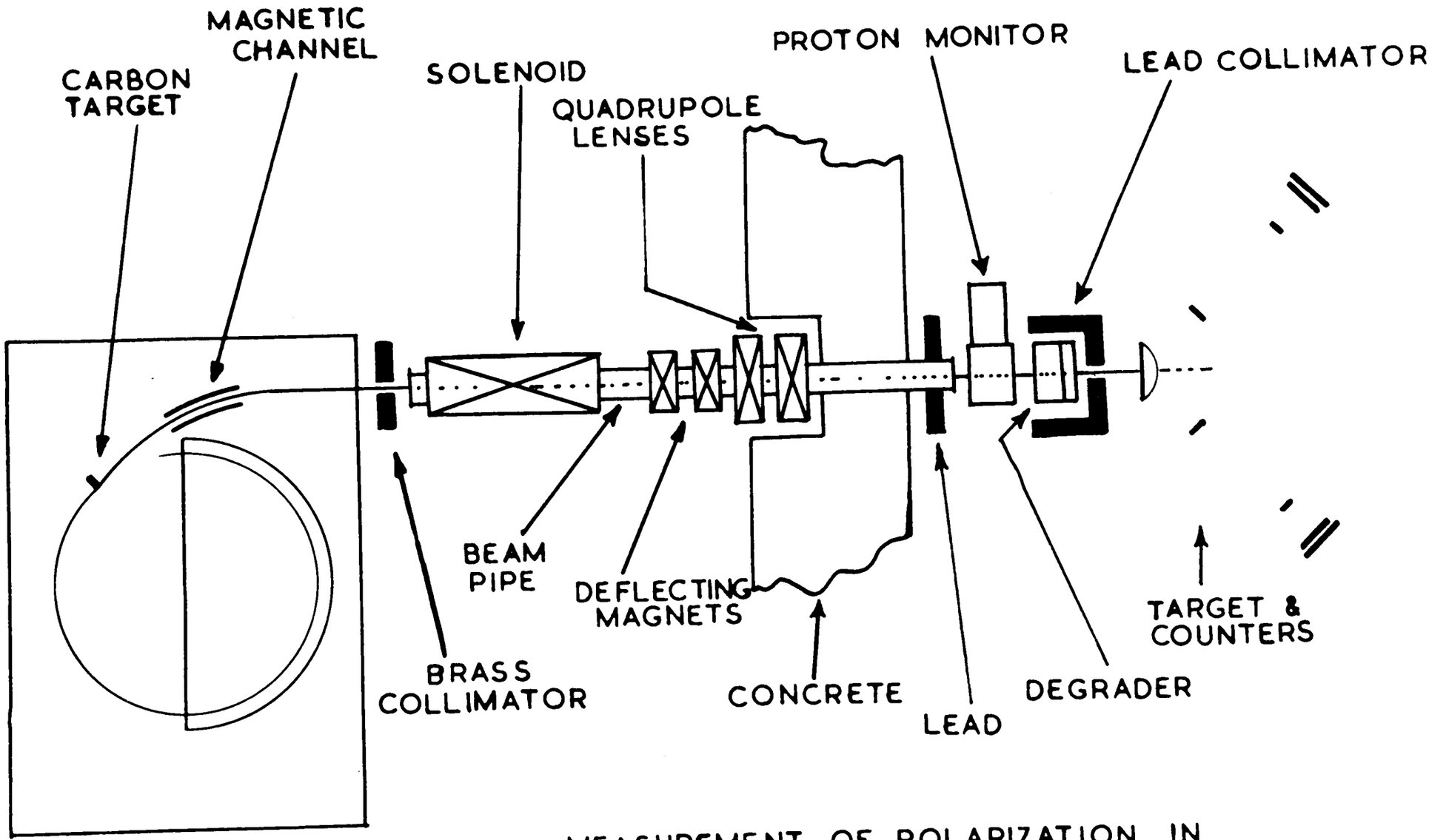

MEASUREMENT OF POLARIZATION IN PROTON–PROTON SCATTERING.
NOT TO SCALE.

FIG 2

necessary in order to obtain sufficient ampere-turns from the available generator. Each solenoid had a single-layer winding built up from overlapping segments of copper plate, separated by a suitable insulator except at the points where they were joined to their neighbours. Water-cooling was used to maintain the temperature at a reasonable level. The displacements of the beam associated with changes in the solenoid current were made smaller by suitable transverse movements of the solenoids, aimed at bringing their axes into coincidence with that of the beam, and were finally reduced to an acceptable level by appropriate adjustments of the steering magnet currents. Estimates of the false asymmetries resulting from the residual movements, together with the appropriate formulae, are given in chapter IV for p-carbon scattering, and in chapter V for p-p scattering.

The steering magnets were used in the way described above and also for positioning the beam relative to the target. At the position of the latter, horizontal and vertical movements of the beam of about 1 ccm. could be produced. The focusing magnets were standard equipment.

(c) Energy Degrader. The choice of degrader was governed by the need to minimise the transverse spread of the beam due to multiple scattering. The latter causes a loss of intensity and an increased background, due to subsequent scattering mostly from the target structure. It was expected that these effects could be minimized by using a substance of rather low atomic number, placed as close

to the target as the geometry would allow. Estimates of the multiple scattering for several light materials indicated that polyethylene was very suitable and this substance was used at all energies. Curves showing the relative multiple scattering for various substances and a table of the multiple scattering for various amounts of polyethylene will be found in Appendix III, together with a summary of the related calculations.

(d) Hydrogen Target. The liquid hydrogen target comprised a cylindrical brass reservoir to the bottom of which a thin-walled scattering chamber was attached, surrounded by a thermal shield which could be cooled by the evaporated hydrogen gas. This system was located in a containing vessel of brass inside which an adequate vacuum was maintained by a 2-inch oil diffusion pump. The reservoir and shield were silver-plated to reduce the influx of heat by radiation. The boil-off rate was about 80 c.c. of liquid hydrogen per hour and refilling was necessary every five or six hours.

To allow the passage of the incident beam and of particles scattered out horizontally at angles up to about 60°, the outer vessel was provided with windows of .004 inch Mellinex; the corresponding parts of the radiation shield were made of .00025 inch aluminium foil. The complete target assembly was located accurately on the scattering table by three set-screws. Two different scattering chambers were used during the experiment, one of which is shown in Fig. 3. Both were about 1 inch thick

FIG.3 SCATTERING CHAMBER FOR LIQUID HYDROGEN TARGET

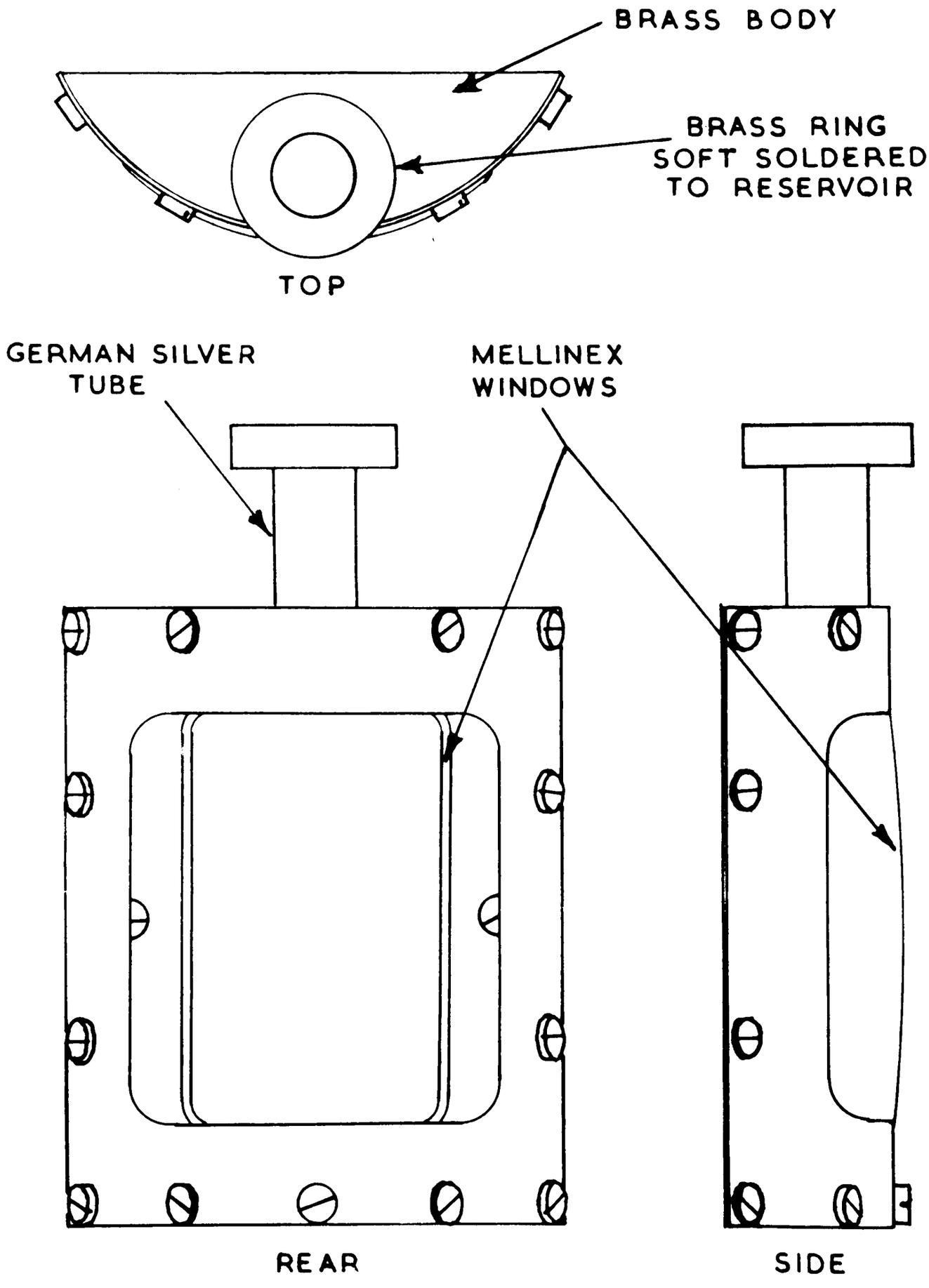

DRAWN ABOUT FULL SIZE

with brass bodies and windows of .002 inch Mellinex. The windows were attached with Araldite adhesive; cold-setting Araldite was used, but baking was needed to obtain a seal which would remain satisfactory at low temperatures. The shape of the chambers, Fig. 3. was chosen to minimize both the energy spread due to the hydrogen and unwanted scattering from the body work.

2. Detection System.

(a) General Description. Protons scattered to the left and to the right in the horizontal plane were detected by similar telescope systems, each of the four counters employing thin scintillation crystals. As already mentioned, the use of two telescopes rendered the system self-monitoring, so that a very precise beam monitor was not required. The monitor used was accurate to a few per cent, which was adequate for applying background corrections; otherwise it served merely as a reference for normalizing the data. Particles which stopped between the last two counters in each telescope were detected as anticoincidences between the back counter and the remaining counters in coincidence. Transistorized coincidence units were used. For each hydrogen measurement the appropriate telescope absorbers were inserted in front of the third counters and the amount of polyethrylene was adjusted to optimize the anti-coincidence counting rates. The energy and energy spread were calculated from the known amount of absorber present, integrating over the effective volume of the

target and allowing for finite penetration into the back crystals. The calculations are described in section 4 of the next chapter.

(b) Counter Telescopes. Each counter comprised a thin rectangular crystal of Nuclear Enterprises NE102 plastic scintillator, attached with Tensol cement to a polished perspex block which was in turn cemented to the perspex disc which formed the top of the photomultiplier can. An E.M.I. type 6097B photomultiplier tube was held in contact with the underside of this disc by springs. Each crystal was covered by a cap of aluminium foil of thickness about .001 inch, coated in its inner surface with magnesium oxide to improve the light collection.

The counters were mounted, as shown in Fig. 4, on an aluminium alloy "sleeve" and the crystals mounted and aligned with the aid of a theodolite. This complete unit could then be mounted on an arm of the scattering table and lined up with the centre of the target. Two different scattering tables were employed during the experiment; both comprised a massive rectangular iron base, upon which was mounted a vertical pillar carrying horizontal arms to which the telescopes could be attached. The mountings for the latter differed in detail, but in both cases the sleeve carrying the counters could be rotated through a few degrees about the axis of the front counter; this rotation was controlled by screws at the rear, as shown in Fig. 4; it sufficed for horizontal alignment. Any vertical adjustments were made by packing metal foil between the sleeve and the arm upon which

FIG.4 COUNTER TELESCOPE & MOUNTING
DRAWN ABOUT ONE THIRD
FULL SIZE

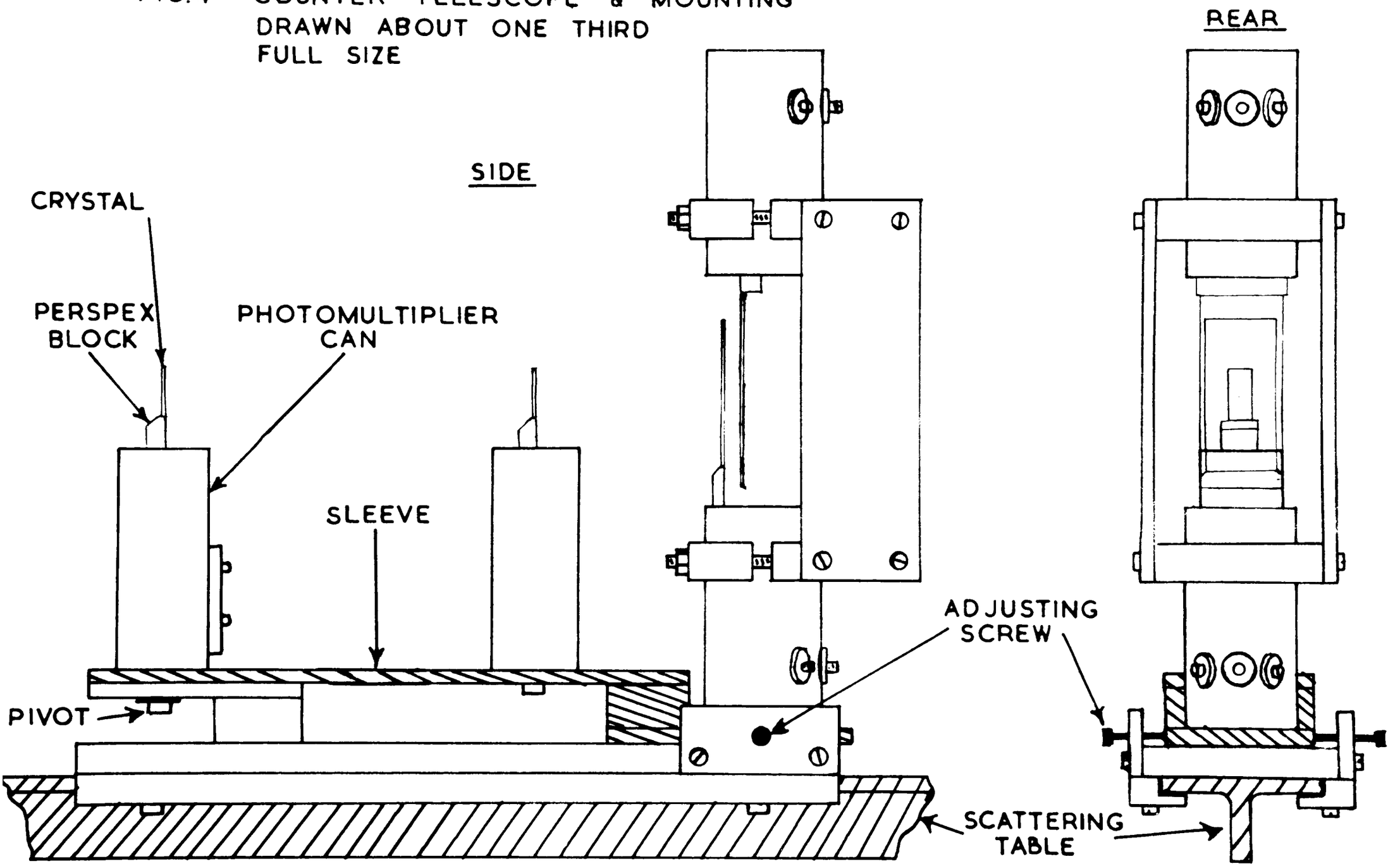

it was mounted.

The procedure for mounting the telescopes was the following: The scattering table was levelled and adjusted to be at the correct height above the floor; it was known that the centre of gravity of the beam was about 50.5 inches above the floor. The theodolite was then set up by trial and error to define a horizontal line through the axis of the scattering table, and at the height above it corresponding to the centre of the scattering chamber. The adjustments described above were then made for each telescope until the centres of the front pair of crystals were located on the reference line defined by the theodolite. The uncertainty in the alignment of the telescopes with the target was estimated to be a few minutes arc. The scattering planes for the two telescopes remained constant and equal to within a small part of a degree. Any counter could be removed and put back without upsetting the alignment; during one run this was necessary, in order to replace a photo tube which had ceased to function.

(c) Geometry. The sizes and separations of the crystals underwent some modification during the experiment, but the main features remained as shown in Fig. 5. In every case the second crystals were 1.8 cm. wide by 3.6 cm. high and were set at 55 cm. from the centre of the target, to define a solid angle of .002 steradian, corresponding to a counting rate of a few anti-coincidences per second from liquid hydrogen. The front crystals

FIG 5 EXPERIMENTAL GEOMETRY

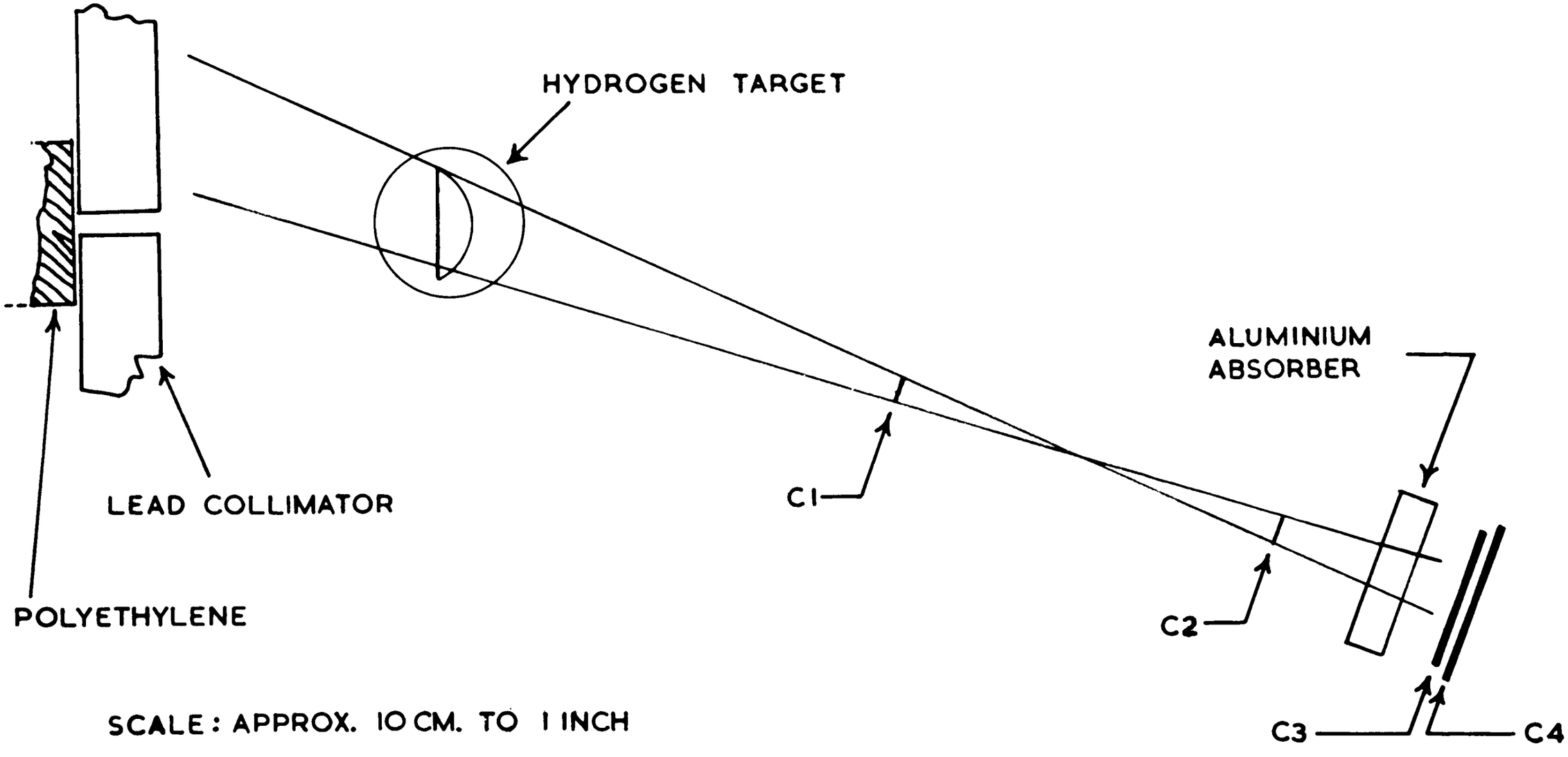

were the same size or slightly wider and were used to reduce the background, in particular to ensure that the telescopes, when set at the smallest angle at which measurements were to be made could not detect coincidences from particles scattered directly out of the polyettrylene.

The rear crystals were required to be quite large, in order to avoid undue loss of counts by scattering from the aluminium absorbers used to define the energy. It was essential to avoid any appreciable loss of this kind between the last two counters, because particles scattered in this manner would be recorded as anticoincidences. The third crystals were in every case 4.5 cm. wide by 9.0 cm. high, and the fourth ones 5.5 cm. by 11.0 cm. The separation of these crystals was about 1 cm.

(d) Electronics. The counters were provided with individual E.H.T. supplies, normally operated between 2.0KV and 2.5KV. They gave negative output pulses of amplitude 3V from protons of energy about 100 MeV. Pulses from each counter were fed, through a 50-yard length of 100-ohms impedence coaxial cable and a delay box, into the appropriate input of one or the other of two identical transistorized coincidence units, one for each telescope, of the type designed by Cándy and Chaplin (R18). The circuit of the coincidence unit is shown in Fig.6. Switching facilities were provided on the four inputs so that these could be studied singly or in any desired combination. The resolving time was about 15 ns. for coincidences and 20 ns. for anticoincidences.

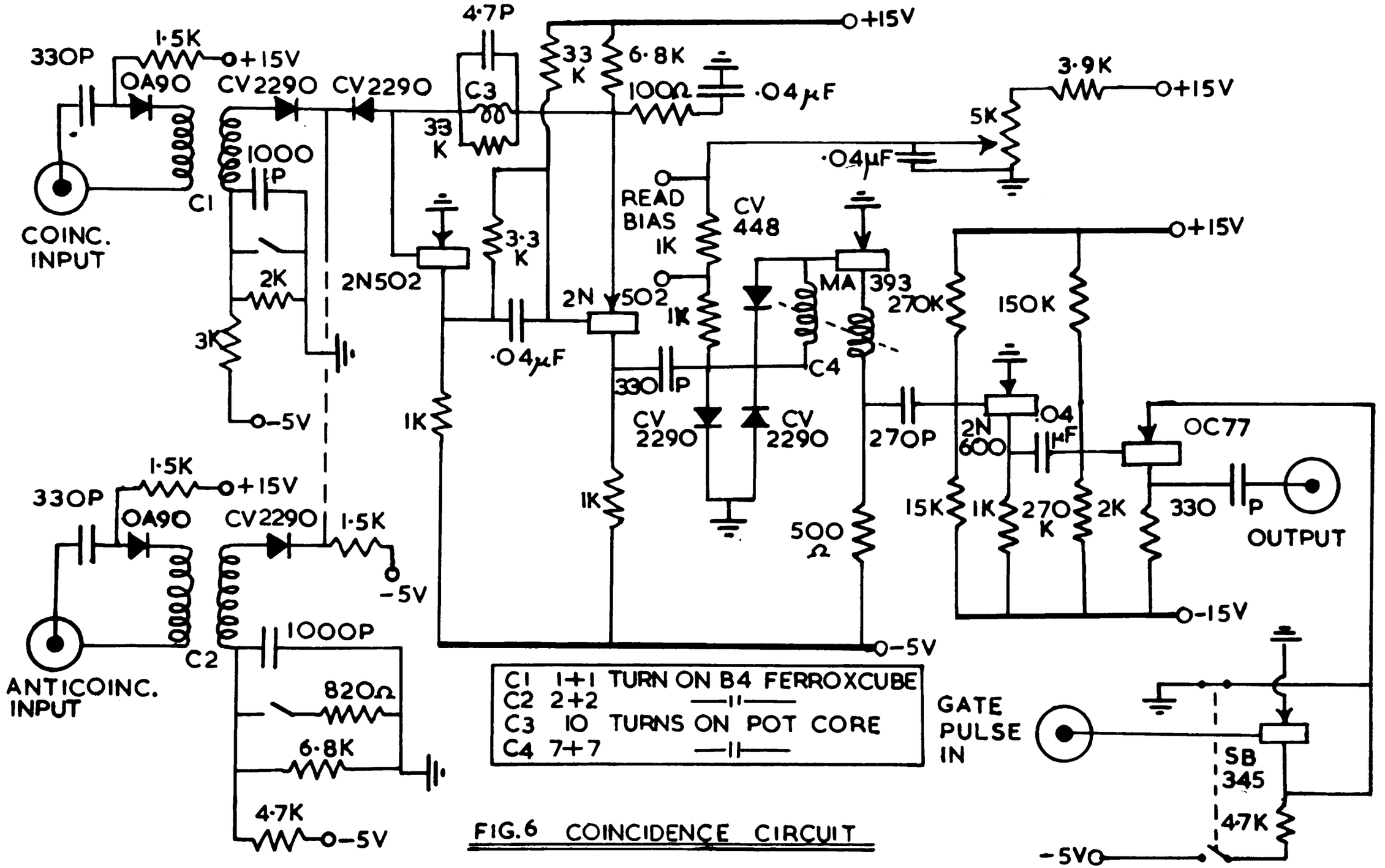

FIG.6 COINCIDENCE CIRCUIT

(1ns. = 10^{-9} sec.) The output from each unit comprised a positive pulse of amplitude 15V. with a measured dead-time of less than 2 μ sec. Facilities were provided for gating the outputs with pulses derived from the cyclotron frequency modulation; these were intended to provide discrimination against low energy particles in the beam and hence a reduction in the background. In the event, however, the background was small enough for gating to be unnecessary.

The outputs from the coincidence units were counted on type 1009 scalers. On later runs a timing unit was added, enabling the scalers to be stopped after a predetermined number of clicks of a mechanical register driven by the beam monitor.

3. Running-Time and Modifications of Apparatus.

There were in all five runs on the machine, each of length about 1 week. As a rule several different energies were considered on each. However, the second run was devoted almost entirely to measurements at 50 MeV and the fourth to 40 MeV. The 30 MeV data were taken on the third and fifth runs.

The runs fell naturally into two groups; the first two were early in 1960 and the last three in the winter of 1960-61. Several modifications inthe apparatus were made in the intervening period; these were the following:

(1) An additional collimator, in front of the monitor and not shown in Fig.2, was dispensed with because it appeared to serve no useful purpose (but see section 1b of chapter V).

(2) The original scattering chamber was replaced by the one shown in Fig.3. The latter was more symmetrical and offered less unwanted obstruction both to the incident beam and to scattered particles.

(3) The scintillation counters on the front pair of counters in each telescope were reduced in thickness from 0.05 inch to 0.02 inch, so that measurements might be extended to lower energies. The rear crystals were reduced in thickness from 0.10 inch to 0.05 inch to reduce the energy spread; there was little point in using thinner scintillators on these counters because at 40 MeV, where most of the later measurements were made, about half the energy spread derived from the hydrogen target. The thickness of the scattering chamber was not reduced below 1 inch because the resulting drop in counting rate would have been intolerable.

(4) New photomultipliers were provided for all counters.

(5) The collection of data was facilitated by the introduction of a timing unit, as mentioned above, to control the scalers.

Chapter IV

Experimental Measurements

1. Adjustment of Apparatus.

(a) General Remarks. This section describes the general procedure for setting up the experiment in readiness for the accumulation of hydrogen data. Some of the operations involved, such as the focussing of the beam, did not require repetition within a given group of runs once they had been performed at the beginning. It was usually possible to mount and align the counters on the scattering table, as described in the last chapter, prior to the run itself; it will be assumed in what follows that this was the case.

(b) Setting Up the Beam. The fixed section of beam pipe which passed through the focusing magnets and the shielding wall was in most cases taken as the reference in positioning the scattering table and the beam monitor. The positioning was done by eye, using cross-wires fastened at each end of the pipe. This rather arbitrary procedure was justified, in the event, by the fact that once the monitor had been set up in this way it rarely had to be moved; any misalignments of the beam which remained after it had been focused were small enough to be corrected with the steering

magnets.

Next, the collimation and focusing were adjusted to give a beam of the required size and shape near the target. The first collimator, close to the cyclotron, was adjusted to a width of 1 inch, known to be sufficient to accept the greater part of the beam, and was then moved horizontally across the beam until the monitor reading was a maximum. In later runs this movement could be performed by remote control from the counting room.

The beam profile was studied with X-ray films. Ilford "Industrial B" films were used; they were exposed to the beam and then developed and fixed in the normal manner. The beam profile appeared as a dark spot on the negative. With the largest available intensity an irradiation of 15 sec. gave a good image. The density of the latter was sufficiently reproducible to allow detailed comparison among a group of exposures; for this purpose measurements were made with a ruler, the negative being held against a white background.

A series of films were taken for various focusing magnet currents, in order to obtain a beam cross-section of the required shape and with the minimum area at a point corresponding to the centre of the degrader. The latter requirement served to reduce the spread of the beam at the target. When a reasonably good beam had been obtained, final adjustments of the width and position of the first collimator were made if necessary to sharpen the outline of the "spot". In a typical instance the resulting image was

about 2.0 cm. high by 0.8 cm. wide at the centre of the target, corresponding to 1.8 cm. by 0.5 cm. at the position of the centre of the degrader. The steering magnets were adjusted to bring this spot into approximate coincidence with a fixed steel marker pin whose point corresponded in position to the centre of the scattering chamber. The pin showed clearly on films exposed behind it.

Next, the solenoids were set up. It was known that a current of about 910 amperes was needed to produce a 180° rotation of the polarization of 150 MeV protons; the movement of the beam caused by the normal and reverse directions of this current were studied, again with X-ray films. For this and subsequent measurements the films were placed near the centre of the scattering table, about 1 cm. behind the marker pin. Some reduction of the spot movement was obtained by transverse movements of the solenoids; by means of the previously calibrated steering magnets the remainder was reduced to less than 0.05 cm. Vertical movements of this order produced entirely negligible false asymmetries, while similar horizontal movements could be tolerated. The latter produced an estimated false asymmetry in p-p scattering of only 0.04 per cent, or about 0.1 of the smallest statistical uncertainty in the results.

Finally, the beam was centred accurately on the marker pin and the second collimator set up. Several different collimators were used during the experiment. On the last three runs, for

example, a 2-inch thick lead block was employed, with a rectangular hole 1.1 inches high by 0.6 inch wide; it was placed about 9 inches in front of the centre of the target.

A check on the above procedure was provided, with the hydrogen target in position, by a shadow photograph taken with a film placed behind the target.

(c) Adjustment of Counter Voltages and Delays. For this purpose the telescopes were set at about 20° to the beam to detect particles scattered from an aluminium or carbon target.

First, curves of counting rate versus counter E.H.T. were plotted and each counter set at a point well above the lower end of its voltage plateau. The relative delays for the counters in each telescope were then established. The procedure was to run a delay curve for the front pair of counters to determine their correct relative delay, and similarly for this pair of counters versus the third counter. Having thus obtained the correct delays for counting coincidences between the first three counters, the correct relative delay was established, in the same way, for counting anticoincidences between the fourth counter and the first three in coincidence. Finally, the E.H.T. values were adjusted, if necessary, until there was no significant change in either the triple coincidence or the anticoincidence counting rates when all the voltages were changed by $\pm$ 50V.

The delays were set up with absorbers present both in the telescopes and in front of the second collimator to simulate

running conditions, namely the detection of particles scattered at reduced energy. The relative delays were energy-dependent and needed to be checked at each new energy and/or scattering angle. The variation with angle arose from the $\cos^2\theta$ dependence of the energy of a particle, in this case a proton, scattered through an angle θ in the laboratory from a stationary particle of equal mass. The energy dependence of the delays derived from two effects, both of which acted in the same sense. Firstly, a slower particle took longer to traverse the distance between the counters. Secondly, the pulse from a slow particle was recorded before that from a fast one, owing to the greater amplitude of the former pulse for the same rise time and the finite threshold of the detecting circuit, here about 0.25V. In a typical instance it was necessary to increase the delays of the front counters by 2ns. in going from 50 MeV to 30 MeV.

(d) Zero Angles for the Telescopes. The zero angle for each telescope was determined by measuring the triple-coincidence counting rate as a function of angle, using the direct beam at reduced intensity. Because the ionization chamber was unreliable at low intensities, time-monitoring was employed. The angles were established to within $\pm 0.25^{\circ}$, which was adequate, remembering that false asymmetries from this source were eliminated by the use of solenoids.

2. Measurement of Beam Energy.

The energy of the beam was obtained from range measurements using calibrated aluminium absorbers. The telescopes were set up to detect particles scattered at 10° or 20° from an aluminium or carbon target, and range curves taken for both simultaneously, by recording triple coincidences between the first three counters in each telescope for varying amounts of absorber between the second and third counters. Measured values of the mean energy and energy spread are given in Table I for each of the two groups of runs.

TABLE I. ENERGY OF POLARIZED PROTON BEAM.

Run	Target	Scattering Angle degrees.	Mean Energy MeV	Energy Spread MeV
1	0.3 c.m. Aluminium	10	144	14
3	1.37 c.m. Carbon	20	145	13

The data refer to the beam emerging from the monitor. The energy spread is the full width at half-height, estimated from the range curve on the assumption that the beam spectrum was Gaussian in form, and corrected for the spread induced by the finite thickness of the third crystal; a correction for range straggling has also been applied, using the calculated results of Sternheimer (R19). Both corrections were small, amounting to a few per cent of the observed spread. For the proton-proton polarization measurements only qualitative information about the energy of the beam was needed, since the energy and energy spread of the scattered particles were defined by the telescope absorbers (see Section 4.e. below).

A reasonably precise value of the beam energy was however required in connection with the measurement of the polarisation of the beam, described below.

3. Measurement of Beam Polarization.

(a) Asymmetry in Proton-Carbon Scattering. For the calculation of p-p polarizations from the measured asymmetries in p-p scattering it was necessary to know the polarization of the beam. The latter, and also the calibration of the solenoids, was infered from measurements of the asymmetry in scattering from carbon for various values of the solenoid current. The "calibration" of the solenoids refers to the current through them required to produce a given rotation of the beam polarization. For setting up the beam, as mentioned above, a current of 910 amperes had been assumed to correspond to a rotation of 180°; it was however, desirable to check this figure experimentally before proceeding further. The proton-carbon scattering measurements and their interpretation will be discussed in some detail; they were important not only for the information, mentioned above, which they provided, but also because they illustrated quantitatively several of the systematic errors to which such measurements are liable.

The measurements were made with a carbon target of thickness 1.37 cm. for which the mean energy of scattering was 139 MeV with a spread of about 13 MeV (see Table I). The telescopes were set at a fixed angle, actually 20° or 15°, to the beam and triple

coincidences between the first three counters in each were recorded for various values of the normal and reverse solenoid currents between zero and 1000 amperes. At both angles about 12 gm/cm^2 of aluminium were placed in each telescope to avoid the detection of low energy particles. All counts were normalized to 1 "click" of the monitor register. The background was measured by removing the carbon and increasing the telescope absorbers by an equivalent amount; it was never more than 2 per cent of the real counting rate, hence a mean background was subtracted from all the data at each of the two angles. At 20° all the normal and all the reverse data were taken at fixed settings of the steering magnets. There was therefore in each case significant horizontal movement of the beam as the current was varied, and this had to be considered when analysing the data. In the 15° measurements the appropriate adjustments of the steering magnets were made to keep the beam stationary relative to the target.

(b) Analysis of the Data. The following effects were taken into account:

(1) A difference between the scattering angles for the two telescopes. The angular dependence of the differential cross-section and polarization at the second scattering led to false asymmetries if the angles were different. The difference in scattering angle comprised in general a term, independent of the solenoid current, due to errors in setting up the telescopes, together with a term arising from beam movement associated with

changes in the solenoid current.

(2) Variations of the normal& reverse beam intensities with the magnitude of the solenoid current.

(3) A difference in the efficiencies of the telescopes.

(4) A difference in the azimuthal angle between the first and second scattering planes.

For a given normal solenoid current i the recorded counts per click for the left and right telescopes were respectively, from equation 2.1,

$$N(iA) = N_{(i)} M_{(i)} I_{(iA)} e_A \left[1 + P_1 P_2 (iA) \cos (\phi + \beta) \right]$$
$$N(iB) = N_{(i)} M_{(i)} I_{(iB)} e_B \left[1 - P_1 P_2 (iB) \cos (\phi + \beta) \right] \qquad 4.1$$

A and B denote the left-and right-hand telescopes respectively,

$N_{(i)}$ = No. of protons incident per second upon the target,

$M_{(i)}$ = No. of seconds/click of the monitor register,

e = telescope efficiency,

I = differential cross-section for p-carbon scattering,

P_1 = polarisation of beam,

P_2 = polarization in p-carbon scattering,

$\phi = ki$ = rotation of polarization due to current i, k being the solenoid calibration,

β = difference in azimuth between the incident polarization P_1 for zero solenoid current and the normal to the second scattering plane, with its sign defined by equations 4.1.

All numerical constants in the above equations have been put

equal to unity.

I and P_2 depend upon the solenoid current through the beam movement accompanying changes in the latter; horizontal movements of the beam are equivalent to changes in scattering angle, hence to changes in the effective cross-section and polarization.

The total difference $\Delta\theta$ between the scattering angles for the telescopes will be defined as follows:

$$2\,\Delta\theta = \theta_A - \theta_B \quad . \qquad 4.2$$

The quantity of greatest interest was the ratio

$$\epsilon_i = N(iA) \,/\, N(iB) \quad . \qquad 4.3$$

Noting that the contributions from (1), (2) and (4), above, were expected to be small compared to unity, the following is obtained:

$$\epsilon_i = \left(\frac{1+\Sigma\cos\phi}{1-\Sigma\cos\phi}\right)\left[\frac{e_A}{e_B}\right]\left[1-\frac{2\Sigma\beta\sin\phi}{1-\Sigma^2\cos^2\phi}\right]$$

$$\times\left[1+2\left(\frac{1}{I}\frac{dI}{d\theta}-\frac{\Sigma^2\cos^2\phi}{1-\Sigma^2\cos^2\phi}\,\frac{1}{P_2}\,\frac{dP_2}{d\theta}\right)\Delta\theta_i\right]. \qquad 4.4$$

P_2 and I now refer to the mean scattering angle, and $\Sigma = P_1P_2$. A similar expression can be written for the reverse direction of i, remembering to change the sign of β. Where appropriate the reverse direction of the current will be denoted by a prime.

From ϵ_i and ϵ_i^1 two quantities were calculated; these were

$$R = r_i / r_i^1 = \left[1 - \frac{4 \sum \beta \sin\phi}{1 - \sum^2 \cos^2\phi}\right]$$

$$\times \left[1 + 2\left(\frac{1}{I}\frac{dI}{d\theta} - \frac{\sum^2 \cos^2\phi}{1 - \sum^2 \cos^2\phi}\ \frac{1}{P_2}\frac{dP_2}{d\theta}\right)(\Delta\theta_i - \Delta\theta_i')\right]. \quad 4.5$$

and $$r^2 = r_i\, r_i^1 = \left(\frac{1 + \sum \cos\phi}{1 - \sum \cos\phi}\right)^2 \left[\frac{eA}{eB}\right]^2$$

$$\times \left[1 + 2\left(\frac{1}{I}\frac{dI}{d\theta} - \frac{\sum^2 \cos^2\phi}{1 - \sum^2 \cos^2\phi}\ \frac{1}{P_2}\frac{dP_2}{d\theta}\right)(\Delta\theta_i + \Delta\theta_i^1)\right]. \quad 4.6$$

The terms in square brackets derive from effects (1) to (4) above. It will be noted that neither R nor r^2 contain the quantities N and M. The data could be combined differently to provide information about the latter; the results indicated that the intensity of the beam at the target varied somewhat with solenoid setting. ~~This point will be mentioned with solenoid setting.~~ This point will be mentioned again during the analysis of the hydrogen data.

(c) Scattering at 20°. The coefficients of β, $\Delta\theta_i$ and $\Delta\theta_i^1$ in the above equations could be evaluated with sufficient accuracy from published cross-section and polarization data, and using the estimated value of 180/910 degrees per ampere for the solenoid calibration. The following were obtained for scattering at 20°.

$$\frac{1}{I}\frac{dI}{d\theta} = -0.275 \text{ per degree (lab.)},$$

$$\frac{1}{P_2}\frac{dP_2}{d\theta} = 0.048 \text{ per degree (lab.)}$$

$$\sum = 0.44 \text{ approximately.}$$

It was concluded that the contribution of the polarization to the

false asymmetry could be neglected in comparison with that of the cross-section, also that the term $\sin\phi(1 - \sum^2 \cos^2\phi)^{-1}$ could be taken equal to $\sin\phi$. Hence, to a good approximation,

$$R = \left[1 - 0.0307\beta \sin(0.198i)\right]\left[1 - 0.55\left(\Delta\theta_i - \Delta\theta_i'\right)\right], \quad 4.7$$

$$r^2 = \left(\frac{1 + \sum \cos ki}{1 + \sum \cos kI}\right)^2 \left[\frac{eA}{eB}\right]^2 \left[1 - 0.55\left(\Delta\theta_i + \Delta\theta_i'\right)\right], \quad 4.8$$

where β, $\Delta\theta_i$ and $\Delta\theta_{i2}'$ are in degrees.

Since the steering magnet currents were fixed for the normal and reverse measurements, the variation of the solenoid current i produced horizontal movements of the beam y (i), y^1(i); these were proportional to the current. The relation between the displacement y and the corresponding change in scattering angle is the following:

$$\Delta\theta = -\left[180\, y \cos\theta / \pi\, L\right] \text{degrees} \quad 4.9$$

where θ is the mean scattering angle and L the distance from the target to the defining counter. The minus sign follows from the definition of $\Delta\theta$, equation 4.2, together with the convention adopted in this work that y is positive for a movement of the beam to the left as seen when looking along the incident beam towards the target. At 20° the largest movement which occurred was about 0.25 cm., which corresponded to a change of very nearly 0.25° in scattering angle.

It was convenient to write the changes in angle as follows:

$$\Delta\theta_i = a + b + c\,i\,,$$
$$\Delta\theta_i' = a + b^1 + c^1\,i\,, \quad 4.10$$

where a, b and c are constants. a represents the error in aligning the

telescopes, estimated to be of order 0.25° (see section 1.d of Chapter III). b and b^1 differed from zero because the fixed steering magnet currents were not those appropriate to zero solenoid current, for which the telescopes had been set up. The difference between b and b^1 was due to the changes in the width of the beam which occurred between the normal and reverse directions of the solenoid current. The quantity R does not involve a ; from equations 4.7 and 4.10 the observed values were

$$R = \left[1 - 0.0307\,\beta \sin (0.192i)\right] \times \left[1 - 0.55\,(b - b^1) - 0.55\,(c - c^1)\ i\right] ; \qquad 4.11$$

b, b^1, c and c^1 were evaluated from information obtained when setting up the beam. They gave the following for the second term in square brackets in equation 4.11. :

$$1.135 - 1.48 \times 10^{-4}\, i .$$

Corrected values of R were obtained which were expected to satisfy the equation.

$$R_{corr.} = \left[1 - 0.0307\,\beta \sin (0.192i)\right] \qquad 4.12.$$

The results are shown in Fig. 7. The indicated least squares fit gave $\beta = 1.1^{\circ} \pm 1.1^{\circ}$

In order to assess the significance of this result, the effects of solenoid - induced vertical movements of the beam must be considered. The latter are equivalent to changes $\Delta\phi$ in ϕ; they cause an additional term in r_i, equation 4.4, of the form

FIG. 7 ESTIMATION OF β FROM P-CARBON SCATTERING

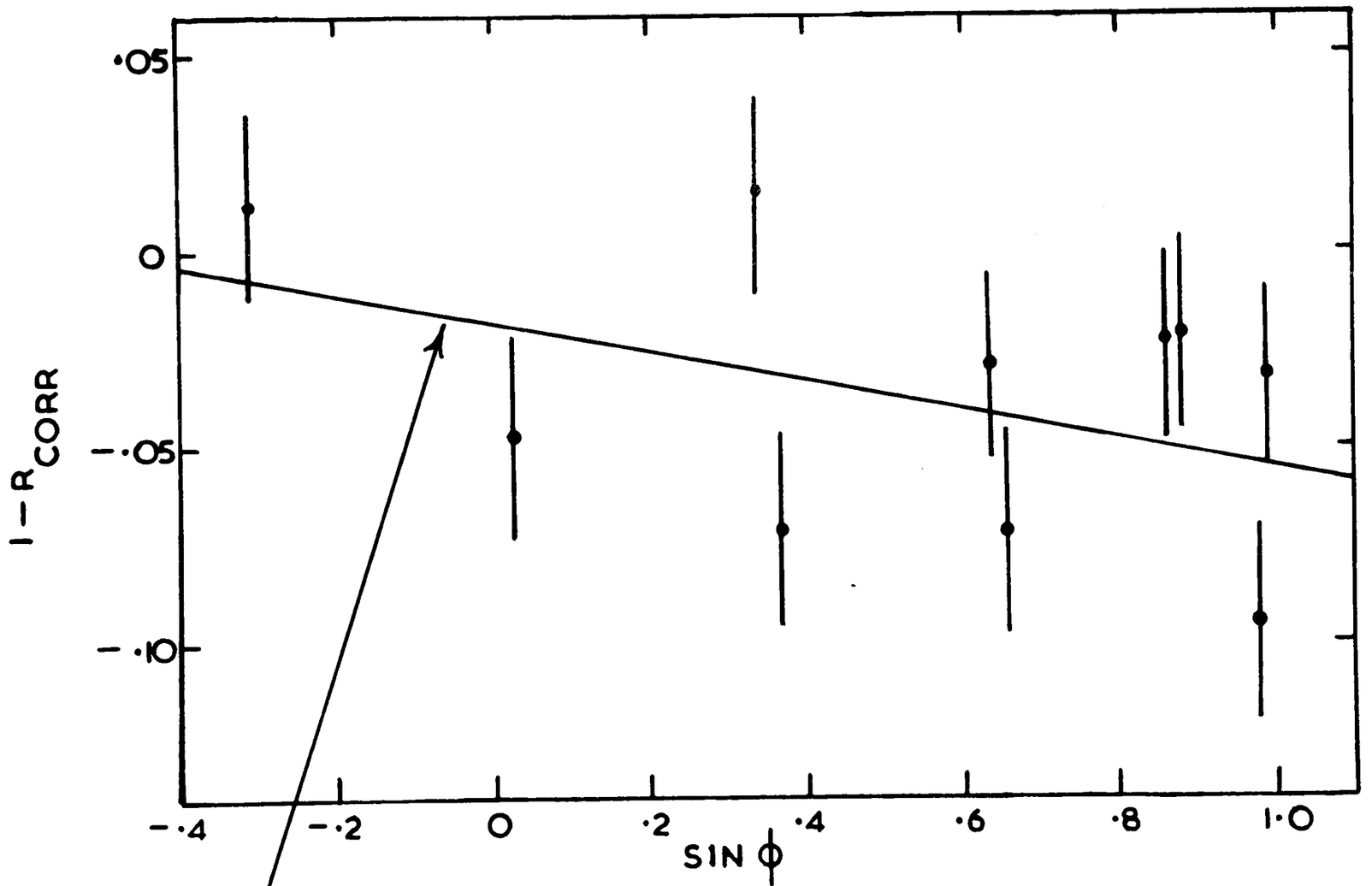

LEAST SQUARES FIT: $1-R_{CORR} = -(\cdot 018 \pm \cdot 023) - (\cdot 034 \pm \cdot 034) \sin\phi$

$$\left[1 - \frac{\Sigma^2 \sin 2\phi}{1 - \Sigma^2 \cos^2 \phi} \quad \Delta\phi_i \right] .$$

In the present case the estimated contribution to R was of the order of 0.1 per cent and was negligible in comparison with the statistical uncertainties. It was therefore, possible to conclude that $\beta = 0$ within the errors of measurement.

Using equations 4.10, equation 4.8 can be written

$$r^2 = \left(\frac{1 + \Sigma \cos ki}{1 - \Sigma \cos ki} \right)^2 \left[\frac{e_A}{e_B} \right]^2 \left[1 - 1.10a \right]$$
$$x \left[1 - 0.55 (b + b^1) - 0.55 (c + c^1) \quad i \right] . \qquad 4.13$$

The term $(e_A/e_B)^2$ $(1 - 1.10a)$ was now regarded as an adjustable parameter K^2 :

$$r_{obs}^2 = \left(\frac{1 + \Sigma \cos ki}{1 - \Sigma \cos ki} \right)^2 \quad K^2 \left[1 - 0.55 (b + b^1) - 0.55 (c + c^1) \; i \right] \qquad 4.14.$$

Proceeding as for R, the term in square brackets was evaluated, and values of r^2 obtained which were expected to satisfy the relation

$$r^2_{corr.} = K^2 \left(\frac{1 + \Sigma \cos ki}{1 - \Sigma \cos ki} \right)^2 \qquad 4.15.$$

Writing $s^2 = r^2_{corr.} / K^2$, it follows that

$$\Sigma \cos ki = (S-1) / (S + 1) . \qquad 4.16$$

Several values of K were taken and for each the calculated values of Σ cos ki were plotted against i. Fig. 8A is typical of the curves obtained. If the correct value of K were chosen, then the curve should be symmetrical, i.e.,

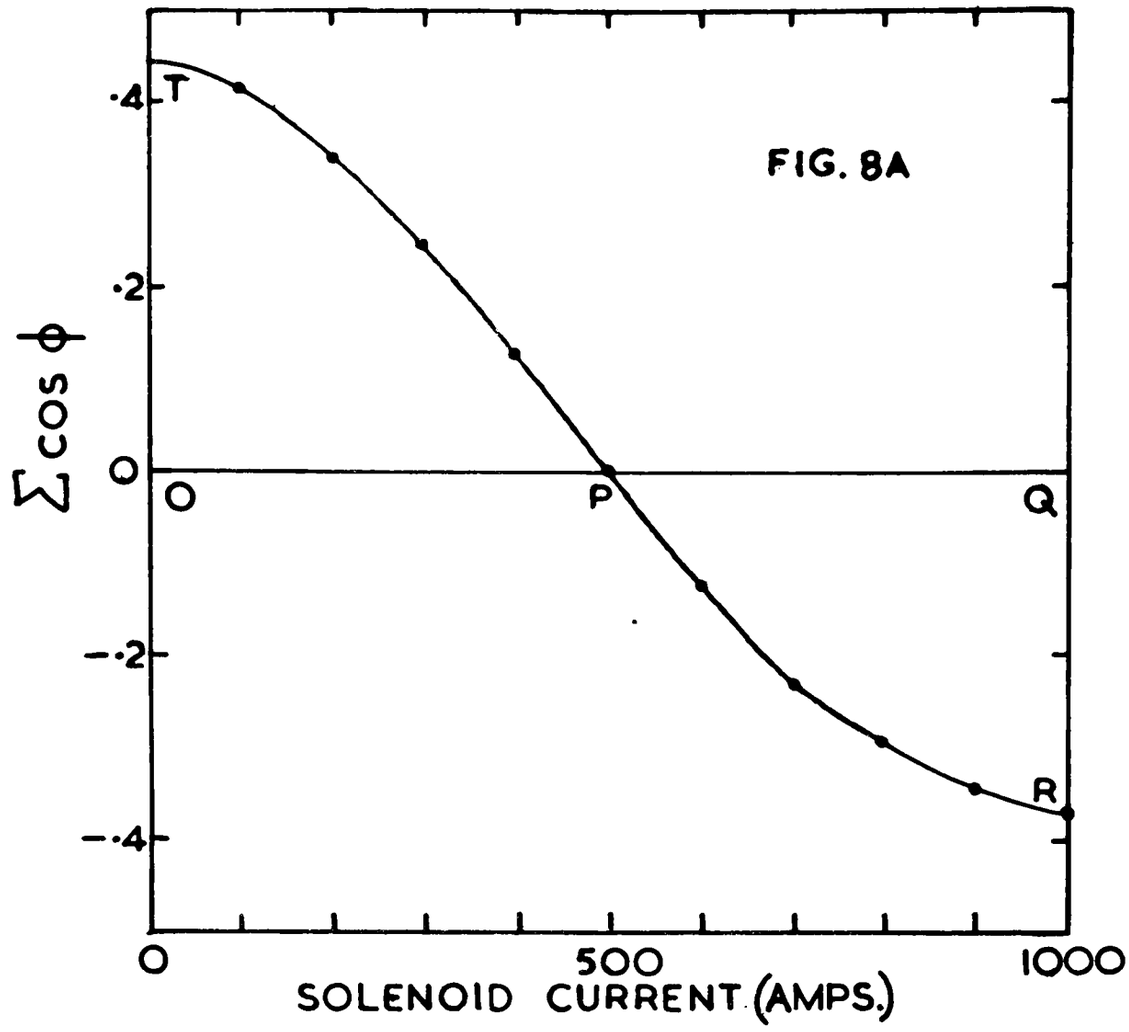

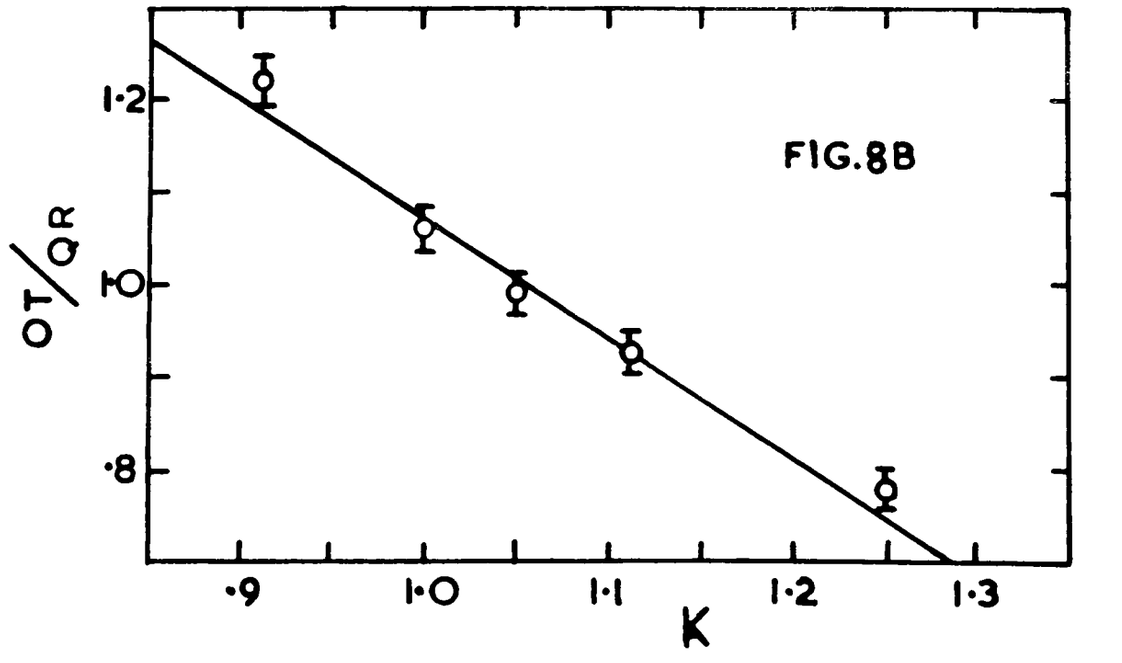

FIG. 8 ANALYSIS OF P-CARBON SCATTERING

$$\frac{OT}{QR} = 1 \qquad \text{where } PQ = OP$$

The solenoid calibration k can be obtained from the intercept OP. The correct value of K was estimated from a plot, shown in Fig. 8B, of OT/QR against K. The value obtained was 1.05 ± .01; the corresponding value of the calibration was 0.200 ± .002 degrees / ampere. Using these results, values of $\sum$ cos ki were obtained and plotted against cos ki as in Fig. 9. A least square fit gave $\sum = 0.396 \pm .008$. The error includes the statistical uncertainties of the data and also the error in fitting them. (formulae for the statistical error on the asymmetry will be found in the next chapter). The errors due to vertical movement of the beam were again negligible.

(d) Polarization of Beam from Asymmetry. In order to obtain the beam polarization from the measured asymmetry, it was necessary to know the polarization in p- carbon scattering, in this case at 20°, 139 MeV. The latter was obtained by interpolation between published data at 135 MeV (R20) and 155 MeV (R21). At 20°, and at 15°, there is a significant contribution to the polarization from inelastic scattering involving the 4.43 MeV excited state in carbon 12. Contributions from the higher excited states are small, at least in comparison with the uncertainties in the present work, and have been neglected. Since the polarized beam is produced by scattering from carbon at 8°, where inelastic effects are negligible, the first scattering can be assumed to be purely elastic. The observed asymmetry could thus be written

$$\varepsilon_{obs} = P_1 P_2 \varepsilon_{el} \frac{1 + \nu\delta}{1 + \nu} , \qquad 4.17$$

where ν is the ratio of the 4.43 MeV inelastic differential cross-section to the elastic cross-section, and δ is the ratio of the inelastic to the elastic polarization. ν and δ were evaluated from the 135 MeV. data.

The final value obtained in this way for the beam polarization, from the 20^0 data, was

$$P_1 = 0.457 \pm 0.34.$$

The error contains 2 per cent from estimating B_2, 3.5 per cent from estimating the inelastic contribution and 2 per cent from the measured asymmetry.

(e) Scattering at 15^0. The procedure was similar to that just described, except that no corrections for movement of the beam were necessary. However, several of the observed values of R differed significantly from unity, in a manner that could not be explained by a non-zero value for β. For this reason the statistical errors of this measurement were all doubled.

The following results were obtained:

$$K = 1.00 \pm .01 ,$$

$$k = 0.194 \pm .004 \text{ degrees / ampere},$$

$$\Sigma = 0.318 \pm .010,$$

and $$P_1 = 0.492 \pm .031$$

(f) Conclusions. When the results at 20^0 and 15^0 were combined, the following mean values were obtained :

(1) Solenoid Calibration,

$$k = 0.199 \pm .002 \text{ degrees/ampere.} \qquad 4.18.$$

(2) Beam Polarization,

$$P_1 = + 47.6 \pm 2.3 \text{ per cent.} \qquad 4.19.$$

The sign of the polarisation was determined by Brinkworth and Rose (R22) from a double scattering measurement using a helium analyser at low energies.

All hydrogen measurements were made with k = 0.198 degrees/ampere, which is to all intents identical with the above value.

The value of the polarization obtained here is in agreement with a previous determination (R23), which gave 46 ± 1 per cent. The value 48 per cent was used when analysing the hydrogen data.

It appears that adequate account has been taken of the various false asymmetries in the p-carbon scattering experiments. This is important because similar effects had to be considered for p-p scattering, where the genuine asymmetries were much smaller. Concerning the effects themselves they were clearly of importance in the p- carbon scattering experiments; the correction applied to R at 20° amounted, as shown above, to more than 10 per cent. For p-p scattering the false asymmetries were smaller, partly because the amount of beam movement was smaller, and partly owing to the near-isotropy of the p-p differential cross-section in the centre-of-mass system, over the ranges of energy and angle considered. Also, the polarization was not expected to change violently with angle.

Finally, a mention of the value obtained for β. Since the second scattering plane was known to be horizontal, it was concluded that the direction of the beam polarization differs from the vertical by

no more than about 1 degree at most. Strictly, this result applies only to the transverse polarization; a longitudinal component is not excluded. However, the latter is known to be very small (R24). β did not enter the expression for the p- carbon asymmetry, equation 4.6. It did occur in the asymmetry measured in p-p scattering, the latter being $\Sigma \cos\beta$ rather than Σ. In the event, however, the difference was clearly negligible.

4. Proton-Proton Scattering.

(a) Accumulation of Data. For each hydrogen measurement the energy and energy spread were predetermined by putting the calculated amount of absorber in the telescopes, in front of the third counters. Calibrated aluminium absorbers were used, whose values ranged in convenient steps from 0.12 to 10.03 gm/cm^2 and were known to within 0.01 gm/cm^2. In no case was absorber added between the back pairs of counters, although provision had been made for this; the energy spread was always the minimum allowed by the absorber built into the apparatus as crystals and the like.

With the target full and the telescopes at the required angle, the amount of polyethylene was varied until the anticoincidence counting rate was a maximum. At the same time the delays were checked to ensure that the maximum was real.

Both real counts with the target full, and background counts with the target empty and an additional 0.44 gm/cm^2 of aluminium in each telescope, were taken in cycles of one or two hours duration. A single polarization measurement consisted of several cycles. Each

cycle comprised eight counts and gave two independent values of the polarisation. These corresponded to the two possible directions of the 180° rotation of the beam polarization, or to the two directions of the 910 amperes solenoid current. Using the notation already introduced for the latter, they will be referred to as the "normal" and "reverse" values of the polarization. Of course, each involved measurements for zero current also. To obtain each value to a statistical accuracy of $\pm$ 1 per cent required about 10^5 counts in all per cycle. All counts were taken for a given number of clicks of the monitor register and were then normalized to counts per click. In all cases the available time was shared between real and background counting in such a way as to minimise the statistical errors.

(b) Background Counts. The background was never unduly large. The greater part of it resulted from scattering of the beam by the target structure. For scattering at 22.5° in the laboratory the background varied from about 5 per cent of the real rate at 98 MeV to 15 per cent at 30 MeV. At 40 MeV, it increased from 2.5 per cent at 35° to about 12 per cent at 22.5°.

There was no significant difference between the background with the target evacuated and with it full of air. This was expected, since particles scattered from air in the target would have energies outside the range detected by the telescopes. In view of this, nearly all backgrounds were taken with air in the target.

(c) Random Counts. The finite resolving time of any multiple coincidence systems implies the possibility of detecting accidental or

random coincidences between the counters. For a triple coincidence array the random counting rate is

$$R = 2\,ABC\,T^2 \qquad 4.20$$

Where T is the resolving time and A, B and C the individual or "singles" rates of the counters. If the accidentals are a significant fraction of the real counts, then a correction must be applied to the latter.

For a system used in conjunction with a pulsed accelerator, the random coincidence rate can be measured by delaying the output of one of the counters by an amount equal to the time between machine pulses. For the Harwell synchrocyclotron this time is 50 ns. and in this experiment the random rates were studied by adding a 50 ns delay to each of the first three counters in each telescope in turn, conditions otherwise being those for recording anticoincidences. No genuine events could now be recorded; the expected counting rate was

$$R^1 = R\,(1 - 2\,DT^1) \qquad 4.21$$

where R has already been defined, D is the singles rate for the back counter and T^1 the anticoincidence resolving time. Since DT^1 was small compared with unity, R^1 was very nearly equal to R. In the event the observed random rates were always so small that they could be neglected.

(d) Dead-Time Losses. It has already been observed that the dead-time on the output of the coincidence circuit was less that 2 μ sec. With counting rates of at most about 10 per second it followed that the associated counting losses were negligible.

(e) Estimation of Mean Energy and Energy Spread. In assigning an energy and energy spread to each measurement there were two effects to be considered. The first of these was purely geometrical; at the lowest energies at which measurements were made, the detected protons lost about half their energy in traversing the hydrogen target, so that it was necessary to consider in some detail the size and shape of the scattering chamber and also the profile of the beam inside it. The former were obtained directly by measurement, while the latter was estimated from the multiple scattering which occurred in the polyethylene (see Appendix III). The lateral distribution of intensity across the target was Gaussian, modified by the structure of the beam; for present purposes it was approximated by a rectangular distribution whose half-width corresponded to the r.m.s. angle of multiple scattering.

The second effect related to the energy definition of the anticoincidence counters. In every case the crystals on the third and fourth counters in each telescope were of equal thickness. If it were not known how far into one of these crystals a proton had to penetrate in order to be detected, then the mean range would be subject to an uncertainty equal to the thickness of either. In the 30 MeV determinations, for example, the rear crystals were equivalent to 0.17 gm/cm^2 of aluminium. This would give an uncertainty of 3.5 MeV in the mean energy for scattering at 22.5° in the laboratory. It was clearly desirable to reduce this uncertainty.

The response of phosphors to charged particles has been

discussed by Taylor et al.(R25). They show that various organic phosphors behave rather similarly; the following remarks are based upon the results given for protons in anthracene.

At high energies the light output L from a given crystal is proportional to the energy lost by the particle in traversing it. Below about 10 MeV the response becomes nonlinear and the phosphor is said to become saturated. The form of the response is then

$$\frac{dL}{dX} = \frac{A\,dE}{dx}\left(1 + kB\,\frac{dE}{dx}\right)^{-1} \qquad 4.22$$

Using published values of A and kB, together with tables of dE/dx against E, L can be plotted as a function of energy for a given crystal. Fig. 10 shows the response curve obtained in this way for the thinner of the crystals used on the rear counters in the present experiment.

On the arbitrary scale of Fig. 10, the light output from a proton of energy 140 MeV is about 0.8. Since this was the energy at which the counters were set up, it follows that 0.8 is an upper limit for the light which a proton must emit in order to be detected. From the left-hand part of the response curve it is found that the minimum energy for detection is 1.6 MeV, corresponding to a minimum penetration of 0.009 gm/cm^2 of aluminium. In scattering at 22.5^0 in the laboratory this represents an uncertainty of only 0.2 MeV in a mean energy of 30 MeV, falling to 0.07 MeV at 100 MeV.

The value of 0.009 gm/cm^2 was confirmed by a similar calculation for the thicker scintillator; it was in all cases taken as the contribution of the third counter to the absorber which defined the mean energy. The resulting error in the latter was negligible. The

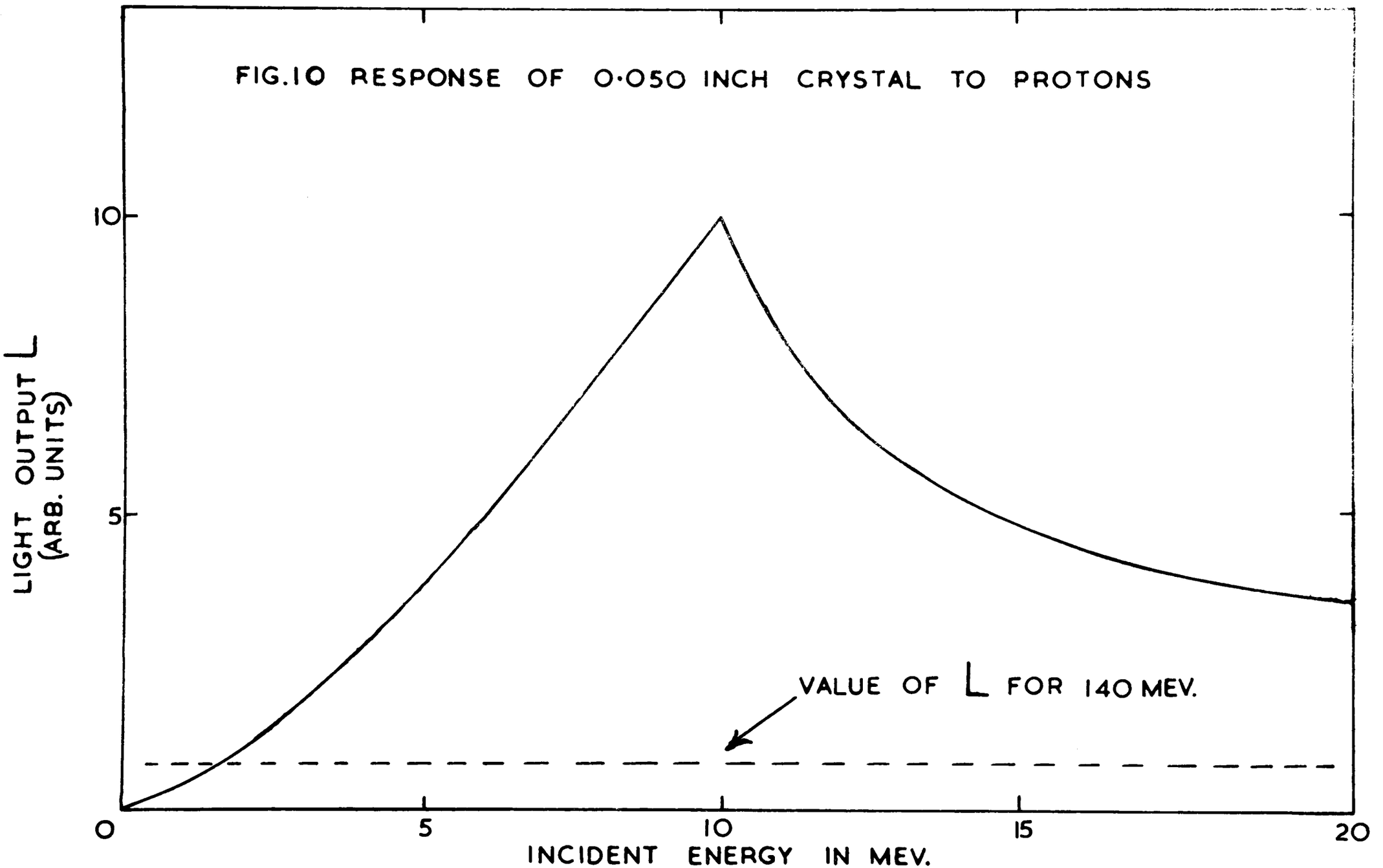
FIG.10 RESPONSE OF 0·050 INCH CRYSTAL TO PROTONS
LIGHT OUTPUT L (ARB. UNITS)
10
5
0
5
10
15
20
INCIDENT ENERGY IN MEV.
VALUE OF L FOR 140 MEV.

contribution of the third and fourth crystals to the energy spread was taken as the thickness of either; the error was again negligible.

To calculate the energy and energy spread, a scale drawing was made of the scattering chamber with the estimated limits of the beam inside it. This drawing was then divided into about 10 thin sections of equal thickness and normal to the axis of the beam. The range of energies detected from each section was estimated and the results combined to give an energy spectrum for all detected particles.

This procedure was carried out for each energy and scattering angle, and for both scattering chambers used during the experiment.

The range of accepted energies had in every case been located on the peak of the degraded beam spectrum by suitable adjustment of the amount of polyethylene. Since this range of energies was always substantially less than the width of the degraded spectrum, between about 0.3 and 0.5 of the latter at 40 Mev for example, it followed that all energies within the range were detected with about equal probability. The same would have been true for the scattered particles if the p-p differential cross-section were independent of energy; the spectra were first obtained on this basis and were then corrected for the preferential scattering of lower energy particles.

A typical energy spectrum is shown in Fig. 11. Each spectrum was a histogram giving on an arbitrary scale the number of detected particles, $N(E)\,dE$, inside an interval dE at energy E. The "mean energy" assigned to the measurement was defined as

FIG.11 TYPICAL ENERGY SPECTRUM

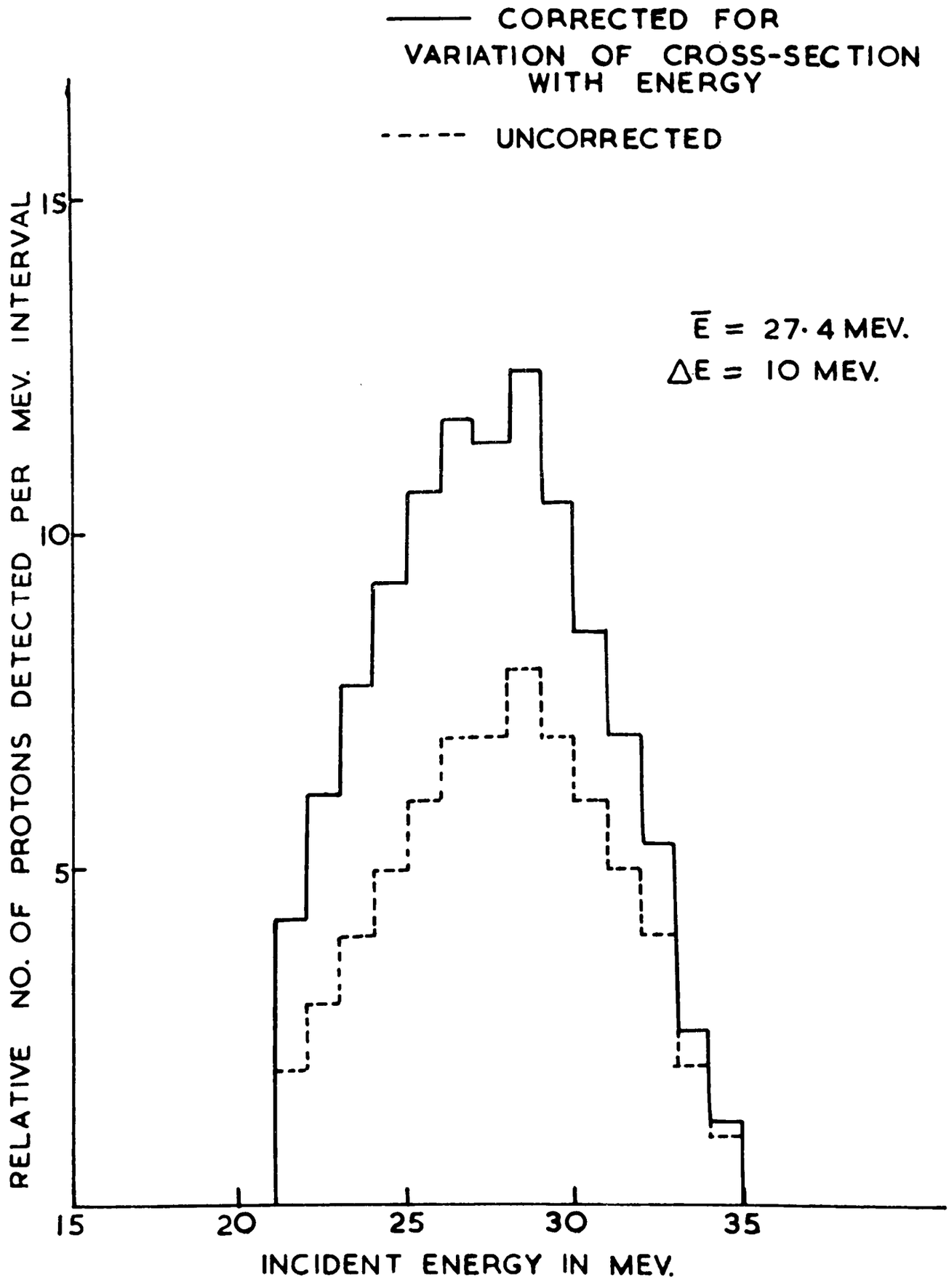

$$\bar{E} = \frac{\sum_{N(E)\,EdE}}{\sum N(E)\,dE} \quad . \qquad 4.23$$

The full-width at half-height, ΔE, of the spectrum was taken as the energy spread.

On the assumption that the polarisation varied linearly with energy over the interval ΔE, the mean polarization, which was the quantity measured, was the same as the polarization at energy $\bar{E}$. In no instance did $\bar{E}$ differ by more than about 3 MeV from the nominal value which had been used to estimate the amount of telescope absorber required for the measurement.

The individual values of $\bar{E}$ and ΔE are given with the measured values of the polarization in Table IV.

(f) Angular Resolution. The geometry was such that the angular resolution for either telescope was determined by the width of the beam at the target, together with the aperture of the defining counter. The resolution could be described approximately by a Gaussian, whose standard deviation increased from about 2.5° c.m. at 100 MeV to 3.5° c.m. at 30 MeV. At a given energy it did not change very much with angle.

Chapter V.

Results

1. Analysis of Data

(a) Calculation of Polarization. Each recorded count, after normalization and subtraction of background, gave the number of protons scattered into a given telescope (T) for a given solenoid setting (S), for one click of the monitor register. A typical count could be written

$$N(TS) = N_{(S)}\, M_{(S)}\, I_{(ST)}\, e_{(T)} \left[1 + P_1 P_2 (ST) \right] \qquad 5.1.$$

where $N_{(S)}$ = No. of protons incident per second upon the target,

$M_{(S)}$ = No. of seconds/click of the monitor register,

$I_{(ST)}$ = p-p differential cross-section in the laboratory frame of reference,

$e_{(T)}$ = efficiency of telescope,

P_1 = beam polarization,

$P_2(ST)$ = p-p polarization.

It will be convenient to introduce, in addition, the quantity

$$m_{(S)} = N_{(S)}\, M_{(S)}.$$

Numerical constants and quantities which remained constant t roughout each measurement, have been put equal to unity in equation 5.1.

The (S,T) dependence of the cross-section and polarization terms derived respectively from any spot movement which accompanied changes in the solenoid current, and from any error in setting up the telescopes.

In principle, the thickness of hydrogen traversed by the beam should have been included as an additional S- dependent term, since the Mellinex windows on the scattering chamber were curved. However, this effect was small enough to be neglected; in any case it did not enter the expression from which the polarization was computed. Making trivial changes in the above notation, the recorded counts in each half-cycle of data could be written as follows:

Spin up, or zero solenoid current:

left telescope, $N(LU) = m(U)\, I(LU)\, e(L)\, (1 + P_1P_2(LU))$

right telescope, $N(RU) = m(U)\, I(RU)\, e(R)\, (1 - P_1P_2(RU))$

spin down, N or R current of 910 amperes:

left telescope, $N(LD) = m(D)\, I(LD)\, e(L)\, (1 - P_1P_2(LD))$

right telescope, $N(RD) = m(D)\, I(RD)\, e(R)\, (1 + P_1P_2(RD))$. 5.2.

The asymmetry, $\Sigma = P_1P_2$, was calculated from

$$r^2 = \frac{N(LU) \times N(RD)}{N(RU) \times N(LD)} \qquad 5.3$$

The following sources of false asymmetry were considered:

(1) a possible difference $\Delta\theta_o$ in the scattering angles for the telescopes due to misalignment; this did not contribute to r^2.

(2) a possible change $\Delta\theta$ in the scattering angle for either telescope due to movement of the beam when the solenoid setting was changed.

$\Delta\theta$ was defined by equation 4.2 and was related to the transverse movement of the beam according to equation 4.9.

Following the discussion of Chapter IV, section 3, the effects of β were neglected. Effects due to the residual vertical movements

of the beam induced by the solenoid were also estimated to be entirely negligible.

The relation between the asymmetry and the measured quantity r^2 was

$$r^2 = \left(\frac{1+\Sigma}{1-\Sigma}\right)^2 \left[1 - 2\left(\frac{1}{I}\frac{dI}{d\theta} - \frac{\Sigma^2}{1-\Sigma^2}\frac{1}{P_2}\frac{dP_2}{d\theta}\right)\Delta\theta\right] \qquad 5.4$$

It will be seen that the system is indeed self-monitoring, since $n(U)$, $n(D)$ do not occur in equation 5.4. From the kinematics of the elastic scattering of particles of equal mass, it can be shown that the laboratory and centre-of-mass scattering parameters are related as follows:

$$\frac{1}{I}\frac{dI}{d\theta} = -\tan\theta + \frac{1}{I_c}\frac{dI_c}{d\theta_c} \qquad 5.5.$$

where the suffix c denotes a quantity measured in the centre-of-mass system. At the energies and angles of scattering considered in this experiment, $dI_c/d\theta_c$ is very small; neglecting this term.

$$\frac{1}{I}\frac{dI}{d\theta} = -\tan\theta \qquad 5.6$$

Using equation 5.6. and noting that $\Sigma^2 \ll 1$, equation 5.4. could be written

$$r^2 = \left(\frac{1+\Sigma}{1-\Sigma}\right)^2 \left[1 + 2\left(\tan\theta + \Sigma^2\frac{1}{P_2}\frac{dP_2}{d\theta}\right)\Delta\theta\right] \qquad 5.7$$

In the event, the beam movement was reduced to less than 0.05 cm. corresponding to a variation in scattering angle of only about 0.05°; it followed that the term in $\Delta\theta$ in equation 5.7 was small. In fact

$$2 \tan\theta \, \Delta\theta \sim 10^{3} \ , \quad 2 \sum^{2} \frac{1}{P_2} \frac{dP_2}{d\theta} \sim 10^{6} \ ,$$

so that both could be neglected. Equation 5.7 thus reduced simply to

$$r^2 = \left(\frac{1+\Sigma}{1-\Sigma} \right)^2 \ . \qquad 5.8$$

From equation 5.8 the asymmetry was calculated, and hence the p-p polarization, using the value given in chapter IV for the beam polarisation.

For reasons given later, the normal and reverse polarization measurements were regarded as equivalent, so that a mean value could be calculated for each cycle. (In calculating means, the individual values were weighted in inverse proportion to the squares of their statistical errors) Finally, from the values for the separate cycles of data, a mean polarization was obtained for each determination.

(b) Additional Information from the Data. In addition to r^2, two other quantities were calculated from each half-cycle of numbers. The first and more important of these was defined as follows:

$$q^2 = \frac{N(LU) \times N(L)}{N(RU) \times N(RD)} = \left(\frac{e(L)}{e(R)} \right)^2 \qquad 5.9.$$

The second equality in equation 5.9 was valid apart from an uncertainty of about 1 per cent. The latter was almost entirely due to a cross-section term; this derived partly from $\Delta\theta$ but mainly from $\Delta\theta_o$ which did not vanish here as it did for r^2. However, any effect due to $\Delta\theta_o$ remained constant during each measurement and so the corresponding uncertainty in q^2 was of no consequence, since one

sought only to detect variations of e(L) / e (R) within the measurement. If this ratio does change, then the quantity calculated from equation 5.8 may no longer be a true measure of the polarization; this point will be referred to again.

The second quantity was S^2, defined as follows:

$$S^2 = \frac{N\,(LU) \times N\,(RU)}{N\,(LD) \times N\,(RD)} = \left(\frac{m\,(U)}{m\,(D)}\right)^2 \qquad 5.10$$

where the effects of spot movement were so small that the second equality could be considered exact.

Table II contains mean normal and reverse values of S, calculated for each run, together with their statistical errors (see below).

TABLE II. MEAN VALUES OF S.

Run	Normal	Reverse
1	0.94 ± .005	0.95 ± .005
2	0.97 ± .006	0.99 ± .006
3	0.89 ± .006	1.08 ± .010
4	0.92 ± .004	1.10 ± .006
5	0.92 ± .003	1.08 ± .005

From equation 5.10, and the definition of m, it follows that

$$\frac{N(U)}{N(D)} = S\,\frac{M(D)}{M(U)} \qquad 5.11$$

where N was defined immediately below equation 5.1.

Using the data of Table II, and typical values of M from the times recorded for the hydrogen counts, the following were

obtained:

TABLE III. APPROXIMATE VALUES OF $N(U)/N_{(D)}$

Runs	Solenoid Settings	
	Zero & Normal (1st half-cycle)	Zero & Reverse (2nd half-cycle)
1-2	1.0	1.0
3-5	0.9	0.8

The variations of beam intensity with solenoid setting observed in last three runs is the more usual condition; it has occurred in other experiments using the polarized beam and solenoids. In the first two runs the intensity was almost independent of the solenoid setting. This is thought to have been due to the use, already mentioned, of an additional collimator of quite small aperture, immediately in front of the monitor.

One other quantity, t^2, was calculated from the data, in this case from each complete cycle of numbers. t^2 was defined as the ratio of the spin-up counts for the first half-cycle, divided by the same ratio for the second half-cycle. It was expected to be unity. The use which was made of the quantities defined here in assessing the accuracy of the experiment is described in Section 3.

(c) Calculation of Statistical Errors. All counting experiments are subject to uncertainties which arise from the statistical nature of the process being studied, and which can be reduced only by accumulating more data.

The significance of the statistical errors in comparison with the other errors in this experiment is discussed in section 3 below. Here, attention will be limited to an example showing how the statistical errors were calculated. Suppose r^2, equation 5.3, were computed from 4 numbers N_χ with statistical errors ΔN_χ: Then the corresponding error in r would be Δr, where

$$2\,\frac{\Delta r}{r} = \left[\sum_{\chi=1}^{4} \left(\frac{\Delta N_\chi}{N_\chi}\right)^2\right]^{1/2} \qquad 5.12$$

The associated error in the asymmetry would be

$$\Delta\Sigma = \frac{2\,\Delta r}{(1+r)^2} \cdot \qquad 5.13$$

The ΔN_χ are understood to contain the errors on both the real counts and the corresponding backgrounds.

2. Tabulated Results.

The results obtained from 20 determinations of the polarization in p-p scattering at various energies and angles are presented in Table IV. The errors given are the statistical standard deviations; the energies and energy spreads were derived by the methods of Chapter IV, section 4.e. The results are tabulated in order of increasing energy, the numbers in the column headed M serving merely as a convenient form of labelling.

The given centre-of-mass scattering angles were obtained from the measured laboratory angles in the non-relativistic approximation. In a number of cases there are several values for the

polarization at the same scattering angle and at closely similar energies. In such cases mean values have been calculated; the 10 values which remained when this was done are given in Table V. For the combined data the quoted energies are mean values, obtained by weighting the individual measurements according to the number of cycles of data of which they were composed.

The measurement for M = 11 has been excluded from Table V; for reasons given below this determination was regarded as suspect.

TABLE IV. PROTON PROTON POLARIZATIONS IN PER CENT. INDIVIDUAL MEASUREMENTS.

Run	M	Energy in MEV		$\theta^{\circ}_{C.M.}$	Polarization
		Mean	Spread		
3	1	27.4	10	45	0.19 ± 0.82
5	2	"	"	"	0.37 ± 0.56
1	3	41.0	13	"	- 1.15 ± 1.24
2	4	41.9	8	"	0.15 ± 0.91
4	5	37.7	7	"	1.51 ± 0.55
4	6	36.8	10	60	2.15 ± 0.54
5	7	"	"	"	0.44 ± 0.60
5	8	"	"	"	0.63 ± 0.57
4	9	"	13	70	1.10 ± 0.49
1	10	50.5	11	45	1.15 ± 0.80
2	11	51.1	7	"	1.89 ± 1.15
2	12	"	7	"	0.11 ± 1.23
3	13	49.4	6	"	3.75 ± 0.84
5	14	"	6	"	2.68 ± 0.52

TABLE IV (contd.)

Run	M	Energy in MEV		$\theta^\circ_{C.M.}$	Polarization
		Mean	Spread		
2	15	51.7	9	60	4.09 ± 1.02
2	16	53.2	13	75	0.84 ± 0.86
5	17	58.5	6	45	4.31 ± 1.05
1	18	70.0	9	"	6.50 ± 0.65
1	19	97.5	7	"	11.75 ± 0.81
3	20	96.5	4	"	13.37 ± 0.85

TABLE V. PROTON-PROTON POLARIZATIONS IN PER CENT.
COMBINED VALUES

M	Energy in MEV		$\theta^\circ_{C.M.}$	Polarization
	Mean	Spread		
1-2	27.4	10	45	0.31 ± 0.46
3-5	38.3	8	"	0.86 ± 0.44
6-8	36.8	10	60	1.14 ± 0.33
9	"	13	70	1.10 ± 0.49
10,12-14	49.7	7	45	2.33 ± 0.37
15	51.7	9	60	4.09 ± 1.02
16	53.2	13	75	0.84 ± 0.86
17	58.5	6	45	4.31 ± 1.05
18	70.0	9	"	6.50 ± 0.65
19-20	97.0	5	"	12.52 ± 0.59

3. Accuracy

(a) Sources of Error. In addition to the statistical errors already mentioned, the measurements were in principle subject to systematic errors, due to inadequate consideration of the factors upon which they depended, and to accidental errors in making the measurements. Because the asymmetries were very small the measurements were extremely liable to systematic errors and it was important to eliminate as many of these as possible.

Since solenoids were used it was expected that the results would be free from systematic error due to misalignment of the telescopes. Errors due to inhomogeneities in the distribution of energy and polarization in the beam should have been eliminated in the same way. The system was self-monitoring and so there should have been no error due to the beam monitor. Errors due to the small residual movements of the beam accompanying changes in solenoid setting were expected to be negligible; the interpretation of the proton-carbon scattering data had indicated that the treatment of these effects was adequate. (There was in principle a possibility of false asymmetries from the observed differences in the beam profile for the three solenoid settings. In the event, however, the normal and reversal polarizations were indistinguishable, indicating that the effects were negligible).

In order to achieve the required statistical accuracy it was necessary, owing to the low counting rates, to spend up to about 30 hours on each measurement, so that the latter were rather liable

to the effects of drifts in the detection system or in the beam transfer system. These effects were largely eliminated, however, by taking the data in cycles. By this means also, mistakes, for example in re-setting the steering magnets when the solenoid condition was changed, were easily detected.

To summarize, it was expected that all other errors would be small compared with the statistical uncertainties remaining after any reasonable counting time. A statistical analysis of the data indicated that this was the case; the analysis will now be described.

(b) Statistical Analysis. The data gave 181 individual half-cycle values (i.e. normal or reverse values from each cycle of data) of the polarization at various energies and angles of scattering; these contained 89 pairs of normal and reverse values from complete cycles.

The paired results were examined first, in order to detect any systematic differences between the normal and reverse values; as already pointed out, there should be no such differences provided the spot movements due to the solenoid were correctly compensated and the asymmetry was insensitive to the details of the beam profile. The "sign test" for paired observations (R26) applied to pairs within the individual measurements failed to detect any significant difference between them. This was followed by an analysis en bloc of the paired data, whose results are shown in Fig. 12A. The distribution is given of the difference between each pair of values,

FIG. 12 STATISTICAL ANALYSIS OF POLARIZATION DATA

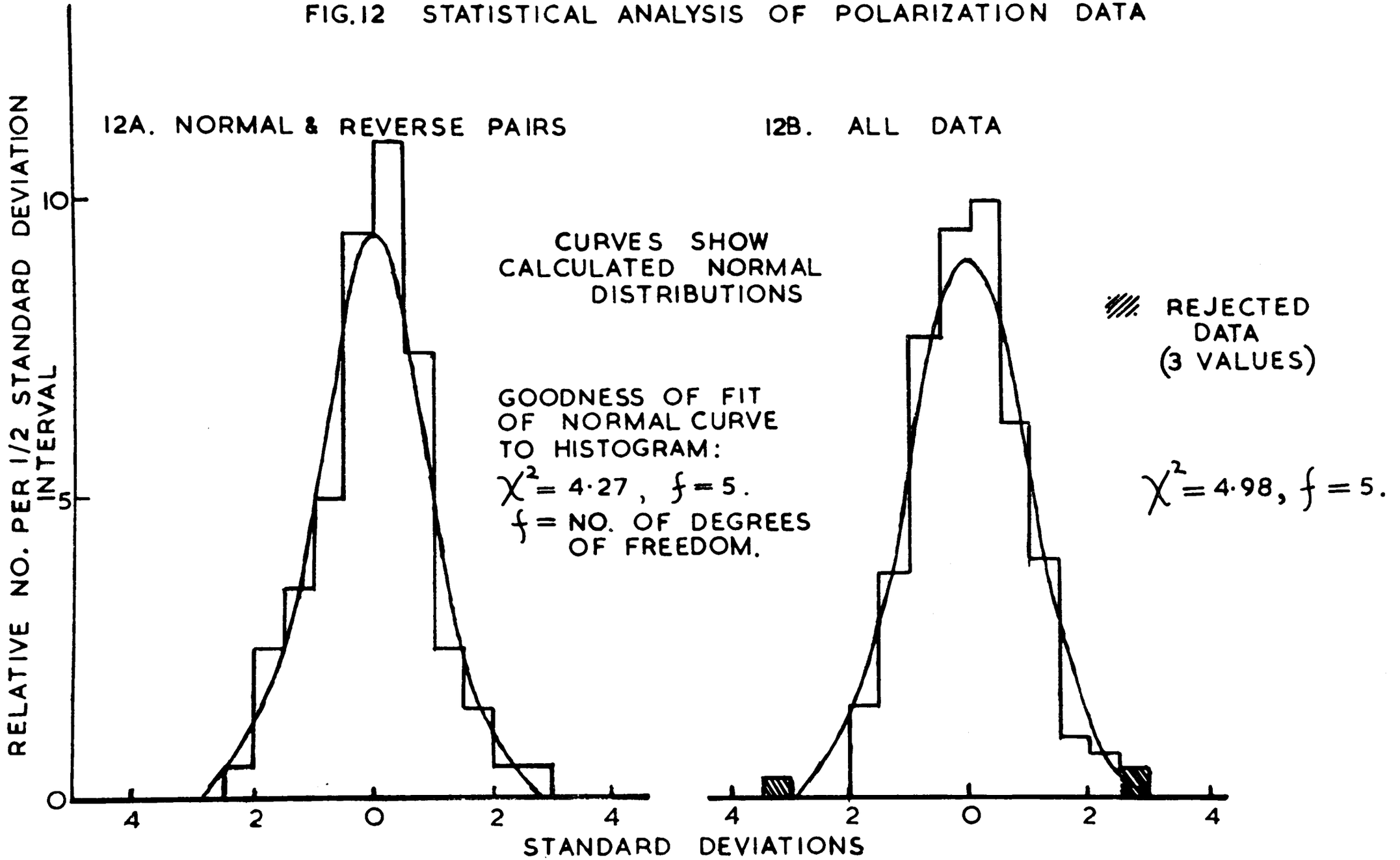

in terms of the error on the difference, also the normal distribution for an assumed mean difference of zero. The normal curve is a good fit to the histogram. For the two groups of runs taken separately, the corresponding distributions were again normal within the errors. It was concluded that the effects of spot movement and of variations in beam profile were negligible. In what follows, the normal and reverse polarizations are regarded as equivalent.

A test similar to those just described was next performed on the 181 individual polarization values, for the distribution about their appropriate means. The results are shown in Fig. 12B; the normal curve is again a good fit to the histogram.

Reference to Fig. 12B shows that there were 3 values, or 1.7 per cent of the total, lying outside the limits $\pm$ 2.5 standard deviations from the mean; the normal curve predicts 1.84 per cent. These three values have been rejected on the grounds that they would otherwise unduly influence the results. They were not included in the remaining analyses.

From Fig. 12B it was concluded that on the average all other errors were small compared to the statistical errors. However, such a conclusion is of limited value since it is the polarizations at particular energies and angles of scattering which are significant, rather than an average effect. For further information the results within each measurement were analysed in the following way: For each measurement values of the

polarization and of the efficiency parameter q^2, with statistical errors, had been calculated from each half-cycle of numbers. Mean values were obtained and the distributions about these of the half-cycle values were subjected to chi-squared tests. Similarly for the values of t^2 within each determination. The results are summarized in Table VI, which corresponds to Table IV. For q^2, the tabulated chi-squared values refer to the distribution about the mean for each measurement. The value for M = 11 is much larger than expected and therefore this measurement has been rejected. In every other case the values are consistent with a constant mean value, while in addition the normal and reverse values were found to be the same within the errors, as required.

For t^2, the chi-squared values in Table VI refer to an assumed mean value of one; all are consistent with this assumption.

As mentioned earlier, results at the same scattering angle for closely similar energies have been combined. In such cases a chi-squared value was computed both for the distribution of the mean values of the polarization from the separate measurements about the overall mean and for the distribution about the same mean of all the individual half-cycle values. The results are given in Table VII. From the right-hand columns of this table it will be seen that there is a possible case for increasing the quoted error on the polarization at 49.7 MeV, 45° c.m.; the

TABLE VI. STATISTICAL ANALYSIS OF DATA

Values of χ^2 and number of degrees of freedom f for individual measurements.

M	r^2		q^2		t^2	
	χ^2	f	χ^2	f	χ^2	f
1	11.2	11	8.0	11	1.9	6
2	2.0	5	6.1	5	3.0	3
3	0.3	2	0.8	4	0.8	1
4	5.1	5	13.5	5	3.2	3
5	11.8	13	14.2	13	8.7	7
6	10.5	10	4.5	10	2.6	5
7	6.1	8	12.5	8	6.4	4
8	7.9	11	11.7	11	5.2	6
9	8.1	11	5.6	11	2.6	6
10	2.3	4	5.8	4	6.2	2
11	5.3	4	24.3	4	0.5	1
12	1.7	3	1.8	3	2.4	2
13	6.9	13	24.4	13	13.2	7
14	13.2	19	24.2	19	7.6	10
15	2.4	3	2.7	3	3.1	2
16	1.3	3	2.9	3	0.6	1
17	10.3	9	9.4	9	4.1	5
18	7.4	5	2.7	5	1.1	3
19	6.3	9	12.4	9	11.3	5
20	7.3	11	17.2	13	3.2	7

probability of observing a chi-squared value larger than 8.7 for 3 degrees of freedom is rather less than 5 per cent. The remaining values in the table have probabilities of 5 per cent or more. Here, no such increase has been made, but in a report of this work submitted to the Rutherford Jubilee International Conference at Manchester, September 1961, the error on the measurement in question was increased by a factor 1.6. Also, the results presented at Manchester for the angular distributions of the polarization near 40 MeV and near 50 MeV differ slightly from those given in Table IX below, since in each case a mean energy was taken and no allowance made for the variation of polarization with energy.

TABLE VII. STATISTICAL ANALYSIS OF DATA

Values of χ^2 and number of degrees of freedom f for combined measurements.

M	Polarization Data			
	Half-Cycle Values		Mean Values	
	χ^2	f	χ^2	f
1-2	13.3	17	.03	1
3-5	21.8	22	4.6	2
6-8	29.3	31	5.7	2
10,12-14	31.4	42	8.7	3
19,20	13.5	21	1.9	1

Chapter VI

Discussion of Results

1. The Energy Dependence of the Polarization at 45° c.m.

(a) The power Law $P = aE^b$ The results obtained in this experiment for the polarization at 45° c.m. are plotted in Fig. 13 together with the corresponding Harvard data below 100 MeV. The measurements agree very well in the region where they overlap; this may be regarded as additional evidence for the reliability of the present results near 30 MeV and 40 MeV. The general form of the energy dependence shown in Fig. 13 suggested that the data might be fitted by a power law of the form

$$P = aE^b \qquad 6.1.$$

The results of several least squares fits of equation 6.1. to the data are shown in table VIII.

TABLE VIII. LEAST SQUARES FITS OF $P = aE^b$

Source of data	Max. energy in MeV	b	$\log_{10}a$	χ^2	f
this work	58.5	3.45 ± 1.73	4.49 ± 2.77	0.08	2
this work	70.0	3.36 ± 1.13	4.36 ± 1.84	0.91	3
this work & Harvard	71	3.42 ± 0.71	4.44 ± 1.18	5.85	7
this work	97.0	3.06 ± 0.72	3.87 ± 1.21	32.1	4

The values of a and b given in the table relate the polarization in

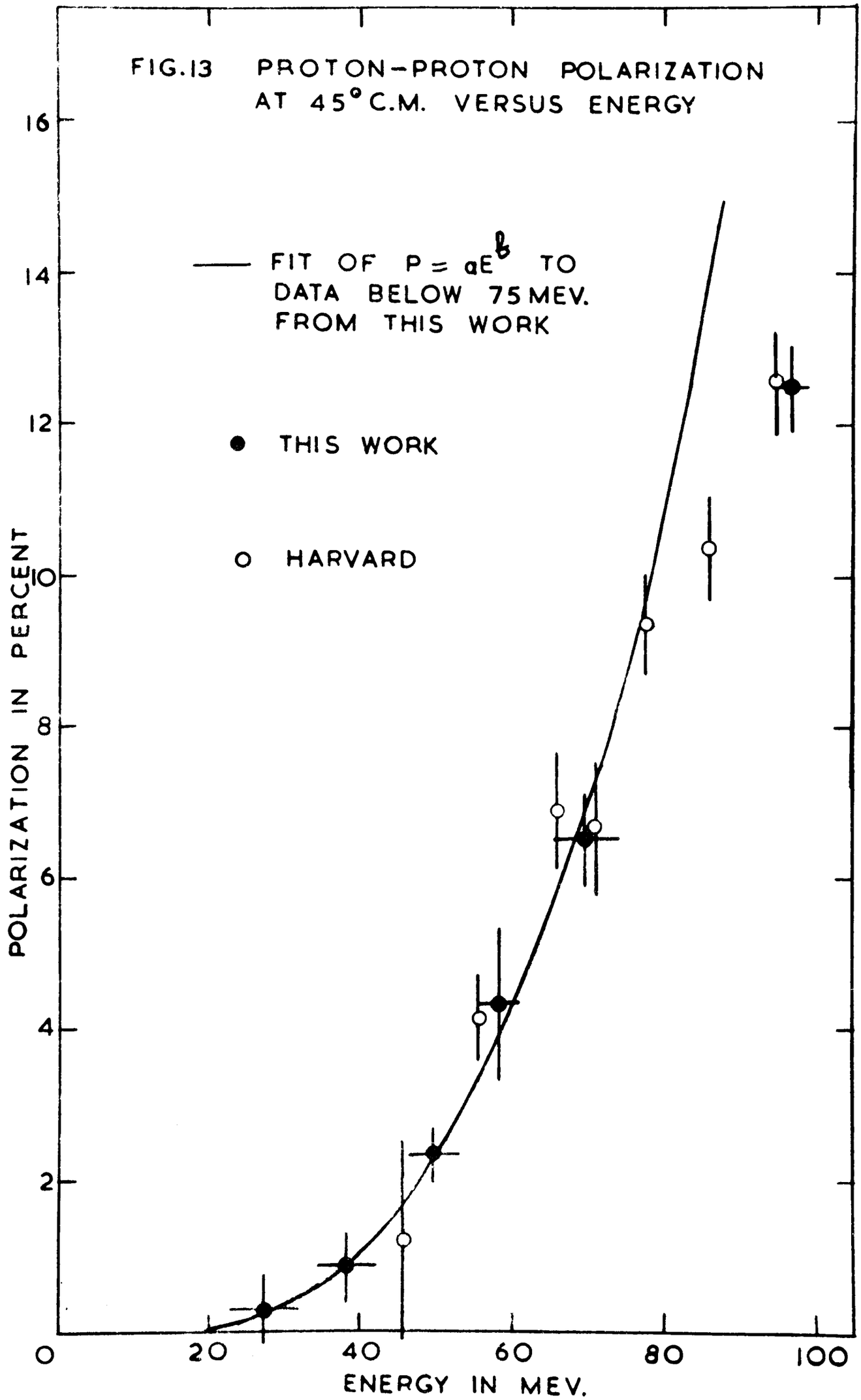
FIG. 13 PROTON-PROTON POLARIZATION AT 45° C.M. VERSUS ENERGY
FIT OF $P = aE^b$ TO DATA BELOW 75 MEV. FROM THIS WORK
THIS WORK
HARVARD
POLARIZATION IN PERCENT
ENERGY IN MEV.
0
2
4
6
8
10
12
14
16
20
40
60
80
100

per cent to the laboratory energy in MeV. For each set, the data were taken from the source given in the first column for energies up to and including that given in the second column. The goodness of fit is indicated by the chi-squared value; f is the corresponding number of degrees of freedom.

Equation 6.1 is a good fit to the data below about 75 MeV; the fit to the present data below this energy is plotted in Fig.13. At higher energies the fit deteriorates rapidly. The significance of these results will be discussed in section 1.c. below.

(b) Use of the Power Law for Interpolation. An immediate application of the results of the previous section is to give a method of interpolating between the experimental data at various energies. This is particularly useful for the angular distributions of the polarization near 40 MeV and 50 MeV, where the individual measurements (see Table IV) refer to energies which differ by as much as 3.5 MeV. From equation 6.1

$$\frac{\Delta P}{P} = b \frac{\Delta E}{E} \qquad 6.2$$

This result is in general true only at 45° c.m. However, it is shown in the next section that the polarization is predominantly due to P-wave scattering at the energies of interest here; equation 6.3 shows that in the P-wave approximation the energy dependence and angular dependence of the polarization are separable so that equation 6.2 remains correct at all angles.

The results in table IX were obtained from the appropriate

data of Table V by using equation 6.2 with b = 3.45. In each case the quoted energy has been chosen to minimise effects due to the neglect of higher partial waves.

TABLE IX. POLARIZATION VERSUS C.M. SCATTERING ANGLE.

Energy in MeV	Corrected Polarization in per cent			
	45°	60°	70°	75°
37.0	0.76 ± 0.44	1.16 ± 0.33	1.08 ± 0.49	- - -
52.5	2.77 ± 0.37	4.31 ± 1.02	- -	0.80 ± 0.86

(c) Significance of the Power Law $P = aE^b$. At energies greater than a few MeV the polarization in p-p scattering consists almost entirely of two terms, a purely nuclear part and a Coulomb-nuclear interference term; polarization effects in Coulomb scattering, and corrections to the phase shifts for vacuum polarization, are negligible at angles greater than a few degrees.

As the energy increases the angular range of the interference region diminishes; at 30 MeV it extends out to about 45° c.m. It is therefore reasonable, in discussing the significance of the results of section 1.a., to regard the measured polarization as purely nuclear in origin and this will be assumed in what follows.

The polarization arises entirely from triplet scattering, and if S- and P- waves only are assumed it is given by equations A2.15 of Appendix II:-

$$k^2 I_P = \rho \sin 2\vartheta \qquad 6.3.$$

where ρ is a function of the ^3P_J phase shifts. The energy

dependence and angular dependence of the right-hand side of equation 6.3 are quite distinct; more generally one has

$$IP = \sum_{n=0}^{2\ell_{max.}-1} a_n \cos^n\theta \sin\theta \qquad 6.4$$

where the a_n are complicated functions of the energy (through the phase shifts), and a straightforward separation is no longer possible.

It is clearly of interest to determine the extent to which equation 6.3 gives an adequate description of the polarization below 100 MeV. With this point in mind the polarization at 45°c.m. has been calculated in the S- and P- wave approximation, using equations A2.14 and A2.15, from the tabulated phase shifts of Gammel and Thaler (R.7) and the results compared with the accurate predictions of their potential. The results are given in Fig.14. The solid curve is that given by Gammel and Thaler, while the points are the values obtained for S- and P- waves only. The predictions agree in the form of the energy dependence and in general order of magnitude, and the difference between them diminishes, as expected, as the energy decreases.

Since the Gammel-Thaler model does not reproduce the details of the experimental data below 100 MeV, the validity of the S-, P- wave approximation has also been tested by calculations using phase shifts extracted from the data by Perring (R27). The results are shown in Table X.

FIG. 14 PROTON-PROTON POLARIZATION FROM S- & P-WAVE SCATTERING

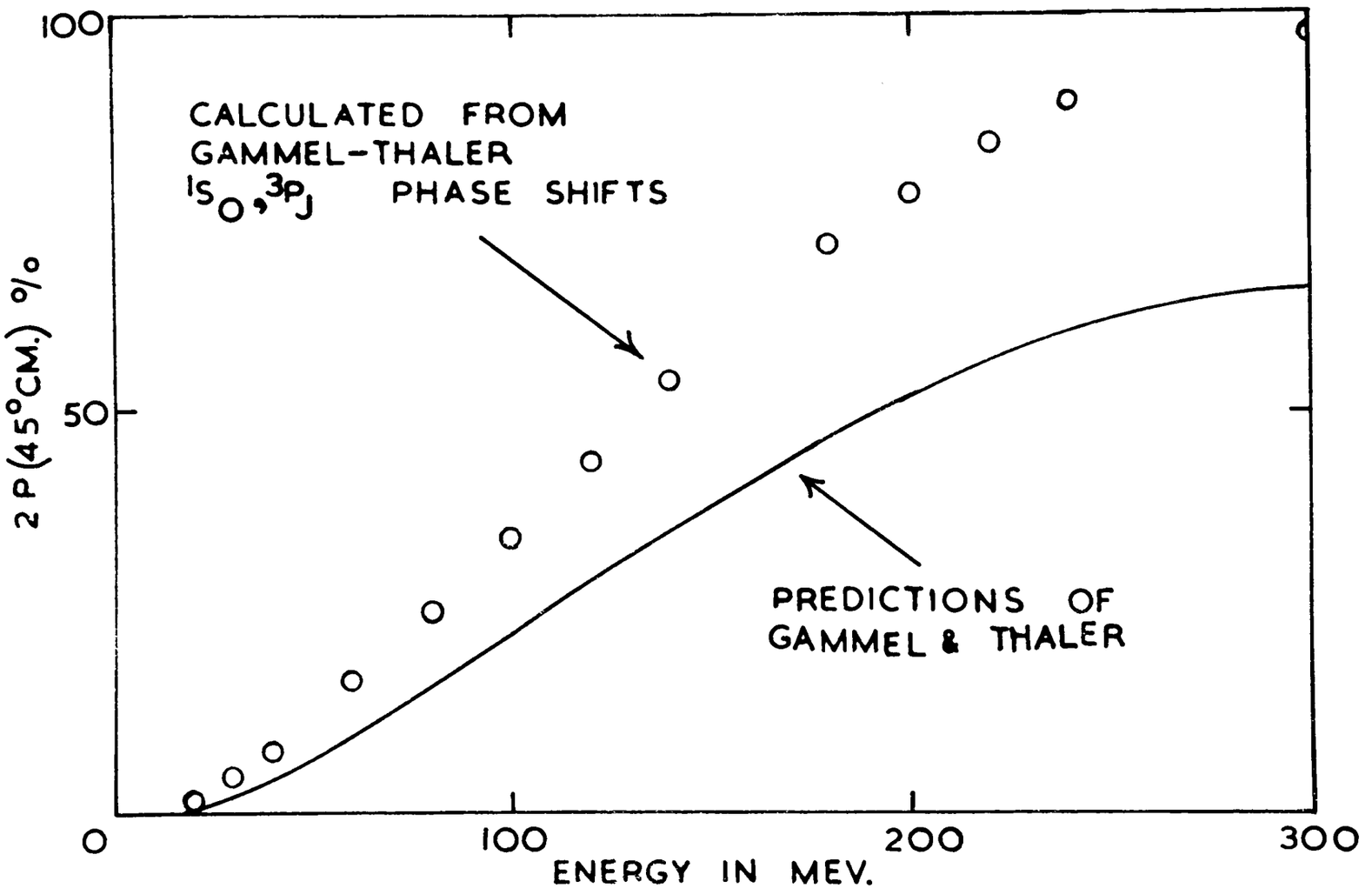

TABLE X. POLARIZATION IN S-, P- WAVE APPROXIMATION

Energy in MeV.	Perring's solution type (R27)	Polarization in Per cent	
		Calculated from S-, P- Phase shifts	Experimental value used in analysis
68	1	7.3	6.9 ± 0.8
"	2	6.5	"
98	1	14.8	12.6 ± 0.7
"	2	10.2	"

The results given above indicate that S- and P- waves give a semi-quantitative description of the polarization data considered in section 1.a. and the latter will now be discussed in terms of these.

As the first step towards understanding the power law fits described earlier, we note that the p-p differential cross-section at 90° c.m. is very nearly inversely proportional to the laboratory energy; a least squares fit to the data gave

$$\log_{10} I = (2.755 \pm 0.129) - (1.055 \pm .083) \log_{10} E. \qquad 6.5$$

where I is the cross-section in millibarns/steradian and E is the energy in MeV. Further, since the c.m. cross-section is almost isotropic above about 40° in the energy region of interest, equation 6.5 can be used for the cross-section at 45° c.m. also. From equations 6.3 and 6.5 it follows that

$$P(45^{\circ}) = \text{constant} \times \rho \qquad 6.6$$

so that the energy dependence of the polarization is directly

related to that of the ^3P_J phase shifts. The energy dependence of the phase shifts takes a rather simple form at low energies, for a potential of finite range (R28); the phase shift for a given orbital angular momentum ℓ can be written

$$\delta_\ell \propto k^{2\ell+1} \quad \text{for} \quad kr_o \ll 1 \qquad 6.7$$

where r_o is the distance at which the potential becomes comparable with the total energy of the incident particle in the centre-of-mass. From equations 6.6 and 6.7, and assuming that the phase shifts are small enough for their sines to be replaced by the angles themselves, we obtain

$$P(45^\circ) = \text{constant} \times E^{4.5}, \text{ for } kr_o \ll 1. \qquad 6.8$$

Both the Gammel-Thaler and Signell-Marshak potentials employ a long range tensor term which dominates the P- wave scattering at low energies. For the Signell-Marshak triplet odd-parity tensor potential r_o is about 1×10^{-13} cm. at 20 MeV, corresponding to a value of about 0.5 for kr_o. Equation 6.8 should therefore apply at energies of several MeV but not at 20 MeV or above; Iwadare (R29) has noted that the ^3P_J phase shifts obtained by MacGregor below 5 MeV vary with energy according to equation 6.7.

The data of table VIII do in fact extrapolate to a value close to 4.5 at zero energy, but the extrapolation is not very meaningful owing to the large uncertainties in the values of b. More significant is the fact that the observed values of b remain consistent with 4.5 up to about 70 MeV; it may be concluded that the energy dependence of the ^3P_J phase shifts up to an energy

of this order is not markedly different from that at very low energies. The failure of the simple power law at higher energies can be attributed to a change in the energy dependence of one or more of the P- wave phase shifts (the $^3P_0$ phase shift of Perring's solution 1 (R27) has a maximum between 50 MeV and 100 MeV for example), together with the increasing importance of higher partial waves.

2. Phase Shift Analysis of Proton-Proton Scattering.

(a) Phase Shift Analyses at 40 MeV and Below. This section will be devoted largely to a discussion of the significance of the polarization measurements near 30 MeV and 40 MeV in terms of phase shift analyses of low energy p-p scattering. The experimental results at higher energies will not be discussed, since they are of note chiefly for their excellent agreement with the Harvard data. Very recently, cross-section measurements near 50 MeV have been reported from Tokyo (R30); these will add considerably to the significance of the present polarization data near that energy.

The 40 MeV analysis of Moyes & MacGregor was referred to in chapter 1. In 1959 MacGregor (R31) extended this work to include cross-section data at a number of energies between 1.855 MeV and 39.40 MeV. The method of analysis was to adjust the phase shifts until a good least squares fit to the data was obtained. The goodness of fit was measured by the quantity

$$M = \sum_{i=1}^{n} \left[\frac{\text{Icalc} - \text{I exp.}}{\Delta \text{I exp}} \right]^2 , \qquad 6.8$$

which has the expected value (n-p), where n is the number of experimental points and p the number of phase shifts. Some relevant features of the work will now be described.

The data at 1.855 MeV could be fitted by Coulomb effects together with a nuclear S- wave. At 10 MeV S_y P- and D- waves were required while at 40 MeV F- waves were also needed, as described in chapter 1. It was established that F- waves were not effective at 20 MeV, but no definite conclusion could be reached at 31.8 MeV, owing to uncertainties in the experimental data. In the region below 40 MeV, where S-, P- and D- waves were adequate, MacGregor found that there is at each energy a semi-infinite region in the S-D plane inside which equally good fits are obtained. For each pair of S, D phases there are four sets of ^3P_J phase shifts, with the characteristics shown in Table XI.

TABLE XI. LOW ENERGY ^3P_J PHASE SHIFTS (R31)

Solution type	$^3P_0$	$^3P_1$	$^3P_2$	P(45°)
I	M+	M-	S+	+
II	L+	S-	S-	-
III	L-	S+	S+	+
IV	M-	M+	S-	-

S, M and L denote small, medium and large phase shifts respectively. The signs of the phase shifts are indicated, also that of the polarization at 45° c.m. predicted by each type of

solution. As an illustration of the multiplicity of solutions, MacGregor noted that at 20 MeV the cross-section at any angle is constant to within 0.1 or 0.2 per cent for all solutions inside the allowed region. However, the results of the present work show rather convincingly that the polarization remains positive at low energies; it follows from table XI that solution types II and IV are excluded. MacGregor has investigated the extent to which a knowledge of the magnitude as well as the sign of the polarization would reduce the remaining ambiguity. He finds that a polarization measurement at 18.2 MeV with an accuracy at all angles of 0.1 per cent would probably distinguish types I and III, but that a whole range of possible S- D combinations would remain. A better way of distinguishing solutions I and III would appear to be a single measurement of the depolarization. There is considerable evidence in favour of solution I (R27); for example, both the Gammel-Thaler and Signell-Marshak potentials predict ^3P_J phase shifts which correspond to this type of solution.

At 40 MeV, where F- waves are important, the multiplicity of solutions fitting the cross-section data alone is even greater. While the results of this experiment do not allow a unique analysis, they appear to reduce the multiplicity quite considerably. For example, of 17 typical solutions given by MacGregor only one gives a polarization consistent with that observed. Although this particular solution is not unique, it may be noted that the order of the ^3P_J phase shifts corresponds to solution type I at lower

energies.

Again, Noyes and MacGregor were unable in their 40 MeV analysis to distinguish between $^3P_2$ - $^3F_2$ mixing with no appreciable F- wave on the one hand, and an appreciable F- wave with no mixing on the other. The former corresponds to a tensor interaction of the type used by Gammel and Thaler, the latter to a large-range spin-orbit potential. Such a spin-orbit term was suggested by the Harvard group (R11) to account for the negative polarization at 40 MeV which seemed to be implied by their measurements. However, the present work shows that the polarization is positive at 40 MeV and eliminates the need, in this respect at least, for such a potential.

Following the success of the modified analysis of Cziffra et al.at 310 MeV, mentioned in chapter I, a similar analysis was carried out for the data below 40 MeV. The one-pion exchange contribution (OPEC) was again used for the higher partial waves. However this analysis did not provide any important results that had not been obtained already from the ordinary analysis (R5).

The present situation at low energies is summarized quite well by Fig. 15, which shows typical solutions obtained by Perring (R32) from phase shift analyses which included preliminary polarization data from this experiment. The experimental points shown differ slightly from those given in this work; the value for M = 4, Table VI, was not included and no correction was applied for the variations of polarization with energy, section 1 above.

FIG. 15 PHASE SHIFT SOLUTIONS OBTAINED BY PERRING

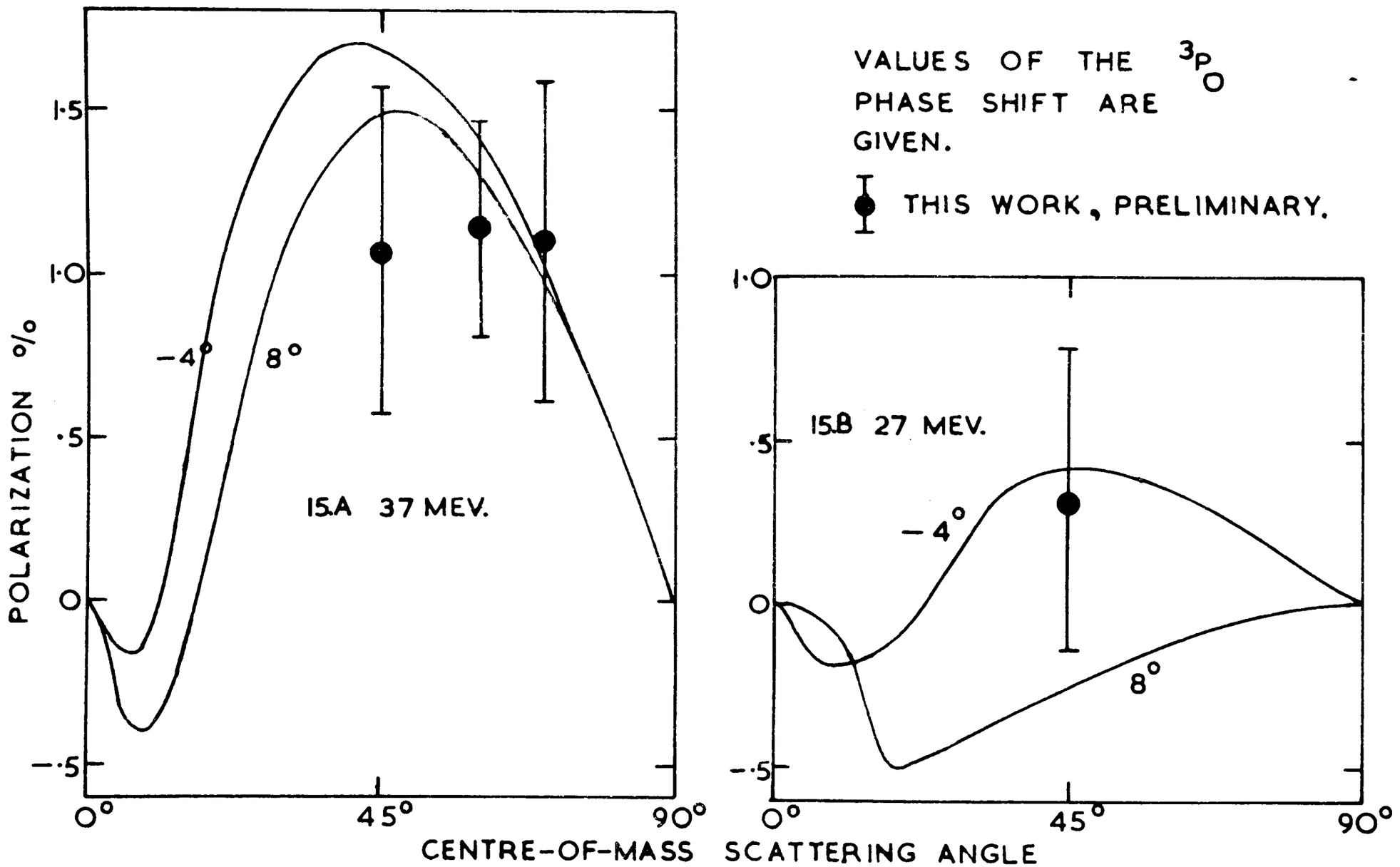

The most serious ambiguity at low energies resides in the $^3P_0$ phase shift. Fig.15 shows that very much more precise data will be required in order to resolve this ambiguity using polarization measurements, also that such measurements should be made in the Coulomb-nuclear interference region.

(b) Proton-Proton scattering above 40 MeV. The most notable advance has been the extraction of a unique set of phase shifts at 210 MeV, following the completion of the programme of p-p triple scattering experiments referred to in chapter I (R33). Less spectacular progress has been made in the region near 100 MeV. Perring, for example, has reported an analysis of p-p scattering between 68 MeV and 142 MeV (R27) in which OPEC was used for partial waves with ℓ greater than 3. He finds two solutions, denoted 1 and 2. Solution 1 extrapolates to the unique solution at 210 MeV and to the popular solution I of Stepp et al. at 310 MeV; it also corresponds to a MacGregor type I solution at low energies. Apart from this evidence in favour of solution 1, solution 2 is regarded as unlikely because it requires a change in the sign of the $^1S_0$ phase shift near 50 MeV. The latter would correspond to a minimum in the cross-section or to a resonance, and there is evidence for neither. Even if solution 1 is correct however, a great deal of work remains to be done before the phase shifts can be determined uniquely at all energies.

Finally, mention must be made of recent analyses by Breit et al. (R34) and by Stapp et al.(R35) in which data at all energies are

treated simultaneously, each phase shift being written as a function of the energy in terms of a number of adjustable parameters. Analyses of this kind are obviously superior to those performed at single energies, but they do not in general define the low energy phase shifts any more precisely; when the fit is insensitive to the phase shifts the solutions obtained are determined by the particular form which has been used for their energy-dependence rather than by the experimental data.

3. Conclusions.

It appears at the present time that there will be little point in performing low energy polarization measurements unless the accuracy can be improved by about an order of magnitude over that of existing measurements. Since these measurements are likely to prove more difficult than triple scattering experiments now that polarized ion sources and polarized targets are becoming available, it would seem preferable to concentrate rather upon the latter. The advantage of the triple scattering and correlation experiments is that the parameters involved may be quite large and show quite pronounced variations with the phase shifts at energies where the polarization is very small, and where both the cross-section and polarization are insensitive to changes in the phase shifts. For example, a depolarization measurement at 68 MeV, and possibly at lower energies, would materially reduce the ambiguity in the $^3P_0$ phase shift, (R27). At 40 MeV and below, Iwadare (R29) has suggested a measurement of the correlation parameter Cnn

to pin down the $^1S_0$ phase shift, followed by a measurement of $R(90^\circ)$ or $A(90^\circ)$ to resolve the ^3P_J phase shifts; according to Noyes (R36), a 5 per cent measurement of $C_{nn}(90^\circ)$ at 40 MeV might fix the $^1S_0$ phase to 0.5° and the D phase also.

CHAPTER VII

The Depolarization in Proton-Proton Scattering near 150 MeV

1. Introduction

(a) General Remarks. Programmes of triple scattering experiments near 150 MeV were initiated several years ago at Harvard and Harwell with the object of providing enough data to allow a unique phase shift analysis at that energy. Since the Depolarization measurement is the easiest of the triple scattering experiments (R37), both groups began with this experiment.

(b) Principle of the Measurement. For the D measurement the three successive scattering planes are parallel. The first scattering produces the polarized beam and the third scattering measures the vertical component of the polarization of twice-scattered particles. From equation A2.13 with the restriction of time-reversal invariance removed, the polarization after the second scattering is given by

$$I_2 \langle \underline{\sigma} \rangle_f = I_{02} \left[(P_2 + D\underline{P}_1 \cdot \underline{n}_2) \underline{n}_2 \right]$$

where

$$I_2 = I_{02} \left[1 + \underline{P}_1 \cdot \underline{A}_2 \right] .$$

Thus

$$\langle \underline{\sigma} \rangle_f = \frac{(\underline{P}_2 + D\underline{P}_1 \cdot \underline{n}_2) \underline{n}_2}{1 + \underline{P}_1 \cdot \underline{A}_2} \qquad 7.1.$$

The asymmetry at the third scattering is

$$\Sigma_3 = \langle \underline{\sigma} \rangle_f \cdot \underline{A}_3 \ . \qquad 7.2$$

With a single telescope set up to view the third scatterer, suppose that counts are accumulated for equal times at the four positions shown in Fig. 16, where it is assumed that the polarization $\underline{P}_1$ of the once-scattered beam is directed out of the plane of the paper. The LL count is given by

$$LL = I_{02} I_{03} (1 + P_1 A_2) \left[1 + A_3 \frac{P_2 + DP_1}{1 + P_1 A_2} \right] ,$$

where various constants have been neglected. It follows that

$$LL = I_{02} I_{03} \left[1 + P_1 A_2 + A_3 \ (P_2 + DP_1) \right] \ ;$$

similarly,

$$\begin{aligned} LR &= I_{02} I_{03} \left[1 + P_1 A_2 - A_3 \ (P_2 + DP_1) \right] , \\ RL &= I_{02} I_{03} \left[1 - P_1 A_2 - A_3 \ (P_2 - DP_1) \right] \\ \text{and } RR &= I_{02} I_{03} \left[1 - P_1 A_2 + A_3 \ (P_2 - DP_1) \right] . \end{aligned} \qquad 7.3$$

From equations 7.3 it follows that

$$D = \frac{1}{P_1 A_3} \ \frac{LL + RL - LR - RR}{LL + RL + LR + RR} \qquad 7.4$$

The "analysing power" $P_1 A_3$ can be determined as the asymmetry at the third scattering for $\theta_2 = 0$, hence D can be obtained.

The measurement could be made by using only one of the two

FIG.16 PRINCIPLE OF THE DEPOLARIZATION MEASUREMENT.

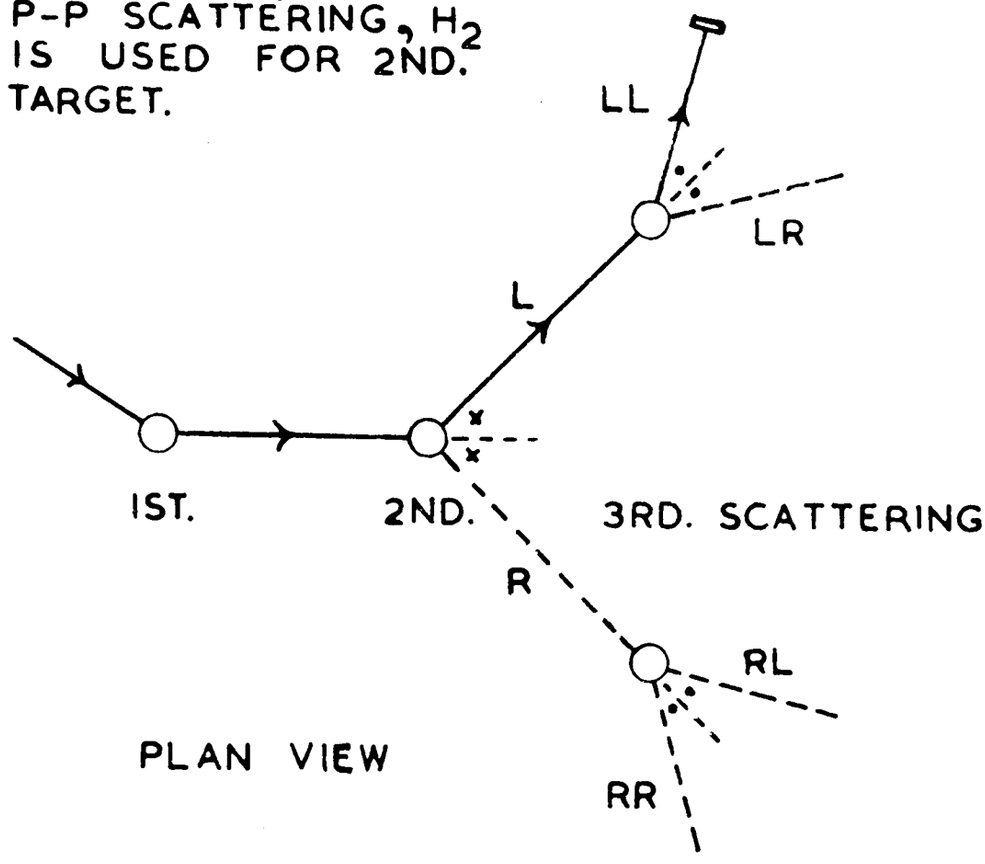

FIG.17 APPARATUS FOR 2ND. HARWELL DEPOLARIZATION MEASUREMENT

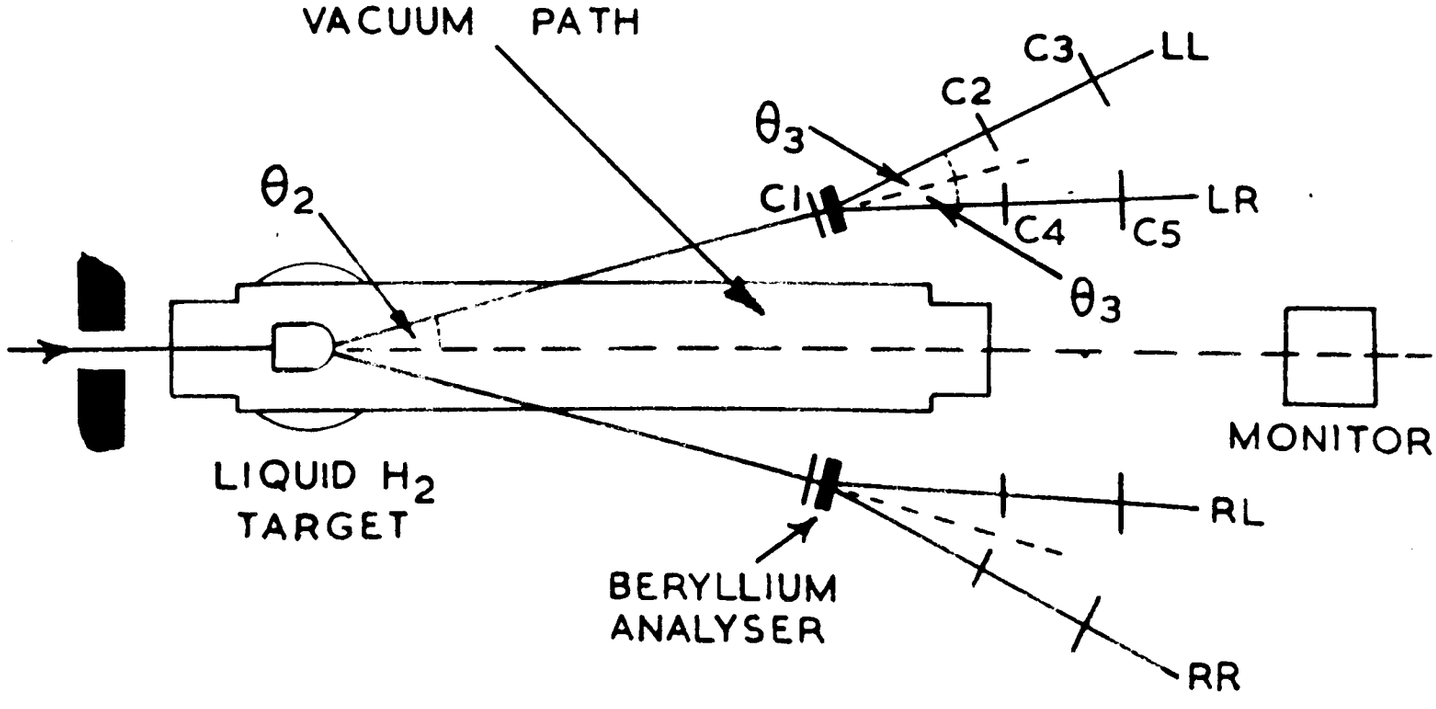

NOT TO SCALE

positions for the third scatterer indicated in Fig. 16, but would then require data from three double scattering experiments instead of one as here, and the results would be correspondingly more liable to error.

(c) Time-Reversal Invariance in Proton-Proton Scattering.

By combining equations 7.3 differently we obtain

$$A_3 P_2 = \frac{LL + RR - LR - RL}{LL + RR + LR + RL} \qquad 7.5$$

Also, by treating the measurement as a double scattering and averaging over the third scatterings,

$$P_1 A_2 = \frac{LL + LR - RL - RR}{LL + LR + RL + RR} \qquad 7.6$$

Since P = A for a spin-zero target owing to parity conservation it follows that the beam polarization P_1 can be determined from a double scattering experiment. A_2 can then be calculated from equation 7.6, while P_2 can be obtained from equation 7.5, knowing $P_1 A_3$. Since P_2 and A_2 have been measured under the same conditions, their comparison provides a direct test of time-reversal invariance in the p-p interaction if the second scattering was from hydrogen. In the paper describing their depolarization measurements the Harvard group (R38) gives 10 measured values of $P_2 - A_2$, 7 of which are consistent with zero.

2. Previous Measurements of D at 142 MeV.

(a) General Remarks. Both the first Harwell measurement (R39) and

the Harvard measurement (R38) were carried out in the general manner described in the previous section. There were however several differences in detail. For example, the Harwell group used a single counter telescope, while the Harvard group employed two telescopes in conjunction with the third scatterer, one on each side of the beam and arranged to be interchangeable. The Harvard group also employed an additional counter located some distance in front of the third target. This not only reduced the background but defined its source more precisely.

From the discussion of double scattering measurements given in Chapter II, Section 2, it will be appreciated that in both experiments it was necessary to take very great care to avoid false asymmetries. The precautions are described fully in the Harvard paper.

(b) Results. The results of both measurements are tabulated in the Harvard paper. The Harvard data cover the angular range from 12° c.m. to 70° c.m., while the Harwell results extend from 30° to 70°. The experiments agree within the errors at 30° with a positive value of order 20 per cent, but diverge strongly at larger angles; the Harvard data remain positive while the Harwell results change sign and become increasingly negative. The former are close to the predictions of Gammel & Thaler (R7) while the latter correspond to those of Signell and Marshak (R9). The Signell-Marshak potential was later modified somewhat (R40), but the predictions for D remained in general agreement with the Harwell measurements.

Although the Harvard experiment is now regarded as superior to

that at Harwell, much of the superiority derives from the fact that the Harwell results were reported by the time the Harvard measurements were just beginning; the Harwell group had shown that such experiments were possible near 150 MeV and had indicated the relative importance of the various types of experimental error. In neither case did there appear to be an error large enough to explain the discrepancy. As a result it was decided to repeat the Harwell measurement by a different method. It was this experiment in which the writer was involved.

3. The Second Harwell Depolarization Measurement.

(a) Principle. In the second measurement of D a solenoid was used, as described in previous chapters, to rotate the polarization of the once-scattered beam through $\pm 180^{\circ}$ and so eliminate geometrical false asymmetries.

The counts given in equations 7.3 were now taken for spin-up (U) and for spin down (D). Remembering that the effect of inverting the spin is merely to change the sign of P_1, it follows that

$$r_1 = \left(\frac{LL^U}{LL^D}\;\frac{RR^D}{RR^U}\right)^{\frac{1}{2}} = \frac{1 + P_1 A_2 + A_3 (P_2 + DP_1)}{1 - P_1 A_2 + A_3 (P_2 - DP_1)}$$

$$r_2 = \left(\frac{LR^U}{LR^D}\;\frac{RL^D}{RL^U}\right)^{\frac{1}{2}} = \frac{1 + P_1 A_2 - A_3 (P_2 + DP_1)}{1 - P_1 A_2 - A_3 (P_2 - DP_1} \qquad 7.7$$

Four telescopes were employed so that counts could be taken simultaneously at all positions indicated in Fig.16. Because of this equations 7.3 should now contain the efficiences of the telescopes, since these will

in general differ. A monitor term dependent on the solenoid setting is also required since all counts were again normalized by reference to a monitor of the once-scattered beam. However, the quantities r_1 and r_2 defined above are independent of both of these terms. From equations 7.7 we define

$$\varepsilon_1 = (1 + P_2 A_3)\ \frac{r_1 - 1}{r_1 + 1} = P_1 A_2 + DP_1 A_3$$

and $$\varepsilon_2 = (1 - P_2 A_3)\ \frac{r_2 - 1}{r_2 + 1} = P_1 A_2 - DP_1 A_3 \qquad 7.8$$

whence

$$\varepsilon_1 - \varepsilon_2 = 2 D P_1 A_3$$

$$\text{and} \qquad \varepsilon_1 + \varepsilon_2 = 2 P_1 A_2 \qquad 7.9$$

In this experiment known values of P_1, P_2 and A_3 were used to extract D and A_2 from equations 7.9.

(b) Apparatus. The beam transfer system was the same as for the polarization measurements described in previous chapters, see Fig 2; a similar size and shape of beam was used. The arrangement of the apparatus in the experimental area is shown in Fig.17. The polarization of the beam had been determined previously to be (46 ± 1) per cent (R23). The mean energy of scattering from hydrogen was 143 MeV, close to that of previous p-p scattering measurements. The scattering chamber was 6 cm. long by 3 cm. wide with windows of .002 inch Mellinex; a small target was used in order to avoid undue energy loss by scattered particles, since the latter would

reduce the analysing power of the third scatterers. The beam was provided with a vacuum path for some distance behind the hydrogen target in order to reduce the background and random counting rates. Particles scattered horizontally emerged through a pair of long Mellinex windows. The third scatterers were 2 gm/cm^2 blocks of beryllium situated 80 cm. from the hydrogen target, and were viewed at 12° on either side as shown in Fig.17 by telescopes employing counters with thin scintillation crystals. Pulses from the five counters associated with each third scatterer were fed into a transistorized coincidence unit (R18), which recorded triple coincidences for C_1, C_2, C_3 and C_1, C_4, C_5 respectively. C_1 was incorporated with the beryllium target as a single unit.

The counters were mounted on plates which could be rotated in the horizontal plane about a pivot located directly below the centre of the hydrogen target. Alignment was carried out with a theodolite and trammel, and was facilitated by using accurately machined counter mountings, each provided with several degrees of freedom. Estimated errors in alignment were 0.040 cm. and 1$'$ of arc. The scattering table, hydrogen target and counters were located with respect to the beam with the aid of X-ray films. The counter arrays were maintained in position by a sine bar which was pinned to the table. In the event, 3 complete sets of counters were employed, 30 counters in all, so that measurements could be made at 3 values of θ_2 simultaneously.

(c) <u>Accumulation of Data.</u> Both senses of the 180° rotation of the polarization were used. The data were taken in cycles to reduce the

effects of drifts, and all counts were normalized by reference to the beam monitor. At each angle a range curve was taken in order to determine the amount of absorber required in the telescopes. Backgrounds were taken with the target empty and additional absorber in the telescopes. The background was 2 per cent or less at all angles except 15° lab, where it was 10 per cent. Most of it derived from the target.

The analysing power A_3 could not be measured without removing the hydrogen target and for this reason interpolated mean values were used.

(d) Systematic Errors. X-ray film studies showed that the residual movement of the beam at the hydrogen target when the solenoid condition was changed was less than 0.05 cm. Measurements with a small counter in the thrice-scattered beam indicated that the corresponding change in the third scattering angle was less than 0.014°. Corrections to the measured asymmetries were calculated using measured values for the rate of change of counting rate with angle; they were small compared to the statistical errors.

As for the polarization measurements described earlier, the data could be combined differently to yield information about the systematic errors. For example, the mean of the ratios

$$\frac{LL^N}{LL^R} \cdot \frac{RR^R}{RR^N} \qquad \text{and} \qquad \frac{LR^R}{LR^N} \cdot \frac{RL^N}{RL^R}$$

was expected to be sensitive to beam movement only. From the known values of the latter and of the variation in counting rate a

mean value for all angles of 1.002 was predicted, while the observed value was 1.002 ± 0.025. Comparisons of this kind indicated that the effects of beam movement had been accounted for correctly.

Finally, measurements at three angles with an unpolarized beam gave a mean asymmetry of $0.0052 \pm .0070$, comparing very favourably with the expected value of zero.

(e) Results. The values of D obtained from this experiment are shown in Fig.18 together with those from the Harvard measurement. The results are tabulated, with those from the earlier experiments, in the published account (R41). The latter also contains the values of A_3 which were used, and measured values of A_2. The present results should be regarded as superseding the previous Harwell measurements.

(f) Discussion. Perring (R27) has reported a phase shift analysis at 142 MeV in which the present results for D were used, together with data on the cross-section, polarization and rotation parameters. As described in Chapter VI, section 2b, two solutions were obtained of which that designated solution 1 is regarded as the more probable.

Perring's solution 1 is shown in Fig. 18. Also shown are the predictions of the Gammel-Thaler potential and of the recent potential of Saylor, Bryan and Marshak (R42). The latter employ energy-independent boundary conditions at a radius of about 0.5×10^{-13} cm., with meson-theoretic tails. The potential gives a very good description of the p-p scattering data up to 310 MeV consistent with solution I of Stapp et al.

FIG. 18 THE DEPOLARIZATION IN PROTON-PROTON SCATTERING AT 143 MEV.

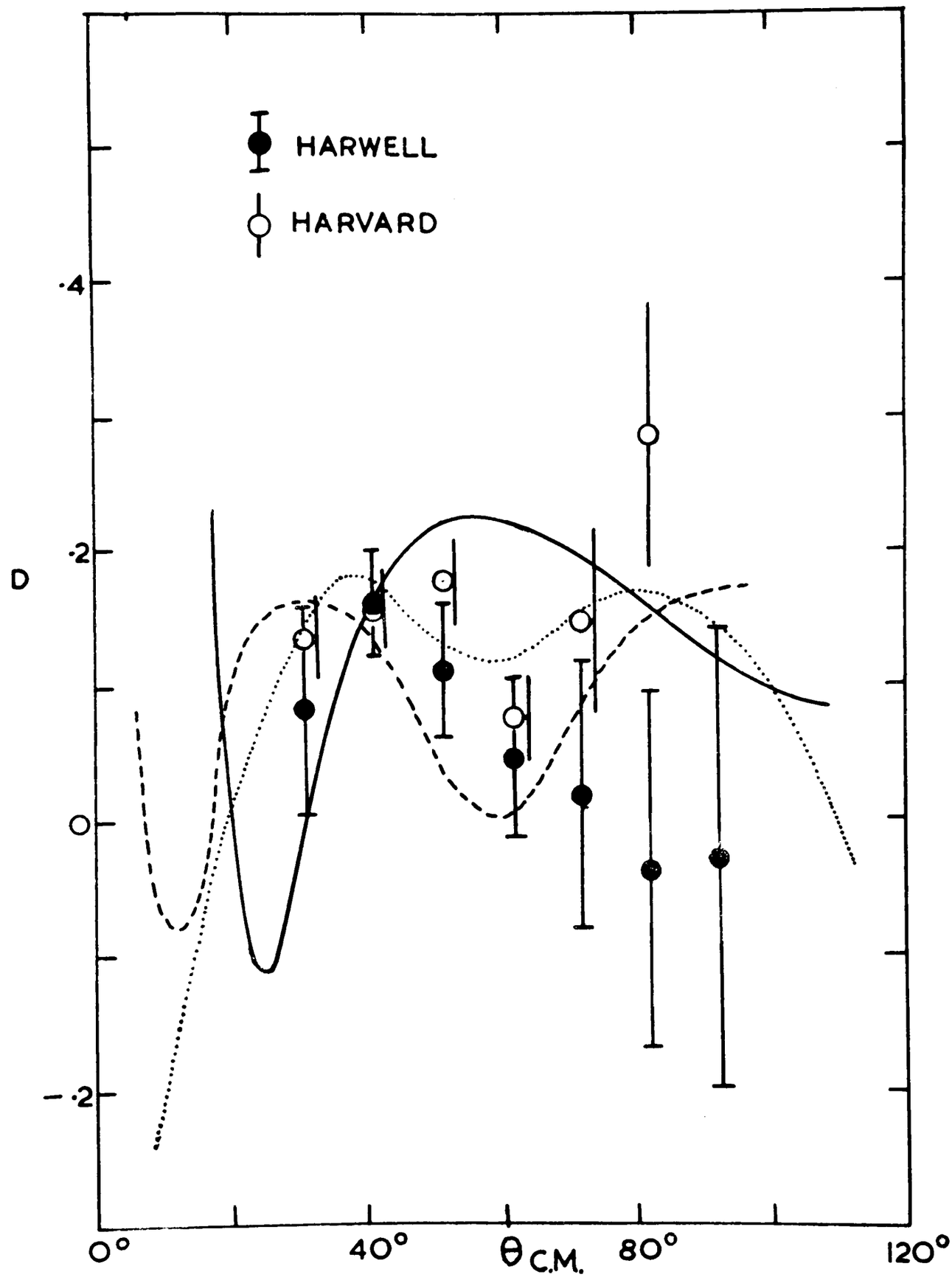

APPENDIX I

Phase Shifts in Nucleon-Nucleon Elastic Scattering.

1. Scattering of Spin-Zero Particles.

We begin with a more precise statement of the definition given in Chapter I of phase shifts for the scattering of spin-zero particles. The discussion is necessarily brief; for full details any textbook on quantum mechanics should be consulted. (e.g. R28)

At distances large compared with the range of the interaction the wave function describing the scattering must take the form

$$\psi = e^{ikz} + f(\theta)\ \frac{e^{ikr}}{r} \qquad \text{A1.1}$$

i.e., a plane wave representing the incident beam and an outgoing spherical wave corresponding to the scattered particles.

The general solution of the Schroedinger equation is, on the other hand, of the form

$$\psi = \sum_{l} A_l P_l(\cos\theta)\ \frac{1}{kr}\ \sin\left(kr - \tfrac{1}{2}l\pi + \delta_l\right). \qquad \text{A1.2}$$

$P_l(\cos\theta)$ is the Legendre Polynomial of order l, identified with particles of angular momentum $\hbar\left(l\,(l+1)\right)^{\frac{1}{2}}$. For a given value of k, A_l and δ_l are constants; δ_l is called a "phase shift".

Now the plane wave in equation A1.1 can be expressed asymptotically as a superposition of spherical waves:-

$$e^{ikz} = \sum_\ell i^\ell (2\ell + 1) P_\ell(\cos\theta) \frac{1}{kr} \sin\left(kr - \tfrac{1}{2}\ell\pi\right)$$

$$= \frac{1}{2ikr} \sum_\ell i^\ell (2\ell + 1) P_\ell(\cos\theta) \left\{ e^{i(kr - \frac{1}{2}\ell\pi)} - e^{-i(kr - \frac{1}{2}\ell\pi)} \right\} \qquad \text{A1.3}$$

From the condition that $\psi - e^{ikz}$ shall be a purely outgoing spherical wave, we find from equations A1.2 and A1.3 that $A_\ell = e^{i\delta_\ell} \times i^\ell (2\ell + 1)$, whence equation A1.2 gives

$$\psi = \frac{1}{2ikr} \sum_\ell i^\ell (2\ell + 1) P_\ell(\cos\theta) \left\{ e^{i(kr - \frac{1}{2}\ell\pi + 2\delta_\ell)} - e^{-i(kr - \frac{1}{2}\ell\pi)} \right\} \qquad \text{A1.4}$$

Comparison of equations A1.3 and A1.4 shows that the phase shifts have exactly the significance ascribed to them in Chapter I.

From the explicit form of the scattered wave we can obtain the scattering amplitude:

$$f(\theta) = \frac{1}{2ik} \sum_\ell (2\ell + 1) \left(e^{2i\delta_\ell} - 1 \right) P_\ell(\cos\theta) \qquad \text{A1.5.}$$

and hence the differential cross-section,

$$I(\theta) = |f(\theta)|^2 = \frac{1}{k^2} \left| \sum_\ell (2\ell + 1) P_\ell(\cos\theta) \sin\delta_\ell \right|^2 \qquad \text{A1.6}$$

The right hand side of equation A1.6 reduces to a power series in $\cos\theta$ whose coefficients are functions of the phase shifts.

2. Scattering of Spin-One-Half Particles.

(a) Pure Nuclear Scattering. The extension to the scattering of particles of spin $\frac{1}{2}$ has been given by Blatt and Biedenharn (B43);

the following remarks are based upon their paper.

It will be assumed that the two-particle interaction is subject to the invariance conditions given in chapter I, section 3.b. Wave functions describing the scattering are written in terms of the total angular momentum J with z component M, and total spin S, all of which are conserved, together with the orbital angular momentum ℓ which is no longer a constant of the motion because of the tensor interaction in triplet states. The spin-angle dependence of the wave functions takes the form

$$\mathcal{Y}^{M}_{J\ell S} = \sum_{m_\ell + m_S = M} (\ell S\ m_\ell\ m_s \mid \ell\ S\ J\ M)\ \ Y^{m_\ell}_{\ell}\ \ \chi^{m_S}_{s} \qquad \text{Al.7.}$$

The term in brackets is a Clebsch-Gordan coefficient, Y is a spherical harmonic and χ a spin wave function. For singlet scattering and for triplet scattering with $\ell = J$ there is no mixing and the complete wave function is

$$\Psi_J = \frac{1}{r}\, U(r)\ \mathcal{Y}^{M}_{J\ell S} \qquad \text{Al.8}$$

where at large distances

$$U(r) = A_\ell e^{-i(kr - \frac{1}{2}J\pi)} - B_\ell e^{+i(kr - \frac{1}{2}J\pi)}.$$

The relation

$$B = SA \qquad \text{Al.9.}$$

defines the "scattering matrix" S, which relates the outgoing part of the complete wave function to the ingoing part of the incident plane wave. When relating the observables to the phase shifts

(Appendix II) it is more convenient to use the R-matrix, defined as

$$R = S - 1 \qquad \text{A1.10.}$$

This relates the outgoing part of the scattered wave to the ingoing part of the incident plane wave. Either of these matrices provides a complete description of the scattering. For each J, S reduces to a single number, of unit magnitude since the scattering is elastic. Thus

$$S = e^{2i\delta_\ell} \qquad \text{A1.11.}$$

This more formal definition of phase shifts is identical, for no mixing, with that given above for particles of zero spin.

In the case of triplet scattering with $\ell = J \pm 1$ there are radial waves $v(r)$ and $w(r)$ for each ℓ and the complete wave function is now of the form

$$\psi_J = \frac{1}{r} v(r) \mathcal{Y}_{J-1} + \frac{1}{r} w(r) \mathcal{Y}_{J+1} ; \qquad \text{A1.12.}$$

for large r,

$$v(r) = A_1 e^{-i(kr-\frac{1}{2}(J-1)\pi)} - B_1 e^{+i(kr-\frac{1}{2}(J-1)\pi)}$$

and similarly for w(r).

For a given J the scattering matrix is now 2 x 2:

$$\begin{pmatrix} B_1 \\ B_2 \end{pmatrix} = S \begin{pmatrix} A_1 \\ A_2 \end{pmatrix} \qquad \text{A1.13.}$$

From general considerations it can be shown that S is both unitary and symmetric. It follows that the 2 x 2 matrix in equation A1.13 can

be expressed in terms of three real parameters; these are called "phase parameters" by analogy with equation A1.11. Blatt and Biedenharn define triplet phase parameters δ_α, δ_β and ϵ, whose significance is the following: The S-matrix now has two eigen-functions which may be labelled α and β, each containing a mixture of $\ell = J-1$ and $\ell = J+1$ partial waves in proportions determined by ϵ. To each eigen function there corresponds an eigenphase shift δ. At very low energies the $\ell = J \pm 1$ partial waves are separated by their different centrifugal barrier effects. This separation implies only that $\sin \epsilon = 0$ at zero energy; with the condition that ϵ shall itself vanish it follows that at zero energy δ_α and δ_β consist entirely of $\ell = J-1$ and $\ell = J+1$ respectively. At other energies the description of the scattering of either partial wave requires all three phase parameters. Stapp et al.(BS) point out that the Blatt-Biedenharn parametization of the S- matrix is in no sense unique and give an alternative definition of phase shifts. These "bar phase shifts" are more convenient when separation of the nuclear and Coulomb terms in proton-proton scattering is considered.

(b) Coulomb Effects in Proton-Proton Scattering. It has already been pointed out that the Coulomb part of the p-p interaction cannot be treated by partial waves because of its infinite range. However the problem has been solved in the non-relativistic approximation; equations such as A1.8 remain valid if (kr) is replaced by (kr-n log2kr) where $n = e^2/\hbar v$, v being the laboratory velocity of the incident proton. S and R now relate to the combined effects of Coulomb and

nuclear scattering. It is convenient to write

$$R = (S-S_c) + R_c$$
$$= \alpha + R_c \qquad \text{A1.14.}$$

the suffix c denoting Coulomb scattering. R_c can be treated exactly and gives the Coulomb scattering amplitude. α on the other hand contains nuclear effects only and can be expanded in terms of phase shifts; for example, when there is no mixing,

$$\alpha_\ell = e^{2i\delta_\ell} - e^{2i\phi_\ell} \qquad \text{A1.15}$$

the Coulomb phase shift ϕ_ℓ being given by

$$\phi_\ell = \sum_{x=1}^{\ell} \tan^{-1}(n/x) \quad .$$

In the absence of nuclear effects the δ_ℓ reduce to ϕ_ℓ. If, and only if, the Coulomb force can be assumed negligible inside the range of the nuclear force then it follows that the scattering in the absence of the former would be described by "nuclear phase shifts" given by

$$\delta_\ell^N = \delta_\ell - \phi_\ell \quad . \qquad \text{A1.16}$$

When mixing occurs, the nuclear bar phase shifts are related to the total bar phase shifts in exactly the same way, whereas the corresponding relations for the Blatt-Biedenharn phase shifts are much more complicated. More generally, equation A1.16 is taken as a definition of nuclear phase shifts and the results of phase shift analyses are usually given in terms of these.

Appendix II

Formalism of Nucleon-nucleon scattering

1. The M- matrix.

From low energy scattering and the properties of the deuteron it was known long ago that the nucleon-nucleon interaction is strongly spin-dependent. Experiments at high energies involve the measurement of quantities which are intimately related to the spin-dependent part of the interaction. Such experiments are most conveniently analysed in terms of transitions between the various initial and final spin states of the two particles. These transitions were described by Wolfenstein & Ashkin (R44) in terms of a 4 x 4 matrix operator M.

Before writing down the general form of the M- matrix certain vectors for the two-particle system must be defined: $\underline{k}$ and $\underline{k}^1$ are unit vectors which define the direction in the laboratory of the incident and scattered particle respectively and $\underline{p},\underline{p}^1$ are similar unit vectors for the motion referred to the centre-of-mass system. In terms of these we define the following:

$$\underline{n} = \frac{\underline{k} \wedge \underline{k}^1}{|\underline{k} \wedge \underline{k}^1|} \quad , \qquad \underline{s} = \underline{n} \wedge \underline{k}^1 \quad ; \qquad \text{A2.1}$$

$$\underline{P} = \underline{p}^1 + \underline{p} \quad , \qquad \underline{K} = \underline{p}^1 - \underline{p} \quad .$$

For particles of equal mass, as here,

$$\underline{k}^1 = \underline{s}_t = \underline{P} \ , \ \underline{k}^1_t = -\underline{s} = -\underline{K} \ , \qquad \text{A.2.2}$$

where the suffix t denotes the target particle.

Wolfenstein and Ashkin show that the M- matrix can be written as follows:

$$M = M(\underline{\sigma}_1, \underline{\sigma}_2, \underline{k}, \underline{k}')$$

$$= A + B(\underline{\sigma}_1 . \underline{\sigma}_2 - 1) + C(\underline{\sigma}_1 + \underline{\sigma}_2).\underline{n}$$

$$+ D(\underline{\sigma}_1 - \underline{\sigma}_2).\underline{n} + E(\underline{\sigma}_1 . \underline{K})(\underline{\sigma}_2 . \underline{K}) + F(\underline{\sigma}_1 . \underline{P})(\underline{\sigma}_2 . \underline{P}) . \qquad \text{A2.3}$$

$\underline{\sigma}_1 . \underline{\sigma}_2$ are the Pauli spin matrices for the particles. The coefficients A to F are functions of the energy and of the scattering angle θ . For p-p scattering D=0 and this is true for n-p scattering also if charge symmetry is assumed.

Using the density matrix representation for the spin wave functions, an equation is obtained which relates the expectation value after scattering of any one of a set of spin operators S to their expectation values before the scattering:

$$I \langle S^\mu \rangle_f = \frac{1}{4} \sum_\nu \langle S^\nu \rangle_i \ \text{Trace}\,(M S^\nu M^\dagger S^\mu) \ . \qquad \text{A2.4}$$

† denotes the adjoint matrix.

It is convenient to take for the operators S the components, 16 in all as required to specify M, of the following operators:

$$1 \ , \ \underline{\sigma}_1 , \ \underline{\sigma}_2 , \ \underline{\sigma}_1 \underline{\sigma}_2 \ . \qquad \text{A2.5}$$

The expectation value of the spin of a beam of particles is referred to as the "polarization" of the beam.

2. Observables.

(a) Double Scattering Experiments. Equation A2.4 has been used by Wolfenstein (R37) to define observables on nucleon-nucleon scattering experiments. The simplest of these involves the scattering of an unpolarized beam by an unpolarized target (it will be assumed that the target is unpolarized, unless otherwise stated). The unpolarized differential cross-section is, from equation A2.4,

$$I_o = \frac{1}{4} \text{ Trace } MM^\dagger, \qquad \text{A2.6}$$

and the spin of the scattered particle is given by

$$I_o \langle \underline{\sigma}_1 \rangle_f = \frac{1}{4} \text{ Trace } MM^\dagger \underline{\sigma}_1 , \qquad \text{A2.7}$$

i.e., the scattering produces a polarization $\underline{P}_1$, where

$$\underline{P}_1 = \langle \underline{\sigma}_1 \rangle_f = \frac{\text{Trace } MM^\dagger \underline{\sigma}_1}{\text{Trace } MM^\dagger} . \qquad \text{A2.8}$$

From the assumption that M conserves parity it can be shown to follow that $\underline{P}_1$ is in the direction of the unit vector $\underline{n}$ defined in equations A2.1.

Until the recent development of polarized ion sources for accelerators (R45), scattering of an unpolarized beam was the only method of producing polarized nucleons.

The beam of polarization $\underline{P}_1$ may now itself be scattered. This will be a double scattering experiment and the cross-section at the second scattering is given by

$$I = \frac{1}{4} \text{ Trace } MM^\dagger + \underline{P}_1 . \frac{1}{4} \text{ Trace } M \underline{\sigma}_1 M^\dagger$$
$$= I_o (1 + \underline{P}_1 . \underline{A}) \qquad \text{A2.9}$$

where

$$\underline{A} = \frac{\text{Trace } M\, \underline{\sigma}_1\, M^\dagger}{\text{Trace } MM^\dagger} \qquad \text{A2.10}$$

$\underline{A}$ is called the "asymmetry". With the usual assumption that M is invariant under time-reversal it can be shown to follow that

$$\underline{A} = \underline{P}_2 \qquad \text{A2.11}$$

where $\underline{P}_2$ is the polarization which would result from the seonnd scattering if $\underline{P}_1$ were zero.

From equations A2.9 and A2.11,

$$I = I_o\,(1 + \underline{P}_1 \cdot \underline{P}_2)\,. \qquad \text{A2.12}$$

If $\underline{P}_2$ is known, then $\underline{P}_1$ can be determined. In other words the double scattering measurement allows the analysis of polarization effects.

(b) Triple Scattering Experiments. In triple scattering experiments the first scattering provides the polarized beam and the third scattering is used to analyse the polarization effects which occur at the second scattering.

Wolfenstein has shown that the polarization produced in nucleon-nucleon scattering with an incident beam of polarization $\underline{P}_1$ can be written as

$$\begin{aligned} I_2 \langle \underline{\sigma} \rangle_f = I_{02} \Big\{ & \left[P_2 + D\, \underline{P}_1 \cdot \underline{n}_2 \right] \underline{n}_2 \\ & + \left[A\, \underline{P}_1 \cdot \underline{k}_2 + R\, \underline{P}_1 \cdot (\underline{n}_2 \wedge \underline{k}_2) \right] \underline{S}_2 \\ & + \left[A^1\, \underline{P}_1 \cdot \underline{k}_2 + R^1\, \underline{P}_1 \cdot (\underline{n}_2 \wedge \underline{k}_2) \right] \underline{k}_2^1 \Big\} \end{aligned} \qquad \text{A2.13}$$

The suffix 2 denotes the second scattering. The triple scattering parameters D, R, R^1, A and A^1 are, like P_2, functions

of the energy and of the angle of scattering; any four of them are independent. D is referred to as the "depolarization"; it is a measure of the probability that the incident polarization remains unchanged by the scattering. R is known as the rotation parameter since it describes the rotation of the incident polarization about the vector $\underline{n}_2$.

From previous remarks a simple scattering cannot be used either to produce or to analyse a beam polarized along its direction of motion. Thus only D and R can be measured by a succession of such scatterings. For the remaining parameters auxiliary magnetic fields are required, to rotate the polarization relative to the direction of motion.

(c) Spin Correlation Experiments. Equation A2.4 also predicts expectation values of the components of the operator $\underline{\sigma}_1 \underline{\sigma}_2$. The associated experiments involve simultaneous measurements of the polarisations of the scattered and recoil particles. Six parameters can be measured, two with an unpolarized beam and four with a polarized beam. Similar experiments involve the use of polarized targets.

(d) Relativistic Corrections. The Wolfenstein-Ashkin formalism is non-relativistic. A completely relativistic treatment has been given by Stapp (R46) who shows that the relativistic correction takes the form of a rotation of the polarization vector about the normal to the scattering plane; it does not therefore affect double scattering or depolarization measurements, for which the successive

scattering planes are parallel (the correction mentioned here is additional to the usual spin-independent kinematic correction.)

3. Observables in Terms of Phase Shifts.

As has been seen in the preceding section, the observables in nucleon-nucleon scattering are described most conveniently in terms of the spins of the individual particles. On the other hand, phase shifts are defined in terms of singlet and triplet states of the two-particle system (Appendix I). Expressions for the observables in terms of the phase shifts have been given by Stapp (R46), using the R-matrix defined in Appendix I. Both p-p and n-p scattering are treated; it is shown that the indistinguishability of the particles in the former can be allowed for by the appropriate antisymmetrization of the scattering matrix.

For p-p scattering in the approximation of S- and P- waves only, the following expressions are obtained for the differential cross-section and polarization:

$$k^2 I(\theta) = \left[\sin^2\delta_0 + \sin^2(\delta^0 - \delta^2) + \tfrac{9}{4}\sin^2(\delta^1 - \delta^2)\right] + 3\left[\sin^2\delta^0 + 3\sin^2\delta^1 + 5\sin^2\delta^2 - \sin^2(\delta^0 - \delta^2) - \tfrac{9}{4}\sin^2(\delta^1 - \delta^2)\right]\cos^2\theta \quad , \qquad \text{A2.14.}$$

$$k^2 I(\theta)\, P(\theta) = \varrho \sin 2\theta, \qquad \text{A2.15.}$$

where $$\varrho = 3\left[\delta^0\ \delta^2\right] + \tfrac{9}{2}\left[\delta^1\ \delta^2\right]$$

and $$\left[x\ y\right] = \sin x \sin y \sin(x-y) \ .$$

k, θ are respectively the wave number and scattering angle in the centre-of-mass system. δ_o is the ^1So phase shift and the δ^J are the ^3P_J phase shifts. These equations represent the purely nuclear interaction; the Coulomb terms for the S- and P- wave approximation have been stated explicitly by Garren (R47).

Appendix III

Multiple Coulomb Scattering

1. Theory

The theory of multiple Coulomb scattering has been described by Rossi (R48). The formulae which are used below are taken from a paper by Rossi and Greisen (R49); they refer to the scattering of singly charged particles only and are approximate to the extent that no corrections have been made either for the finite size of the nucleus or for screening of the nuclear charge by electrons. However, these corrections are unimportant for the applications to be described (R48).

There are two cases of interest:

(1) Scattering by thin foils, with no energy loss. The mean square multiple scattering angle, projected onto a fixed plane containing the axis of the beam, is

$$\langle \theta^2 \rangle = \frac{1}{2} \left(\frac{E_s}{P\beta} \right)^2 t \qquad \text{A3.1.}$$

where

E_s = constant = 21 MeV ,

P = momentum of particle in MeV/c.,

β = v/c as usual,

and t = thickness of foil in "radiation lengths".

The radiation length X_o of a substance determines the rate at

which electrons lose energy in passing through the substance, according to the equation

$$E_x = E_o e^{-\frac{x}{x_o}} \quad ; \qquad \text{A3.2.}$$

some typical values are given in Table XII.

TABLE XII RADIATION LENGTHS FOR VARIOUS SUBSTANCES

Substance	X_o in gm/cm^2
H	138
He	144
Be	85
CH_2	57
CH	55
C	52
Al	26.3
Cu	13.3

(2) Scattering by a thick foil with loss of energy. In this case

$$\langle\theta^2\rangle = \frac{1}{2}\left(\frac{z_s}{m}\right)^2 t \frac{\log_n\left(\frac{1+y_2}{1+y_1}\frac{p_1}{p_2}\right)}{\left(y_1+\frac{1}{y_1}-y_2-\frac{1}{y_2}\right)} \cdot \qquad \text{A3.3}$$

Suffixes 1 and 2 refer respectively to particles entering and leaving the material, while

$$y = (E + m)/m$$

where E is the kinetic energy and m the rest energy of the

particle, both in MeV.

2. Applications

The following remarks relate to the geometry shown in Fig.19A, which was that used in the experiment, and to the scattering of protons.

(1) Comparison of various materials. For this purpose equation A3.1 may be written

$$\langle \theta^2 \rangle = \text{constant} \left(X_o \frac{dE}{dx} \right)^{-1} \qquad \text{A3.4}$$

where dE/dx is the stopping power in MeV.gm^{-1}. cm^2., and X_o the radiation length in gm/cm^2. The corresponding lateral distribution at the target is given by

$$\langle y^2 \rangle = \ell^2 \langle \theta^2 \rangle \qquad \text{A3.5}$$

where ℓ = PC as in Fig. 19A. In every case the value of ℓ has been taken to correspond to the amount of material required to slow down the beam from 150 MeV to 40 MeV; the value of 0.4 used to locate the effective scattering centre, Fig.19A, was obtained from calculations for polyethylene. Fig.19B shows r.m.s. values of θ and of y plotted against the reciprocal of the radiation length. Polyethylene, CH_2, is clearly a very suitable substance for degrading the beam from the point of view of small multiple scattering effects; it is also a very convenient material to handle, and for these reasons it was used at all energies.

(2) Multiple Scattering in Polyethylene at Various Energies.

The data of Table XIII were obtained from equation A3.3

FIG. 19 MULTIPLE COULOMB SCATTERING

19.A GEOMETRY

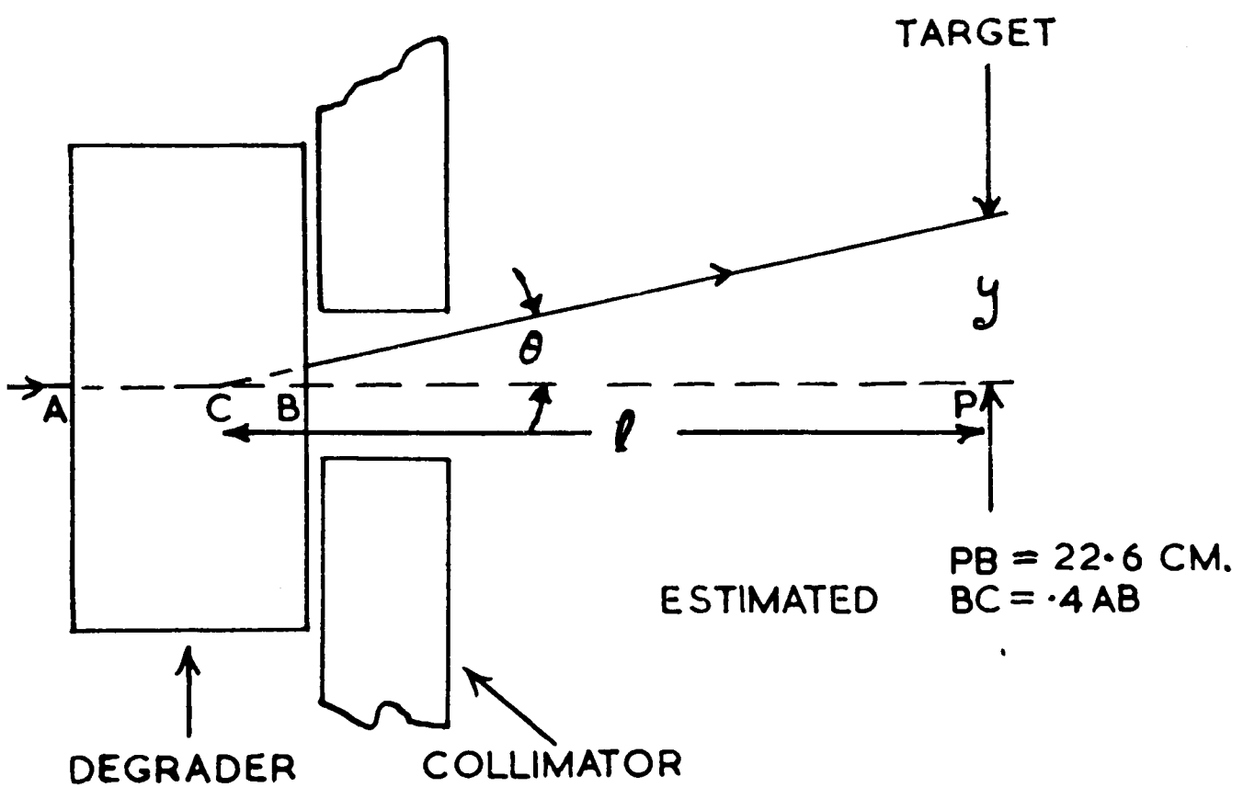

19.B. COMPARISON OF VARIOUS MATERIALS

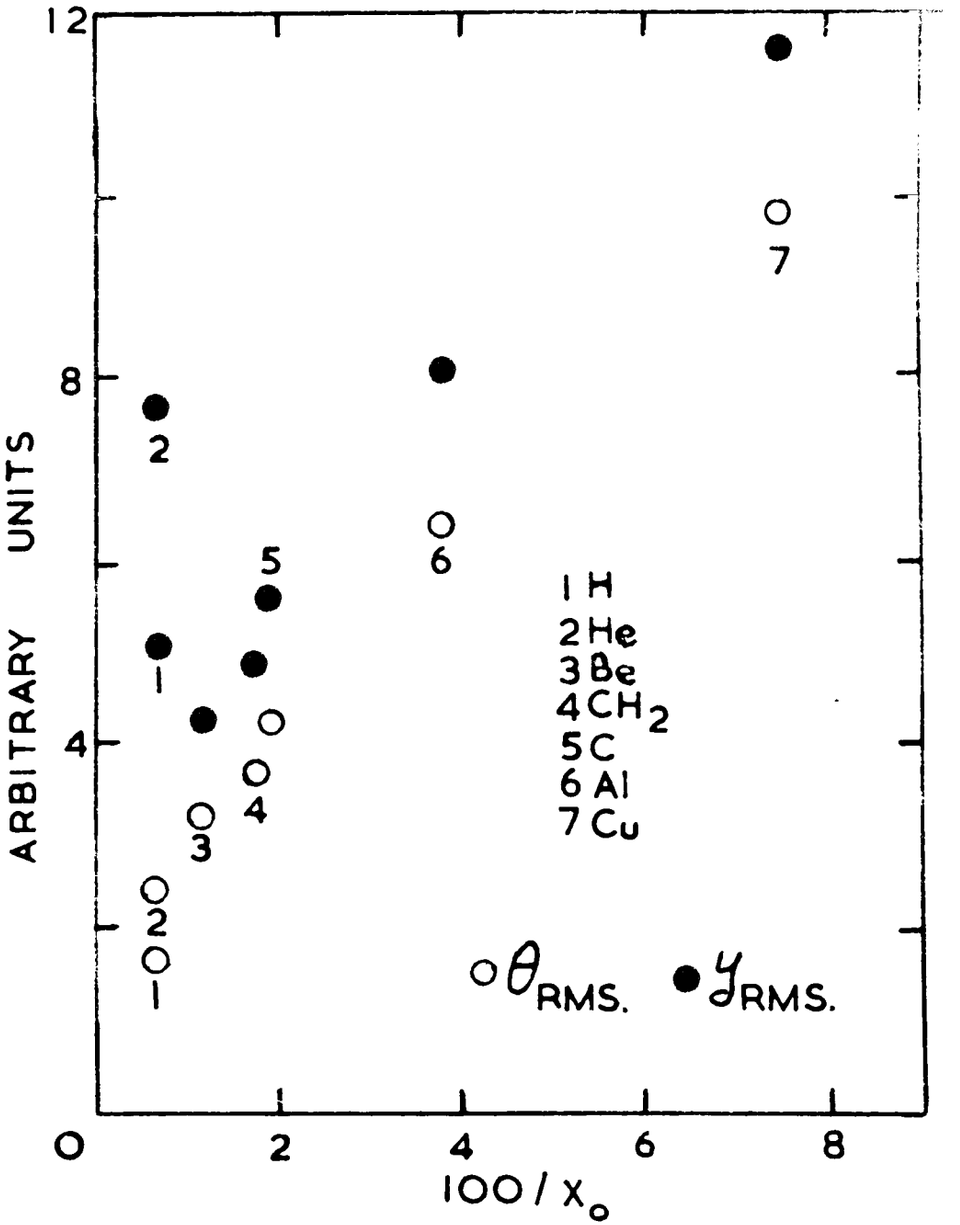

and again refer to the geometry of Fig. 19A. The second column refers to a full-energy beam of zero cross-section (point beam), and the third column to the beam used. The natural width of the latter was about 0.8 cm., and has been approximated here by a Gaussian of standard deviation 0.2 cm.

The height of the full-energy beam at the target was about 2 cm. Allowing for this, it has been estimated that well over half the beam intensity was accepted by the hydrogen target at energies as low as 30 MeV. This conclusion is consistent with the observed counting rates,

TABLE XIII. MULTIPLE SCATTERING IN POLYETHYLENE

Final Energy MeV	r.m.s. spread of beam at target in cm.	
	point beam	finite beam
20	1.44	1.46
40	1.21	1.22
60	0.99	1.01
80	0.78	0.81
100	0.62	0.66
120	0.44	0.48
150	0.00	0.20

REFERENCES

(1) E. Wigner, Phys. Rev., 43, 252, 1933.

(2) J.M. Blatt & V.F. Weisskopf, Theoretical Nuclear Physics, John Wiley & Sons, 1952.

(3) J.L. Gammel & R.M. Thaler, Progr. in Cosmic Ray Phys., 5, 99, 1960.

(4) R.N.J. Phillips, Rep. Progr. Phys., 22, 562, 1959.

(5) M.H. MacGregor, M.J. Moravcsik & H.P. Stapp, Ann. Rev. Nucl. Sci., 10, 291, 1960.

(6) L. Wolfenstein, Phys. Rev., 76, 541, 1949.

(7) J.L. Gammel & R.M. Thaler, Phys. Rev., 107, 291, 1957.

(8) H.P. Stapp, T.J. Ypsilantis & N. Metropolis, Phys. Rev., 105, 302, 1957.

(9) P.C. Signell & R.E. Marshak, Phys. Rev., 109, 1229, 1958.

(10) P. Caiffra, M.H.MacGregor, M.J. Moravcsik & H.P. Stapp, Phys. Rev., 114, 980, 1959.

(11) J.N. Palmeiri, A.M. Cormack, N.F. Ramsey and R. Wilson, Annals of Physics, 5, 299, 1958.

(12) L.H. Johnson and D. Swenson, Bul. Am. Phys. Soc., 2, 180, 1957.

(13) H.P. Noyes, University of California Report, UCRL - 4947, 1957.

(14) H.P. Noyes and M.H. MacGregor, Phys. Rev., 111, 223, 1958.

(15) P. Hillman, G.H. Stafford and C. Whitehead, Nuovo Cimento, 4, 67, 1956.

(16) D.N. Edwards and B. Rose, Nucl. Instr. & Methods, 7, 135 1960.

(17) L. Wolfenstein, Phys. Rev., 75, 1664, 1949.

(18) G.B.B.Chaplin & C.J.N. Candy, Nucl. Instr. & Methods, 5, 242, 1959.

(19) R.M. Sternheimer, Phys. Rev., 117, 485, 1960.

(20) J.M.Dixon & J.M. Salter, Nuovo Cimente, 6, 235, 1957.

(21) R.Alphonce., A.Johansson & G.Tibbell, Nucl. Phys., 3. 185, 1957

(22) M.J.Brinkworth & B.Rose, Nuovo Cimento, 3, 195, 1956.

(23) A.E.Taylor, E.Wood & L.Bird, Nucl. Phys. 16, 320, 1960

(24) B.Rose, Proceedings of the 1960 Annual International Conference on High Energy Physics at Rochester, University of Rochester, 1960.

(25) C.J.Taylor, W.K.Jentschke, M.E.Remley, F.S.Eby and P.G.Kruger, Phys. Rev., 84, 1034, 1951.

(26) E.L.Crow, F.A.Davis & M.W.Maxfield, Statistics Manual, Dover Publications Inc., 1960.

(27) J.K.Perring, Harwell preprint, AERE - T/P 81, 1961.

(28) L.D.Landau & E.M.Lifshitz, Quantum Mechanics, Pergamon Press, 1958.

(29) J. Iwadare, University of Pennsylvania preprint, 1960.

(30) J.Samada, private communication to B.Rose.

(31) M.H.MacGregor, Phys, Rev., 113, 1559, 1959

(32) J.K.Perring, private communication.

(33) H.P.Noyes, University of California Report, UCRL 6108-T, 1960.

(34) G. Breit, M.H.Hull, K.E.Lassila & K.D.Pyatt, Phys. Rev., 120, 2227, 1960

(35) H.P.Stapp, M.J.Moravcsik & H.P.Noyes, Proceedings of the 1960 Annual International Conference on High Energy Physics at Rochester, University of Rochester, 1960.

(36) H.P.Noyes, Proceedings of the Rutherford Jubilee International Conference, 1961. Heywood & Co., to be published.

(37) L.Wolfenstein. Ann. Rev. Nucl. Sci. 6, 43, 1956.

(38) C.F.Hwang, T.R.Opel, E.H.Thorndike & R.Wilson, Phys. Rev. 119, 352, 1960.

(39) A.E.Taylor & E.Wood, 1958 Annual International Conference on High Energy Physics at CERN. CERN, Geneva, 1958.

(40) P.S.Signell, R.Zinn and R.E.Marshak, Phys. Rev. Letters. 1, 416, 1958.

(41) L.Bird, P.Christmas, A.E.Taylor & E.Wood, Nucl. Phys. to be published.

(42) D.P.Saylor, R.A.Bryan & R.E.Marshak, Phys. Rev. Letters, 5 266, 1960.

(43) J.M.Blatt & L.C. Biedenharn, Rev. Mod. Phys. 24, 258, 1952.

(44) L. Wolfenstein & J. Ashkin, Phys. Rev. 85, 947, 1952.

(45) L.J.B.Goldfarb, Proceedings of the Rutherford Jubilee International Conference, 1961. Heywood & Co., to be published.

(46) H.P.Stapp, Thesis, UCRL-3098, 1955.

(47) A.Garren, Thesis, Carnegie Inst. of Tech., NYO-7102, 1955.

(48) B.Rossi. High Energy Particles, Prentice-Hall Inc., 1952.

(49) B.Rossi & K.Greisen, Rev. Mod. Phys. 13, 240, 1941.
